

Correlated electron dynamics and memory in time-dependent density functional theory

Von der Universität Bayreuth
zur Erlangung des Grades eines
Doktors der Naturwissenschaften (Dr. rer. nat.)
genehmigte Abhandlung

von

Mark Thiele

geboren in Frankfurt/Main

1. Gutachter: Prof. Dr. S. Kümmel
2. Gutachter: Prof. Dr. M. Axt

Tag der Einreichung: 28. Mai 2009
Tag des Kolloquiums: 28. Juli 2009

Abstract

Correlated electron dynamics play an important role for nonlinear and linear processes in atoms and molecules such as strong field and photoabsorption excitations. However, the theoretical description of correlation is generally difficult. Furthermore, strong field applications require a nonperturbative treatment. In principle the time-dependent many-electron Schrödinger equation (TDSE) provides the exact solution for any type of process, but the numerical workload becomes too big even for small systems in strong fields.

Here time-dependent density functional theory (TDDFT) presents an alternative as it both accounts for correlation effects and allows for a nonperturbative approach of the strong field regime. TDDFT is an exact reformulation of the TDSE, where the problem of many interacting electrons is mapped onto the Kohn-Sham system of noninteracting particles which reproduces the exact electronic density. As this auxiliary system relies on single particle equations numerical calculations can be performed much more efficiently than in the TDSE case. In the Kohn-Sham system all non-classical many-body effects are incorporated in the exchange-correlation potential which is in general unknown and needs to be approximated. This approach constitutes a well-defined way to deal with the many-body problem.

An important aspect of the necessary approximations regards the treatment of so-called memory effects in the exchange-correlation potential. The latter quantity is in general an unknown functional which depends nonlocally in space on the previous history of the electronic density. The neglect of the nonlocality in time and hence of memory effects constitutes the adiabatic approximation. In practice this approach is usually combined with an approximation of the spatial nonlocality. This combination complicates the interpretation of TDDFT results. Especially in the context of strong fields TDDFT is affected by problems whose relations to memory effects are not well understood up to know. But also in the case of linear excitation spectra memory effects play an important role. It is the goal of this thesis to investigate the connection between memory effects and correlated electron dynamics in strong and weak fields.

To this end one-dimensional two-electron singlet systems are studied as in this case it is possible to compute both the solution of the TDSE as an exact benchmark and the relevant quantities of TDDFT. At the same time these systems include the one-dimensional helium atom model, which is an established system to investigate the crucial effects of correlated electron dynamics in external fields.

The studies presented in this thesis show that memory effects are negligible for typical strong field processes. Here the approximation of the spatial nonlocality is of primary importance. For the photoabsorption spectra on the other hand the neglect of memory

effects leads to qualitative and quantitative errors, which are shown to be connected to transitions of double excitation character. To develop a better understanding of the conditions under which memory effects become important quantum fluid dynamics has been found to be especially suitable. It represents a further exact reformulation of the quantum mechanic many-body problem which is based on hydrodynamic quantities such as density and velocity. Memory effects are shown to be important whenever the velocity field develops strong gradients and dissipative effects contribute. This has consequences for the interpretation of the electrons as a viscoelastic fluid. These and further results have been reported in four publications which are attached at the back of this thesis.

Kurzfassung

Korrelierte Elektronendynamik ist für nichtlineare und lineare Prozesse in Atomen und Molekülen von großer Bedeutung. Dies betrifft insbesondere die Wechselwirkung mit starken Feldern und die Photoabsorptionsspektren. Die theoretische Beschreibung der Korrelationen gestaltet sich jedoch im Allgemeinen schwierig. Außerdem erfordern Anwendungen im Bereich starker Felder einen nicht-perturbativen Zugang. Im Prinzip liefert die zeitabhängige Vielteilchen-Schrödingergleichung (TDSE) die exakte Lösung für beliebige Prozesse. Allerdings wird der numerische Rechenaufwand bereits für kleine Systeme in starken Feldern zu groß.

Eine Alternative bietet hier die zeitabhängige Dichtefunktionaltheorie (TDDFT), die sowohl die Berücksichtigung von Korrelationseffekten als auch einen nichtperturbativen Zugang bei starken Feldern erlaubt. Bei der TDDFT handelt es sich um eine exakte Umformulierung der TDSE, bei der das Problem vieler wechselwirkender Elektronen auf das Kohn-Sham-System nicht-wechselwirkender Teilchen abgebildet wird, das die exakte Elektronendichte reproduziert. Da dieses Hilfssystem auf Einteilchengleichungen beruht, können numerische Berechnungen wesentlich effizienter durchgeführt werden als auf Basis der TDSE. Die gesamten nicht-klassischen Vielteilcheneffekte werden im Kohn-Sham-System über das Austausch-Korrelations-Potential berücksichtigt, das jedoch im Allgemeinen unbekannt ist und daher angenähert werden muss. Dieses Vorgehen stellt einen wohldefinierten Zugang zur Beschreibung des Vielteilchen-Problems dar.

Ein wichtiger Aspekt dieser notwendigen Näherung betrifft die Berücksichtigung sogenannter Gedächtniseffekte im Austausch-Korrelations-Potential. Letzteres ist nämlich im Allgemeinen ein kompliziertes Funktional, das nichtlokal im Raum von der gesamten Vorgeschichte der Elektronendichte abhängt. Werden die Nichtlokalität in der Zeit und damit die Gedächtniseffekte vernachlässigt, spricht man von der adiabatischen Näherung. Diese wird in der Regel mit einer Näherung der räumlichen Nichtlokalität kombiniert. Durch diese Verknüpfung wird die Interpretation von TDDFT-Ergebnissen häufig erschwert. Insbesondere bei der Beschreibung starker äußerer Felder treten im Rahmen der TDDFT Probleme auf, deren Beziehung zu den Gedächtniseffekten bisher unklar ist. Aber auch im Falle der linearen Anregungsspektren spielen die Gedächtniseffekte eine wichtige Rolle. Ziel dieser Arbeit ist es daher, den Zusammenhang zwischen den Gedächtniseffekten und der korrelierten Elektronendynamik in starken und schwachen Feldern zu untersuchen.

Zu diesem Zweck werden eindimensionale Zwei-Elektronen-Singulett-Systeme untersucht, da hier sowohl die Lösung der TDSE als exakte Referenz als auch die Berechnung der relevanten TDDFT-Größen möglich ist. Gleichzeitig schließen diese Systeme das eindimensionale Helium-Atom-Modell ein, das ein etabliertes System zur Untersuchung der

charakteristischen Effekte korrelierter Elektronendynamik in äußeren Feldern darstellt.

Bei diesen Untersuchungen hat sich gezeigt, dass Gedächtniseffekte für Starkfeld-Prozesse nur eine untergeordnete Rolle spielen. Hier ist vielmehr die korrekte Näherung der räumlichen Nichtlokalität entscheidend. Bei den Photoabsorptionsspektren hingegen führt die Vernachlässigung der Gedächtniseffekte zu qualitativen und quantitativen Fehlern. Es zeigt sich, dass diese Probleme mit dem Auftreten von Doppelanregungen zusammenhängen. Um ein besseres Verständnis zu entwickeln, unter welchen Umständen Gedächtniseffekte wichtig werden, hat sich die sogenannte Quanten-Hydrodynamik als äußerst nützlich erwiesen. Hierbei handelt es sich um eine weitere Darstellungsmöglichkeit des quantenmechanischen Vielteilchen-Problems, die auf hydrodynamischen Größen wie Dichte und Geschwindigkeit basiert. Man findet, dass Gedächtniseffekte immer dann wichtig werden, wenn das Geschwindigkeitsfeld starke Gradienten ausbildet und Dissipationseffekte auftreten. Daraus ergeben sich interessante Schlussfolgerungen für die Interpretation der Elektronen als viskoelastische Flüssigkeit. Diese und weitere Ergebnisse sind in vier Publikationen enthalten, die sich am Ende dieser Arbeit finden.

Contents

I	Introduction	1
1	Motivation	3
2	Correlated electron dynamics	5
2.1	Electrons in weak fields	5
2.2	Electrons in strong fields	8
3	Theoretical background	11
3.1	Wave function theory	11
3.2	Static density functional theory	13
3.2.1	The Hohenberg-Kohn theorem	13
3.2.2	The static Kohn-Sham system	14
3.2.3	Static linear density response	15
3.2.4	Approximate static density functionals	16
3.3	Time-dependent density functional theory	16
3.3.1	The Runge-Gross theorem	16
3.3.2	The time-dependent Kohn-Sham system	17
3.3.3	Time-dependent linear density response	18
3.3.4	The adiabatic approximation	20
3.4	Quantum fluid dynamics	23
4	The two-electron singlet system	25
4.1	Theoretical description	26
4.2	Numerical aspects	28
5	The role of memory effects	31
5.1	Validity of the adiabatic approximation for typical strong-field applications	31
5.2	Hydrodynamic interpretation of memory effects	32
5.3	Memory effects and double excitations	33
5.4	Adiabatic approximation of the xc kernel	35
5.5	Summary and outlook	36
	Bibliography	39

Acknowledgment	44
Erklärung	45
II Publications	47

Part I

Introduction

1 Motivation

Power is nothing without control.
Pirelli advertisement slogan

Today strong lasers can generate field strengths comparable to those experienced by valence electrons in atoms and molecules¹⁵. This allows to directly ionize atoms or to break molecular bonds. As strong laser fields do also have the ability to align and orient molecules⁶⁸, these techniques can be used to visualize and manipulate simple chemical processes.

Furthermore the interaction of strong fields and atoms or molecules can be used to generate high intensity attosecond pulses^{15,35,37}. The latter now also match the time scales of electronic motion which makes them an even more powerful tool to analyze and manipulate atomic and molecular processes. Of course there is great hope that one day these techniques can be used to control and steer electron dynamics.

However, while laser technology provides us with mighty tools to probe the molecular world, even the interaction of simple atoms with powerful external fields is only poorly understood. The reason for this is that the mutual Coulomb interaction of electrons plays an important role for their strong-field dynamics. Furthermore, many available theoretical techniques apply only to interactions with weak external fields, which obviously do not include the high-intensity regime.

But even in the weak field linear response regime electronic correlations are not easily accounted for. Here they qualitatively and quantitatively influence the excitation spectra of atoms and molecules, which constitute a primary source of information on the properties of matter.

So if one really wants to understand and control the electron dynamics in external fields there is definitely a need for fully-correlated and also non-perturbative theoretical approaches. One such approach is provided by time-dependent density functional theory (TDDFT). TDDFT represents an exact reformulation of the quantum many-body problem that enables practical calculations when certain well-defined approximations are introduced. An important aspect of this approximation process is the treatment of so-called memory effects. It is the purpose of this thesis to investigate the influence of memory on correlated electron dynamics in strong and weak field applications.

These two regimes are introduced in chapter 2, followed by a discussion of the relevant theoretical concepts in chapter 3. Thereafter we present the systems used for our studies in chapter 4. The obtained results are presented in chapter 5, where we focus on the key results of four publications related to this work. The original publications which are referred to as *Pub1* - *Pub4* are provided at the back of this thesis.

2 Correlated electron dynamics

*This is getting out of hand!
Now there are two of them!*

Nute Gunray in the movie
'Star Wars: Epsiode I'

Towards the end of university quantum mechanic courses probably all of us have experienced a moment of disillusionment: Having mastered the analytically solvable one-electron problems, of which the hydrogen atom is the most prominent representative, we encounter the threatening many-particle problem, that haunts also many other areas of physics. Suddenly the rigor of the full Schrödinger equation apparently has to be abandoned in favor of a list of recipes that either apply to specific situations only or involve strong approximations. This is the negative way of looking at it.

From a positive point of view we have already reached the ground on which modern physics confronts some of its most interesting challenges. In this chapter we will illustrate this situation for finite many-body quantum systems, specifically in the context of atomic physics. Consequently the many-electron regime is entered by proceeding from hydrogen to helium. As we will see in the following, the addition of a second electron does already introduce some of the most crucial aspects of correlation that are topics of current research. These affect atomic spectra as well as ionization dynamics in the course of interaction with a strong laser field. In this context, atomic systems also serve as an important benchmark for correlated electron dynamics in molecules.

2.1 Electrons in weak fields

The electronic excitation spectrum of an atom can be determined experimentally by spectroscopic means, i. e., by studying the interaction of the atom with the light field. From a theoretical point of view this amounts to investigating electronic transitions between ground and excited states of the system. Usually this problem is treated within linear response theory for weak perturbations by the external field. In this section we will sketch some of the general challenges for theoretical approaches.

Our qualitative understanding of many-electron atoms is based on the independent particle picture, which assumes that each electron only interacts with the effective field generated by the nucleus and the other electrons^{23,43,69}. When this concept is applied to atoms in their ground states it leads to an approximate build-up scheme for atomic many-electron systems. The resulting shell-structure is the basis for the periodic table

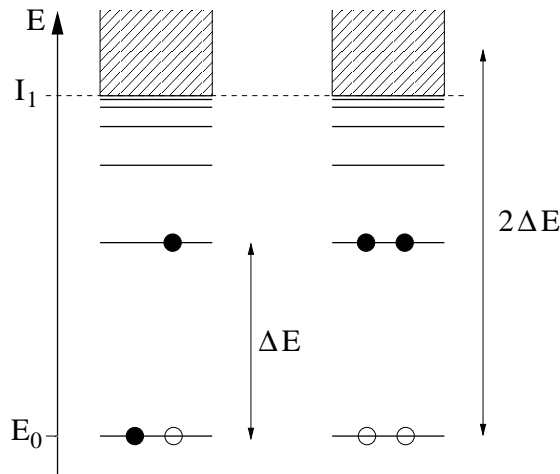


Figure 2.1: Lowest single (left) and double excitation (right) of a two-electron atom together with the corresponding total energy change.

of the elements^{23,43}. Here we discuss its consequences for the description of excited states of atoms in the context of helium.

In the helium ground state both electrons are assumed to occupy their lowest eigenstates, i. e., we have a $1s^2$ state in the usual notation. The bound excited states correspond to single excitations, i. e., one electron remaining in the $1s$ state and the other one occupying one of the excited single particle states. The corresponding spectrum displays the characteristic atomic level spacing shown in figure 2.1, which is a consequence of the Coulombic asymptotics of the effective single-particle potential. Thus, with increasing energy the spectrum will go through a Rydberg series and finally cross over into the continuum at the first ionization threshold I_1 where one electron gets ionized and a He^+ ion remains. This part of the helium spectrum is found to be properly classified by the independent particle picture.

When it comes to the quantitative description the independent particle picture is only applicable to the high single excitations. Here the excited electron is “far away” from the nucleus and the ground state electron, so that the effective field concept works well. However, this is only a tiny part of the whole spectrum. When one electron is excited to one of the lower energy levels the system is more appropriately described by a configuration of two interacting electrons in the field of the nucleus. Thus effects like particle exchange and correlation become important. These lead to corrections of the independent particle picture.

Another more spectacular situation, where the independent particle picture is questionable, is provided by doubly excited states. Here both electrons occupy excited states. As we see in the right part of figure 2.1 this leads to a situation where due to the spacing of the energy levels the doubly excited configuration is energetically no longer in the discrete part of the spectrum but above the first ionization threshold. Hence the double

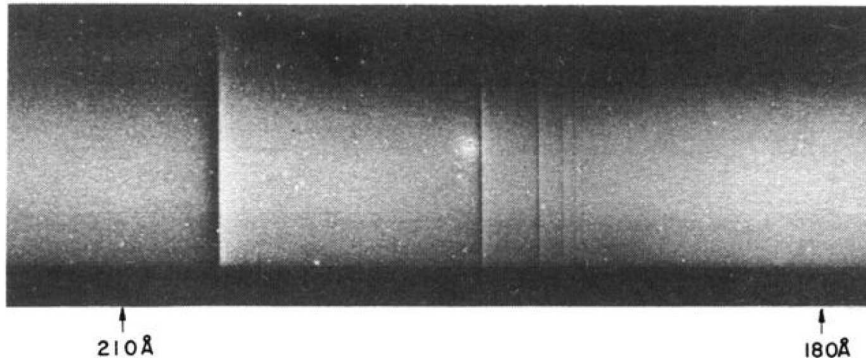


Figure 2.2: Absorption spectrum of helium according to Madden and Codling⁴⁵. There are clear signatures of discrete resonances embedded in the single particle continuum.

excitations are configurations with a discrete spectral structure that are embedded in the continuum. The double excitations form resonances because they are degenerate with a single excitation, where one electron is ionized. These states are known as autoionizing or Fano resonances^{22,26}.

The independent particle picture can still be used to classify the double excitations according to $2s^2$, $2s2p$ etc. and to calculate corresponding transition energies. These predictions were tested by the 1963 key experiment of Madden and Codling⁴⁵ using synchrotron radiation to obtain the absorption spectrum of helium. As shown in figure 2.2 discrete bound states are indeed present within the single particle continuum. However both the energies and intensities of the observed lines were found not to agree with the predictions. The discrepancies indicate that electronic correlations lead to selection rules and quantitative corrections that are crucial for these double excitations^{6,69}.

The importance of electronic correlations for the double excitations makes sense also in the context of their resonance character: As mentioned above they can decay via autoionization by transferring energy between both electrons. This means that one electron has to lose energy by falling back to a lower level, so that the other electron can take up this energy and escape from the atom⁶⁹. Thus there is a need of the two electrons to interact with each other in a dynamical and correlated way which is not accounted for by the independent particle description.

The autoionizing resonances are ubiquitous in the remaining spectrum of helium up to the double ionization threshold where both electrons leave the atom: A whole Rydberg series of resonances appears below the second ionization threshold I_2 at which one electron is removed and the helium ion remains in the first excited configuration. Further resonant series appear below each ionization threshold and even start to overlap with each other for higher energies. This leads to an ever increasing complexity as we approach the two-particle ionization threshold. Correlation effects in this part of the spectrum are the topic of a whole field of research⁶⁹.

We have seen that already for the spectrum of an atom as simple as helium electronic correlation produces significant qualitative and quantitative effects. To account for these features we need a linear response formulation that properly accounts for correlation. One such method is linear density response theory that will be introduced later in the context of TDDFT.

2.2 Electrons in strong fields

In the previous section we have seen that correlated electron dynamics are important for the correct description of electronic transitions in atoms. The underlying theory was based on the assumption that the applied external field, which triggers the excitation, is weak. This condition allows one to use first-order perturbation theory for the light-matter interaction. As a result only one-photon absorption or emission processes are accounted for. But due to modern laser technology it is possible today to expose atoms also to very strong fields of high photon intensity. This is the regime of multiphoton processes, where perturbative approaches are no longer applicable^{2,18,24,79}.

Once again the helium atom has turned out to be a prototype for the relevant physics. Its strong field ionization yields, shown in figure 2.3, have been explored in the 1994 experiment by Walker et al.⁸⁴. The single ionization yield ($\text{He} \rightarrow \text{He}^+ + e^-$) is correctly explained by single active electron calculations, where one electron is kept fixed together with the nucleus. On the other hand the double ionization (DI) yield ($\text{He} \rightarrow \text{He}^{2+} + 2e^-$) is enhanced by several orders of magnitude compared to calculations assuming a sequential process where one electron is removed after the other. Consequently, the increased double ionization yield has been termed nonsequential. The corresponding structure of the curve is usually referred to as the double ionization “knee”.

It took the combined effort of theoretical^{4,5,14,21,41,44,63} and experimental^{53,86,87} studies to establish the so-called “recollision” mechanism as a partly classical explanation for the enhanced DI yields^{2,14,15}.

This mechanism assumes that the first electron escapes to the continuum either through tunnel or multiphoton ionization². In a second step this electron is accelerated in the laser field. Now two things can happen: If the electron takes up enough energy in the laser field to escape from the atom-laser system, single-electron ionization takes place. If, however, the electron gets pushed back by the field towards the atom it becomes a rescatter electron which can enter three possible reaction channels¹⁴: (1) The rescatter electron recombines with the ion and a photon is emitted. Its energy is determined by the ionization potential of the atom and the kinetic energy of the rescatter electron. This process leads to high harmonic generation. (2) The returning electron scatters off the ion and is accelerated further by the field. This leads to highly energetic photo electrons. (3) The rescatter electron kicks out a second electron and both electrons leave the atom simultaneously. This is the nonsequential double ionization introduced above.

From the recollision model we see immediately that the double ionization process

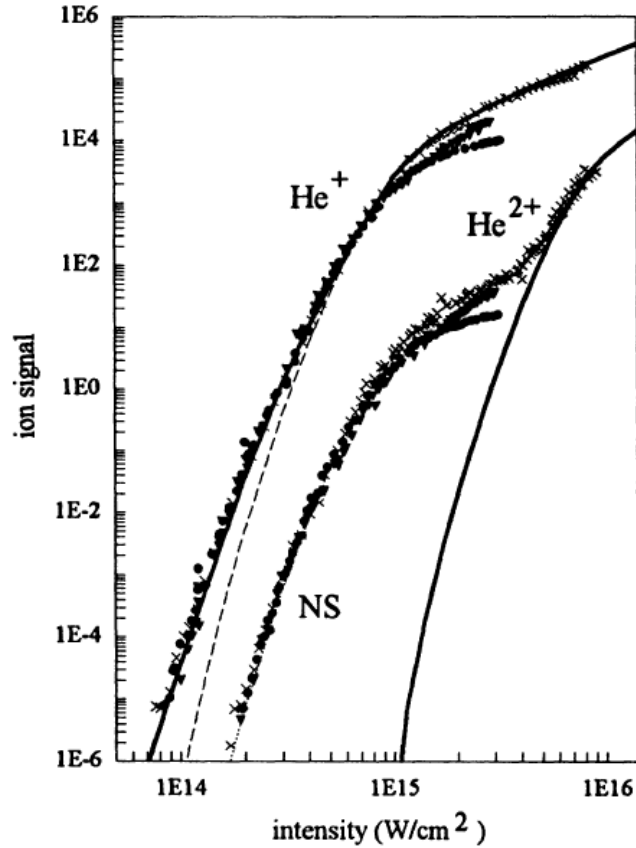


Figure 2.3: Single and double ionization yields of helium exposed to linearly polarized laser light of 780 nm wave length. Experimental values (dots) are compared to calculations (solid lines) which are based on the single active electron model for the He^+ -yield and on a sequential process for the double ionization yield (see text). From Walker et al.⁸⁴.

does crucially depend on electron-electron correlation. Hence it is not surprising that, e.g., time-dependent Hartree-Fock methods fail to reproduce the DI knee^{38,62}. As a consequence, there is great hope that correlated methods like TDDFT will be able to describe this type of process⁵².

3 Theoretical background

There is a theory which states that if ever anyone discovers exactly what the Universe is for and why it is here, it will instantly disappear and be replaced by something even more bizarre and inexplicable. There is another theory which states that this has already happened.

‘The restaurant at the end of the universe’
by Douglas Adams

We have seen that correlated electron dynamics is crucial for the correct description of electronic excitations and the interaction with intense laser fields. Furthermore, the latter application requires a nonperturbative time-dependent approach.

Of course all these requirements are met by the Schrödinger equation for the many-body problem but only at a tremendous computational cost. We will briefly discuss this approach mainly to introduce the formalism and highlight the difficulties. Then we will introduce first static density functional theory (DFT) followed by its time-dependent formulation TDDFT. We will also briefly touch quantum fluid dynamics which is intimately related to TDDFT and turns out to provide useful complementary information on certain aspects of correlated dynamics.

3.1 Wave function theory

The static N -electron problem is described by the Hamiltonian

$$\begin{aligned} H_0 &= T + V_{\text{ext},0} + V_{\text{ee}} \\ &= -\frac{\hbar^2}{2m} \sum_{i=1}^N \nabla_i^2 + \sum_{i=1}^N v_{\text{ext},0}(\mathbf{r}_i) + \frac{1}{2} \sum_{i>j}^N \frac{e^2}{|\mathbf{r}_i - \mathbf{r}_j|}. \end{aligned} \quad (3.1)$$

This means that we neglect relativistic effects and make use of the Born-Oppenheimer approximation to obtain a separate electronic problem on time scales where the atomic nuclei are static. The external potential $v_{\text{ext},0}$ is due to the positively charged ions. This system is described by the static Schrödinger equation (SE) $H_0\psi_i = E_i\psi_i$, where $\psi_i(\mathbf{r}_1, \mathbf{r}_2, \dots, \mathbf{r}_N)$ is the spatial wave function of the i th eigenstate of the Hamiltonian (3.1). As we will only be concerned with spin-unpolarized systems and external fields that do not couple to the spin we suppress any reference to the spin in the following chapters.

When a time-dependent electrical field is applied externally its potential is combined with that of the ions so that we have $H = H(t)$ with $v_{\text{ext}}(\mathbf{r}, t)$ instead of $v_{\text{ext},0}(\mathbf{r})$. The evolution of the system is now governed by the time-dependent Schrödinger equation (TDSE)

$$i \hbar \partial_t \psi(\mathbf{r}_1, \mathbf{r}_2, \dots, \mathbf{r}_N, t) = H \psi(\mathbf{r}_1, \mathbf{r}_2, \dots, \mathbf{r}_N, t). \quad (3.2)$$

The solution ψ is a highly complicated $(3N + 1)$ -dimensional object which contains the complete information about the system at time t . Thus it can provide us with the expectation value of any quantum mechanical operator $\hat{Q}(t)$ according to $Q(t) = \langle \psi | \hat{Q} | \psi \rangle$.

Two important quantities for our purposes are the density operator

$$\hat{n}(\mathbf{r}) = \sum_{j=1}^N \delta(\mathbf{r} - \mathbf{r}_j) \quad (3.3)$$

and the current density operator

$$\hat{\mathbf{j}}(\mathbf{r}) = \frac{\hbar}{2i} \sum_{j=1}^N (\nabla_j \delta(\mathbf{r} - \mathbf{r}_j) + \delta(\mathbf{r} - \mathbf{r}_j) \nabla_j). \quad (3.4)$$

Their expectation values $n(\mathbf{r}, t)$ and $\mathbf{j}(\mathbf{r}, t)$ are related by the continuity equation

$$\dot{n}(\mathbf{r}, t) = -\nabla \cdot \mathbf{j}(\mathbf{r}, t). \quad (3.5)$$

The calculation of the atomic spectra is trivial if the SE can be solved as the excited states properties can easily be obtained from the ψ_i and E_i . However even for simple two-electron atoms sophisticated approaches are required to obtain the E_i of highly excited states let alone the actual eigenstates ψ_i .^{47,64,69} Thus, numerical approaches to the spectra based on the full SE are out of the question for many-electron systems.

In the case of the strong field double ionization process the observables of interest are the ionization yields. Their practical definition is based on the pair density

$$\rho(\mathbf{r}_1, \mathbf{r}_2, t) = N(N-1) \int d^3r_3 \dots \int d^3r_N |\Psi(\mathbf{r}_1, \dots, \mathbf{r}_N, t)|^2 \quad (3.6)$$

for times t long after the laser pulse^{3,38,62}. As ρ represents the probability density to find one electron at \mathbf{r}_1 and another at \mathbf{r}_2 , integrals over certain regions of space can provide the desired ionization yields. This is visualized in figure 3.1 for a one-dimensional projection. Integrating the pair density, e.g., over the shaded areas, where both electrons are sufficiently far away from the nucleus at the origin provides the double ionization probability.

To construct the pair density we need the time-dependent wave function for the whole double ionization process. But in order to represent the full dynamics of the rescatter process introduced above, tremendous grid sizes are required. As the wave function of

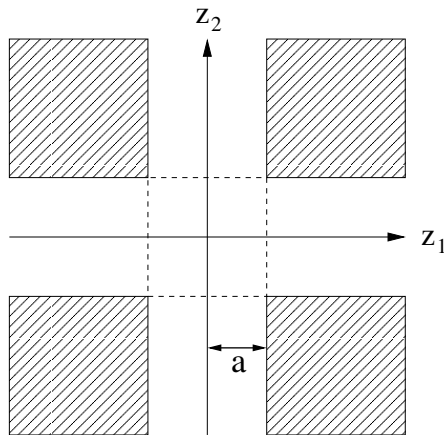


Figure 3.1: Integration regions for the pair density. The electrons are assumed to be bound when they are both in the box of width $2a$ around the nucleus.

helium depends on 6 spatial coordinates this is an enormous numerical workload. Even continuing efforts to solve the problem for helium on supercomputers were not yet able to reach the relevant physical regime of strong field double ionization^{21,58,71}. Thus in the nonperturbative time-dependent regime we need an alternative to the wave function description even more desperately.

3.2 Static density functional theory

Our first goal is a reformulation of the N -electron ground state problem as represented by (3.1). This means that we need a new basic variable that replaces the complicated $3N$ -dimensional wave function. As we will see in the following a suitable alternative is provided by the electronic density.

3.2.1 The Hohenberg-Kohn theorem

Static density functional theory is founded on the famous Hohenberg-Kohn (HK) theorem³³. It provides the mathematical proof that there exists a unique mapping between the ground state potential $v_{\text{ext},0}$ and the ground state density

$$n_0(\mathbf{r}) = N \int \int \dots \int |\psi_0(\mathbf{r}, \mathbf{r}_2, \dots, \mathbf{r}_N)|^2 d^3r_2 d^3r_3 \dots d^3r_N \quad (3.7)$$

for a fixed number of electrons N and a specified type of interaction V_{ee} . The implications of the HK theorem cannot be overestimated: The electronic density as a mere function of 3 spatial coordinates completely determines $v_{\text{ext},0}$ and hence H_0 . But from H_0 follows ψ_0 as a function of $3N$ spatial coordinates, which can in turn be used to obtain any ground state observable. As the Hamiltonian also determines the ψ_i for $i > 0$, even excited state properties should in principle be encoded in the ground state density.

Unfortunately the HK theorem does just provide uniqueness and existence information, i. e., it is not a constructive proof that tells us how to actually calculate ψ_0 from n_0 . This means that up to now we know nothing more than that $v_{\text{ext},0}[n_0]$ and $\psi_0[n_0]$ represent well-defined functionals.

3.2.2 The static Kohn-Sham system

In order to obtain a practical implementation of DFT a further step is required. As mentioned above the HK mapping can be established for any type of electron-electron interaction. Thus the theorem does also hold for particles which do not interact at all. This property is the basis for the Kohn-Sham (KS) system of N independent auxiliary particles³⁶. These particles are described by orbitals $\varphi_j(\mathbf{r})$, which are constructed so that the resulting density

$$n_0(\mathbf{r}) = \sum_{j=1}^N |\varphi_j(\mathbf{r})|^2 \quad (3.8)$$

is equal to the true interacting density. The orbitals are governed by the static KS equation (KSE)

$$h_0 \varphi_j(\mathbf{r}) = \left(-\frac{\hbar^2}{2m} \nabla^2 + v_{\text{s},0}(\mathbf{r})\right) \varphi_j(\mathbf{r}) = \varepsilon_j \varphi_j(\mathbf{r}), \quad (3.9)$$

where the effective KS potential $v_{\text{s},0}[n_0]$ is a unique functional of the density by virtue of the HK theorem.

At this point it is instructive to look back for a moment. In the previous chapter the concepts of independent particles and effective fields or potentials were playing an important role for the understanding of atoms. Now this approach is much more rigorous: First of all it is important to realize that the independent KS orbitals do not represent electrons but just auxiliary particles. Secondly, we no longer attempt to construct the many-particle wave function from single-particle orbitals as, e. g., in Hartree-Fock theory. Instead we construct the interacting many-electron density from single particle orbital densities. Finally, the effective potential is a uniquely-defined multiplicative quantity, which by construction includes all electron exchange and correlation effects in contrast to Hartree-Fock theory, where exchange is handled by a nonlocal integral potential operator and correlation is neglected.

We have seen that simple effective single-particle approaches can already account for important physical properties. This is due to the fact that a significant contribution to any effective potential is of course provided by the ionic $v_{\text{ext},0}$ and by the classical mean field contribution of the electron-electron-interaction, also called Hartree potential,

$$v_{\text{h}}(\mathbf{r}) = e^2 \int \frac{n_0(\mathbf{r}')}{|\mathbf{r} - \mathbf{r}'|} d^3 r'. \quad (3.10)$$

Thus it makes sense to split up $v_{\text{s},0}$ according to

$$v_{\text{s},0}(\mathbf{r}) = v_{\text{ext},0}(\mathbf{r}) + v_{\text{h}}(\mathbf{r}) + v_{\text{xc},0}(\mathbf{r}), \quad (3.11)$$

where all the nonclassical many-body effects are incorporated into the exchange-correlation (xc) potential $v_{xc,0}$. Due to its relation to the other potentials given by (3.11) the xc potential is also a unique functional of the ground state density.

Up to now, no approximations have been made and we are still dealing with an exact reformulation of the N -electron problem. But as $v_{xc,0}[n_0]$ is in general unknown, it needs to be approximated. It is important to note that due to the mathematical rigor of the HK theorem and the construction of the effective potential $v_{s,0}$ in terms of $v_{xc,0}$ and other components, any approximation enters DFT in a well-defined way. Furthermore there exist exact constraints that $v_{xc,0}$ has to satisfy^{59,60}. They provide guidance for the development of approximate xc functionals.

3.2.3 Static linear density response

When we take the functional derivative of $v_{xc,0}$ evaluated at the ground state density n_0 we obtain the static xc kernel

$$f_{xc,0}[n_0](\mathbf{r}, \mathbf{r}') = \left. \frac{\delta v_{xc,0}(\mathbf{r})}{\delta n_0(\mathbf{r}')} \right|_{n_0}, \quad (3.12)$$

which is also uniquely defined by n_0 . The kernel is the susceptibility for the xc potential response to small perturbations of the ground state density, i. e.,

$$\delta v_{xc,0}(\mathbf{r}) = \int f_{xc,0}(\mathbf{r}, \mathbf{r}') \delta n_0(\mathbf{r}') d^3 r'. \quad (3.13)$$

When we take the functional derivative of equation (3.11) we see that the xc kernel connects the corresponding susceptibilities χ_0^{-1} and $\chi_{s,0}^{-1}$ of the interacting and the KS system according to

$$\chi_{s,0}^{-1}(\mathbf{r}, \mathbf{r}') = \chi_0^{-1}(\mathbf{r}, \mathbf{r}') + \frac{e^2}{|\mathbf{r} - \mathbf{r}'|} + f_{xc,0}(\mathbf{r}, \mathbf{r}'). \quad (3.14)$$

Here

$$\chi_0^{-1}[n_0](\mathbf{r}, \mathbf{r}') = \left. \frac{\delta v_{ext,0}(\mathbf{r})}{\delta n_0(\mathbf{r}')} \right|_{n_0} \quad (3.15)$$

describes the response of $v_{ext,0}$ to changes in n_0 , and $\chi_{s,0}$ is defined analogously.

χ_0^{-1} is the inverse of the interacting density-density response or correlation function, i. e., the linear response of the ground state density $n_0(\mathbf{r})$ to a perturbation $\delta v_{ext,0}$ of the ground state potential is given by

$$\delta n_0(\mathbf{r}) = \int \chi_0(\mathbf{r}, \mathbf{r}') \delta v_{ext,0}(\mathbf{r}') d^3 r'. \quad (3.16)$$

Again a similar equation holds for the noninteracting density response.

Hence we see that also on the level of static linear response theory the xc contribution (in the form of the kernel) allows to obtain the interacting density response from the noninteracting one^{28,59}. This concept is important for the computation of the exact transition energies and oscillator strengths in the context of TDDFT, which will be introduced further below.

3.2.4 Approximate static density functionals

In the previous sections we have set up the formal framework of static Kohn-Sham DFT and identified the need to develop approximate density functionals for $v_{xc,0}[n_0]$. These approximations are required to solve the KS equations iteratively until self-consistency of the KS orbitals and $v_{xc,0}$ is reached.

We will not go into the details of xc functional development in DFT here. For our purposes it is sufficient to note that most approximations can be classified according to their degree of nonlocality with respect to the density. An extreme case is provided by the local density approximation which assumes that $v_{xc,0}$ depends on the density only locally^{33,36}. Hence it should be approximately valid for the case of slowly varying densities. Nevertheless it has been found to perform surprisingly well also in other cases.

There is another important aspect of functional development that has only appeared indirectly before. When we have solved the KS scheme with the help of an approximate $v_{xc,0}$ we end up with an approximation of the exact ground state density $n_0(\mathbf{r})$. But how can we obtain any further observables? As mentioned before all observables are unique functionals of n_0 for a nondegenerate ground state, but when the functional dependency is unknown, further approximations have to be introduced. As a consequence within DFT the computation of any observable, which is not an explicit functional of the density, is affected by two approximations: that of $v_{xc,0}$ and that of the observable functional itself.

For our purposes we definitely require information about the transition energies to be able to describe atomic spectra. One obvious possibility is to resort to the KS excited states to construct the transition frequencies in the single particle picture. However, these quantities can only serve as a zeroth order approximation^{27,52}; we need TDDFT to go beyond this level.

3.3 Time-dependent density functional theory

We have seen that DFT provides an attractive approach to include correlation in the description of a static many-electron system in its ground state. On the other hand it does not offer a practical way to determine excited states properties or to tackle fully time-dependent problems. Both challenges are met by TDDFT.

3.3.1 The Runge-Gross theorem

Static DFT is based on the unique mapping between ground state density and external potential provided by the HK theorem. For a time-dependent version of DFT one seeks a similar relation between the time dependent density $n(\mathbf{r}, t)$ and the external potential $v_{\text{ext}}(\mathbf{r}, t)$ which may now include external fields that vary in time. This connection can indeed be established for potentials $v_{\text{ext}}(\mathbf{r}, t)$, that are Taylor-expandable around the initial time t_0 , through the Runge-Gross (RG) theorem^{40,66}.

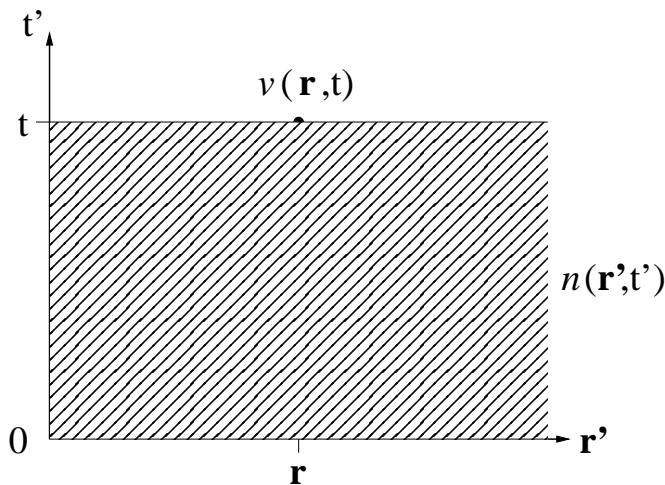


Figure 3.2: Schematic representation of the nonlocal-in-space and nonlocal-in-time dependency of the potential on the density.

The RG theorem states that for a given type of particle-particle interaction the initial state Ψ_0 at t_0 and the time dependent density evolving from t_0 uniquely define the external potential $v_{\text{ext}}(\mathbf{r}, t)$ up to an additive time-dependent constant. As a consequence $n(\mathbf{r}, t)$ and Ψ_0 uniquely determine the time-dependent wave function up to a purely time-dependent phase. The latter is not affecting the expectation values of any quantum mechanical operator, which are thus unique functionals of the density and the initial state.

Formally, we have $v_{\text{ext}}[\Psi_0, n(\mathbf{r}', t')](\mathbf{r}, t)$ and $\psi[\Psi_0, n(\mathbf{r}', t')](\mathbf{r}_1, \dots, \mathbf{r}_N, t)$ for $t_0 \leq t' \leq t$. For most applications and also for our purposes the initial state is the ground state of the system, i. e., $\Psi_0 = \psi_0$. As ψ_0 is uniquely defined by n_0 via static DFT the initial state dependence can be completely absorbed by the density-dependence⁴⁹. Hence for time-dependent processes starting from the ground state we have $v_{\text{ext}}[n(\mathbf{r}', t')](\mathbf{r}, t)$ for $t_0 \leq t' \leq t$. This means that in TDDFT we do not only have the spatially nonlocal functional relation familiar from static DFT but also a nonlocal history dependence on the density: At a given time t , $v_{\text{ext}}(\mathbf{r}, t)$ depends on the density at all points in space at all previous times (cf. figure 3.2). The history dependence is usually referred to as memory effects being present in $v_{\text{ext}}(\mathbf{r}, t)$ and generally also in any observable.

3.3.2 The time-dependent Kohn-Sham system

Similar to the static case the RG theorem allows one to map the interacting N -electron problem to a time dependent Kohn-Sham (TDKS) system of noninteracting particles^{28,66}. These particles are described by orbitals which are governed by the time-

dependent KS equation equation (TDKSE)

$$i \hbar \partial_t \varphi_j(\mathbf{r}, t) = \left(-\frac{\hbar^2}{2m} \nabla^2 + v_s(\mathbf{r}, t)\right) \varphi_j(\mathbf{r}, t) \quad (3.17)$$

and, by construction, add up to provide the exact density

$$n(\mathbf{r}, t) = \sum_{j=1}^N |\varphi_j(\mathbf{r}, t)|^2. \quad (3.18)$$

Here the effective KS potential is defined analogously to the ground state case, i. e.,

$$v_s(\mathbf{r}, t) = v_{\text{ext}}(\mathbf{r}, t) + v_h(\mathbf{r}, t) + v_{\text{xc}}(\mathbf{r}, t). \quad (3.19)$$

Once again we have to pay for this gain in simplicity by introducing the time-dependent xc potential which depends on $n(\mathbf{r}, t)$ at all points in space at previous times (cf. figure 3.2) and needs to be approximated. However as soon as v_{xc} is provided we can solve the KS equations for external fields $v_{\text{ext}}(\mathbf{r}, t)$ both in the linear response regime and in a strong field scenario⁵². Due to the single-particle character of (3.17) this method is expandable to systems of many electrons. The memory in v_{xc} is the central concept on which this thesis focuses.

There exist several exact constraints that have to be satisfied by the exact v_{xc} . One of them is the zero-force theorem⁸⁰, which states that the net xc force exerted on the whole system vanishes, i. e.,

$$\int d^3r n(\mathbf{r}, t) \nabla v_{\text{xc}}(\mathbf{r}, t) = 0. \quad (3.20)$$

This result is a direct consequence of Newton's third law.

Another important result that is especially important for our purposes is the harmonic potential theorem (HPT)²⁰, which applies to interacting N -electron systems. If the electrons are confined by a parabolic potential and a time-dependent dipole field is applied, we have $v_{\text{ext}}(\mathbf{r}, t) = (k/2) r^2 + \mathbf{E}(t) \cdot \mathbf{r}$. Now it can be shown that under these conditions, the electron density is rigidly translated according to $n(\mathbf{r}, t) = n_0(\mathbf{r} - \mathbf{X}(t))$. Here, $\mathbf{X}(t) = (1/N) \int d^3r \mathbf{r} n(\mathbf{r}, t)$ is the center-of-mass coordinate obeying

$$m \ddot{\mathbf{X}}(t) = -k \mathbf{X}(t) - \mathbf{E}(t). \quad (3.21)$$

Only if the xc potential rigidly follows the translated density, the TDKSE will satisfy the HPT. This property is also denoted generalized translational invariance⁸⁰.

3.3.3 Time-dependent linear density response

TDDFT naturally provides a framework for calculating the time-dependent linear response of the density. Currently this is the most important method available to study

the electrical response of matter in the absence of magnetic fields^{52,55}. It is especially relevant in our case, because the time-dependent density-density response function

$$\chi(\mathbf{r}, \mathbf{r}', t - t') = \left. \frac{\delta n(\mathbf{r}, t)}{\delta v_{\text{ext}}(\mathbf{r}', t')} \right|_{n_0} \quad (3.22)$$

can provide the transition energies and oscillator strengths for excitations of the interacting system^{7,11,61,93}. This is most clearly seen from the exact eigenstate representation of its Fourier-transform to frequency-space,

$$\chi(\mathbf{r}, \mathbf{r}', \omega) = \frac{1}{\hbar} \sum_{n>0} \left(\frac{\rho_{0n}(\mathbf{r}) \rho_{0n}^*(\mathbf{r}')}{\omega - \omega_{0n} + i\eta} - \frac{\rho_{0n}^*(\mathbf{r}) \rho_{0n}(\mathbf{r}')}{\omega + \omega_{0n} + i\eta} \right), \quad (3.23)$$

with the transition frequencies $\omega_{0n} = (E_n - E_0)/\hbar$ and the transition densities

$$\rho_{0n}(\mathbf{r}) = N \int \dots \int \psi_0(\mathbf{r}, \mathbf{r}'_2, \dots, \mathbf{r}'_N) \psi_n^*(\mathbf{r}, \mathbf{r}'_2, \dots, \mathbf{r}'_N) d^3 r'_2 \dots d^3 r'_N. \quad (3.24)$$

Hence the poles of (3.23) immediately provide the exact excitation energies. The corresponding oscillator strengths can be obtained from the residues of χ ⁷.

Now, similar to the case of static linear response (cf. section 3.2.3) the inverse response functions can be related by taking the functional derivative of equation (3.19). This leads to

$$\chi_s^{-1}(\mathbf{r}, \mathbf{r}', \omega) = \chi^{-1}(\mathbf{r}, \mathbf{r}', \omega) + \frac{e^2}{|\mathbf{r} - \mathbf{r}'|} + f_{\text{xc}}(\mathbf{r}, \mathbf{r}', \omega). \quad (3.25)$$

Here the frequency-dependent xc kernel $f_{\text{xc}}(\mathbf{r}, \mathbf{r}', \omega)$ is the Fourier-transform of the functional derivative of v_{xc} ,

$$f_{\text{xc}}(\mathbf{r}, \mathbf{r}', t - t') = \left. \frac{\delta v_{\text{xc}}(\mathbf{r}, t)}{\delta n(\mathbf{r}', t')} \right|_{n_0}, \quad (3.26)$$

which is a retarded function of time. This is a consequence of the memory effects in v_{xc} . The exact constraints on v_{xc} carry over to the xc kernel in the linear response regime. They lead to sum rules that have to be satisfied by the exact response functions and by the xc kernel⁸¹.

Thus TDDFT opens a route for the calculation of a system's spectral properties based on f_{xc} . Practical applications usually rely on a matrix formulation¹¹ (also called Casida formalism), where the exact excitation energies ω_{0q} follow from the eigenvalues $\lambda_q = \omega_{0q}^2$ of the matrix

$$\Omega_{qq'} = \delta_{qq'} \omega_{s,q}^2 + 4 \sqrt{\omega_{s,q} \omega_{s,q'}} F_{qq'}, \quad (3.27)$$

with $q = (i, j)$ denoting the occupied-unoccupied KS transition $i \rightarrow j$ so that $\omega_{s,q} = (\varepsilon_j - \varepsilon_i)/\hbar$. The coupling term is given by

$$F_{qq'} = \int \int \varphi_i^*(\mathbf{r}) \varphi_j(\mathbf{r}) f_{\text{hxc}}(\mathbf{r}, \mathbf{r}', \omega) \varphi_{i'}(\mathbf{r}') \varphi_{j'}^*(\mathbf{r}') d^3 r d^3 r', \quad (3.28)$$

where the φ_i are the KS eigenstates and $f_{\text{hxc}}(\mathbf{r}, \mathbf{r}', \omega) = f_{\text{xc}}(\mathbf{r}, \mathbf{r}', \omega) + e^2/|\mathbf{r} - \mathbf{r}'|$. The oscillator strengths of the exact transitions are obtained from the eigenvectors of $\Omega_{qq'}$ ¹¹.

This shows us that the effects of exchange and correlation correct the bare KS excitation energies to provide the exact ones. These corrections do not just consist of quantitative shifts: Due to the frequency-dependence of f_{xc} the eigenvalue problem for $\Omega_{qq'}$ constructed out of N KS transitions can generate more than N eigenvalues. This is achieved by ‘‘mixing’’ of KS transitions to obtain additional excitations⁵⁰.

It is also possible to obtain the excited states data without using f_{xc} : The TDKSE (3.17) can be solved in real-time based on $v_{\text{xc}}(\mathbf{r}, t)$ for an applied time-dependent perturbation of, e. g., dipole type. As the solution of the TDKSE provides the time-dependent density, the dipole moment

$$\mathbf{d}(t) = \int \mathbf{r}(n(\mathbf{r}, t) - n_0(\mathbf{r}))d^3r \quad (3.29)$$

can be easily obtained. From its Fourier transform one can obtain the dynamic dipole polarizability $\alpha_{ij}(\omega)$ which is related to χ by

$$\alpha_{ij}(\omega) = \int x_i \chi(\mathbf{r}, \mathbf{r}', \omega) x_j d^3r d^3r'. \quad (3.30)$$

In this way the poles and residues of dipole-active transitions can be recovered by studying the dipole spectra^{9,51,67,92}. Quadrupole-active transitions⁵⁴ analogously require the use of an external quadrupole perturbation (*Pub3*).

There are thus two complementary ways to obtain excited state properties within TDDFT, one based on f_{xc} and one on v_{xc} . More details on the two approaches can be found in *Pub3* and *Pub4*. Especially the Casida approach is extensively used for the study of atomic and molecular excitations⁵².

3.3.4 The adiabatic approximation

When one is faced with the task to find an approximate functional for v_{xc} , a common first step is to get rid of its inherent history dependence. This means that the xc potential will no longer depend on the density at previous times but only on the instantaneous density. However, as we have seen before, the time-dependent v_{xc} can only be uniquely defined by the complete history of the density from the initial ground state to the time at which the xc potential is evaluated (cf. figure 3.3 left).

So, how can this prehistory be neglected while retaining a well-defined mapping between density and xc potential? The only known way to establish a unique correspondence between density and v_{xc} as mere functions of space is provided by the Hohenberg-Kohn theorem³³ of ground state DFT, which has been introduced earlier. Consequently, to neglect memory, we have to treat the density at any instant in time as a ground state density, which then uniquely defines a corresponding $v_{\text{xc},0}$. This is the essence of the

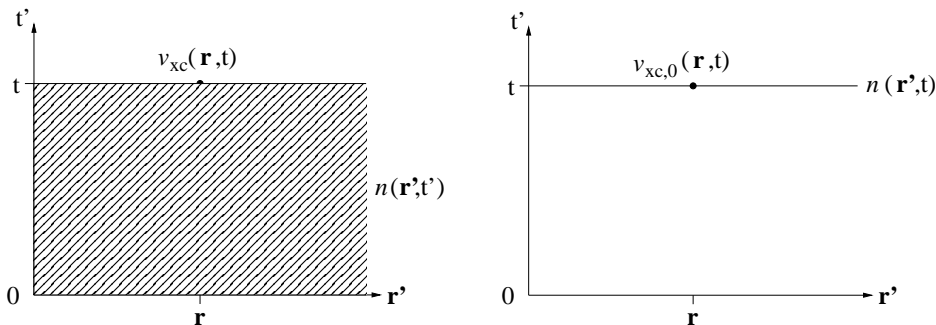


Figure 3.3: Schematic representation of the exact (left) and the AE (right) density-dependence of the xc potential.

adiabatically exact (AE) approximation (*Pub1*), which is adiabatic in time but treats the spatial nonlocality exactly⁵². It is a central concept of TDDFT and of this thesis. More formally it implies that $v_{xc}[n(\mathbf{r}', t')](\mathbf{r}, t)$ with $t' \leq t$ is approximated by $v_{xc,0}[n(\mathbf{r}', t)](\mathbf{r}, t)$ as shown in figure 3.3.

The adiabatic approximation directly carries over to the xc kernel f_{xc} , which is also replaced by its static counterpart $f_{xc,0}$ introduced in the context of static linear response. As a consequence the xc kernel loses its frequency-dependence. The effect of the adiabatic approximation is particularly clear in this linear response context: The matrix formulation (3.27) turns into an ordinary eigenvalue problem, which can only produce the same number of excitations as the underlying KS system. Thus the neglect of memory effects leads to excitations that are not accounted for. From this we see that memory effects manifest formally in the matrix equations for the exact excitation energies. Thus any discussion of memory effects in TDDFT is inevitably connected to the linear response theory.

We note here for completeness that the AE approximation satisfies exact constraints such as the zero-force theorem and the HPT.

By means of the adiabatic approximation we have transferred the question for the xc functional back to DFT. However as we have seen before the exact $v_{xc,0}$ and $f_{xc,0}$ are also unknown. This means that within adiabatic TDDFT one has to resort to approximate ground state functionals, which can then be used as adiabatic approximation. Again the most extreme case is provided by the adiabatic local density approximation, which is local both in space and time. It is important to note that spatial and temporal nonlocality are intimately related, e. g., it is not possible to construct an approximation that is local in space but nonlocal in time²⁹ without violating important constraints on the exact v_{xc} ^{20,81}.

The combination of spatial and temporal approximations does in many cases complicate the analysis of TDDFT performance. For instance it has been claimed that using an adiabatic approximation of the xc kernel in linear density response theory one will miss doubly excited states. However, it is difficult even to pin down what is meant by

a double excitation in TDDFT. After all the KS system is constructed to reproduce the correct density and not the wave function. Only if the wave function is represented by some set of orbitals does it make sense to talk about single and multiple excitations. Practically it is of course possible to construct product wave functions out of the KS orbitals. To tell whether an exact transition is of double excitation character one would need to project the KS product states on the fully correlated excited state wave function. But the latter is in general not available.

Even if we would somehow know that a specific excitation is of double excitation character, it is very difficult to tell how the matrix eigenvalue problem (3.27) does generate it. This is especially questionable if not the adiabatically exact xc kernel is used but only a spatial approximation of $f_{xc,0}$. It is one of the goals of this thesis to shed some light on the relation between the concept of double excitation and the role of memory in linear density response theory.

Finally we come to the TDDFT performance in the strong field regime. Here TDDFT has been successfully applied to the study of clusters^{10,12,65} and high harmonic generation. However it has been found that the common functionals for v_{xc} that are adiabatic in time and approximate in space fail to reproduce the crucial features of the double ionization process like the knee structure^{38,62}. As no explicit density functionals exist for the ionization yields (cf. section 3.1) they have to be approximated within TDDFT⁹¹. So there are two possible sources for TDDFT's failure: the approximation of v_{xc} and that of the ionization yields. However it has been shown³⁸ that the qualitative error (the missing knee) is due to the approximation of v_{xc} whereas the ionization yields introduce a quantitative error. In the following we will only be concerned with the more fundamental problem of obtaining the correct density evolution for a strong field process. This means that we will focus on the approximation of v_{xc} .

It has been commonly believed, that due to the highly nonlinear dynamics in the applied field the wave function builds up a complicated phase dependence. As this phase information should somehow be reflected in the memory effects of v_{xc} it has been assumed, that the strong field failure is mainly due to the adiabatic approximation that is memory-free. On the other hand some recent results indicated that spatially nonlocal effects in v_{xc} can account for much of the strong-field behavior^{42,90}.

So in the strong field regime there is also some need to clarify the role of memory effects. Here it is rather more difficult to pin down the underlying mechanisms as a formal manifestation of memory like in the linear response regime is absent. Thus both regimes have to be considered together to make some progress in memory-related questions.

It is the purpose of this thesis to clarify the role of memory effects in the linear response regime and for strong-field excitations in the nonlinear regime. To achieve this the spatial approximation of v_{xc} and f_{xc} has to be separated from the adiabatic one, i. e., we really need to obtain the AE approximation which is exact in space. Although this approximation is generally unknown, it can be constructed in certain cases as we will see in chapter 4.

3.4 Quantum fluid dynamics

For the understanding of memory effects in TDDFT it is instructive to exploit another closely related reformulation of the quantum many-body problem. This approach which is called quantum fluid dynamics (QFD) is almost as old as wave-function quantum mechanics itself. It was introduced in 1926 by Madelung⁴⁶ for the one-electron problem described by the wave function $\varphi(\mathbf{r}, t)$. The equations are obtained by inserting $\varphi(\mathbf{r}, t) = R(\mathbf{r}, t)e^{i\alpha(\mathbf{r}, t)}$ with R and α real into

$$i\hbar\partial_t\varphi(\mathbf{r}, t) = \left(-\frac{\hbar^2}{2m}\nabla^2 + v_{\text{ext}}(\mathbf{r}, t)\right)\varphi(\mathbf{r}, t). \quad (3.31)$$

Now, real and imaginary part of the equation can be separated. Introducing the electronic density n according to $R^2 = |\varphi|^2 = n$ and defining the velocity field $\mathbf{u} = \frac{\hbar}{m}\nabla\alpha$ one arrives at

$$(\partial_t + \mathbf{u} \cdot \nabla)n = -n\nabla \cdot \mathbf{u} \quad (3.32)$$

and

$$m(\partial_t + \mathbf{u} \cdot \nabla)u_j = -\frac{1}{n}\partial_i P_{ij}^1 - \partial_j v_{\text{ext}}, \quad (3.33)$$

where we use index notation and the Einstein sum convention. Here,

$$P_{ij}^1 = \frac{\hbar^2}{4m} \left(\frac{(\partial_i n)(\partial_j n)}{n} - \delta_{ij}\nabla^2 n \right) \quad (3.34)$$

is the single particle quantum stress tensor^{17,25,72}. These equations show strong analogies to the continuity and momentum equations of classical fluid dynamics^{19,25,34}.

It is also possible to obtain QFD equations for a system of N interacting particles⁷²⁻⁷⁴. These equations follow from the Heisenberg equations of motion for the density and the current,

$$\partial_t n(\mathbf{r}, t) = \frac{i}{\hbar}\langle [H, \hat{n}(\mathbf{r}, t)] \rangle, \quad (3.35)$$

$$\partial_t \mathbf{j}(\mathbf{r}, t) = \frac{i}{\hbar}\langle [H, \hat{\mathbf{j}}(\mathbf{r}, t)] \rangle, \quad (3.36)$$

where \hat{n} and $\hat{\mathbf{j}}$ are the operators defined in equations (3.3) and (3.4). Introducing the velocity $\mathbf{u} = \mathbf{j}/n$ one arrives at

$$(\partial_t + \mathbf{u} \cdot \nabla)n = -n\nabla \cdot \mathbf{v}, \quad (3.37)$$

$$m(\partial_t + \mathbf{u} \cdot \nabla)u_j = -\frac{1}{n}\partial_i P_{ij} - \partial_j(v_{\text{ext}} + v_{\text{h}}). \quad (3.38)$$

Now the quantum stress tensor P_{ij} is a complicated function of two-point quantities like the pair-correlation function that can be derived from the N -particle wave function⁷²⁻⁷⁴. This dependency seems to imply that not much has been gained by the reformulation.

One needs additional equations for the two-point quantities, which would lead us to the famous Bogoliubov-Born-Green-Kirkwood-Yvon hierarchy of equations which is ubiquitous in many-particle physics and appears here in a hydrodynamic version¹⁹.

On the other hand we can now evoke the RG theorem, which tells us that the wavefunction and hence P_{ij} are unique functionals of the density. From the continuum mechanics point of view we are thus dealing with an electron fluid, and its material properties are defined by an unknown but well-defined constitutive relation $P_{ij}[n]$. This means that the system of equations (3.37), (3.38) can be formally closed. In the same spirit it is possible to derive fluid equations for a system of noninteracting KS particles.

It might seem a bit odd that few-particle problems are cast into a hydrodynamic form. After all we know that a classical fluid description can only be obtained for the continuum limit of an enormous amount of particles. However in quantum mechanics we already start from a continuum or field description in terms of the wave function. Thus the transition to QFD is an exact reformulation and does not depend on continuum assumptions^{16,19}.

The QFD approach represents an alternative approach to Kohn-Sham TDDFT: The density is the basic variable and the mathematical rigor of the method relies also on the RG theorem. But instead of mapping the many-particle problem on the noninteracting KS system, we resort to a fluid description introducing the velocity as a secondary variable. To get a practical scheme one needs to approximate P_{ij} ¹⁹.

It is interesting to note that in the QFD picture the quantum mechanical eigenstates correspond to stationary configurations ($\partial_t n = \partial_t \mathbf{u} = 0$) which are either static ($\mathbf{u} = 0$) or dynamic ($\mathbf{u} \neq 0$)^{25,74}. The ground state is stable with respect to small perturbations while the excited states are unstable²⁵.

Recent applications of the QFD approach range from transport and turbulence in nanostructures^{8,16,17,19} to the description of the atomic shell structure in terms of viscoelastic stress balances⁷⁰.

For our purposes it is not required to turn the QFD formulation into a practical scheme for computations. It will rather serve as a conceptual framework to gain a better understanding of memory effects in TDDFT.

4 The two-electron singlet system

*Time flies like an arrow;
fruit flies like a banana.*

Groucho Marx

When we want to investigate the role of memory effects in the TDDFT description of correlated electron dynamics, we need to study a system that is both physically relevant for the questions we ask and numerically tractable. With respect to the first requirement we may conclude from chapter 2 that a two-electron system like helium does already show the important features of correlated electron dynamics both in the linear and nonlinear regime.

The numerical considerations are more involved: First of all we need a benchmark system, which defines the exact solution. Of course the ultimate benchmark are experimental measurements which could be compared to the TDDFT results. But the experiment does neither provide the sophisticated control of the system, nor does it yield all the quantities that we need for our comparison with TDDFT calculations. To gain detailed insight into the mechanisms of TDDFT we need a benchmark system which provides an exact controllable reference on all levels: the time-dependent density, excited states properties, ionization yields etc. We basically need the exact correlated wave function itself!

However, as mentioned before, the TDSE solution for a typical strong field process for helium is not available. As the electron number cannot be reduced any further the only option is thus to reduce the dimensionality of the problem. Fortunately it is already well established that also the one-dimensional (1D) helium (singlet) atom captures most of the crucial correlated electron physics^{3,30,38,39,41,44}. In fact it has been the workhorse of the theoretical investigation of the helium double ionization effect. For the interaction with a strong linearly polarized laser field the major electron dynamics happens along the polarization axis so that a one-dimensional approach can account for most aspects. Also for the exploration of highly excited states the 1D system provides a relevant model system^{31,57,64}.

The 1D helium atom belongs to a broader class of one-dimensional two-electron singlet systems. These systems are the “fruit flies” of correlated electron dynamics in the context of atomic physics. They are used to study phenomena such as strong field ionization, resonant states³⁰ and quantum chaos^{64,85}. At the same time they possess the attractive intuitive relation to what we remember from our quantum mechanic courses: one electron in one dimension, which can be solved analytically. Now we just add a

second one and although most formulas still look familiar we are already confronted with many new physical phenomena. The theoretical and numerical properties of one-dimensional two-electron singlet systems will be discussed in the following. Several new concepts developed in the course of this thesis will also be introduced on the way.

Here and in the following we will mostly use Hartree atomic units denoted by “a.u.”. This means that energies are given in Hartrees and distances in Bohr.

4.1 Theoretical description

The 1D two-electron singlet system possesses several advantageous features that are manifest in all three approaches to the quantum many-body problem presented in the previous chapter. These aspects will be briefly outlined here.

In wave function quantum mechanics the two-electron singlet is treated by splitting off the antisymmetric spin part from the wave function. As we are not interested in interactions that couple to the spin we can neglect this part. This means that we are dealing with a symmetric spatial two-particle wave function, i. e., with fully correlated eigenstates $\psi_i(z_1, z_2)$ and time-dependent wave functions $\psi(z_1, z_2, t)$. The Coulomb singularity requires special attention in 1D as it prevents the electrons from bypassing each other or the nucleus (when dealing with an atomic system). The common approach here is to replace the Coulomb potential by the soft-core interaction $W(z) = e^2/\sqrt{z^2 + 1}$ for the electron-electron interaction V_{ee} and also for the external potential of the helium atom (see below). This replacement was found to preserve the correlation features crucial for strong and weak field interaction^{3,30,31,38,39,41,44,57,64}.

Most of our studies are based on two representatives of the 1D two-electron singlet systems family. One is of course the 1D helium atom, where $v_{\text{ext},0}(z) = -2W(z)$, which is especially relevant for the strong-field double ionization process. However for some studies it is favorable to have a system that is completely confined and thus has an exclusively discrete spectrum. This requirement is met by the second system called anharmonic Hooke’s atom which is characterized by $v_{\text{ext},0}(z) = (k/2)(z^2 + \tilde{k}z^6)$ with $k = 0.1$ a.u. and $\tilde{k} = 0.01$ a.u. (see *Pub2*). It is derived from the Hooke’s atom^{32,56} by adding a small term $\sim z^6$ to the otherwise quadratic potential. The anharmonic term is introduced to avoid any special harmonic-oscillator properties like motion according to the HPT in the presence of external dipole fields (cf. section 3.3.2). Ground state potentials and densities of both systems are shown in figure 4.1.

It turns out that 1D two-electron singlet systems are especially suited to study properties of (TD)DFT: From the two-particle singlet character it follows that, within KS theory, we only have two identical spatial orbitals φ with $|\varphi|^2 = n/2$. This means that effectively the problem can be formulated just in terms of the density, i. e., we are particularly close to the essence of DFT. This is especially important for the TDKS system, which is completely determined by $\varphi(z, t) = \sqrt{n(z, t)/2}e^{i\alpha(z, t)}$. Here, the phase $\alpha(z, t)$

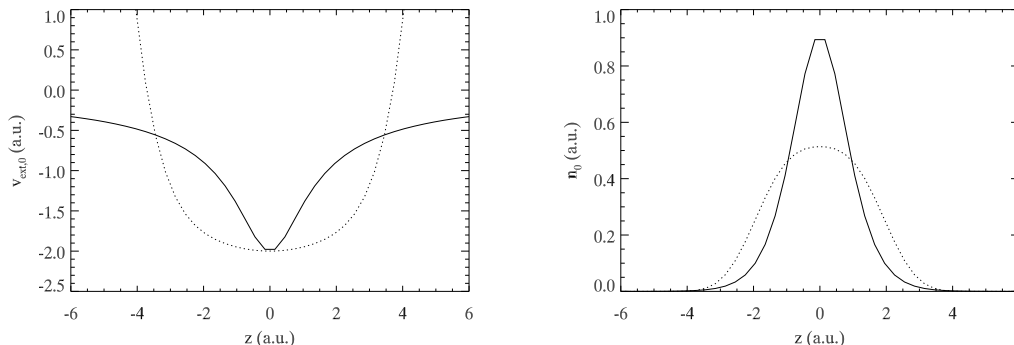


Figure 4.1: Ground state potentials (left) and densities (right) of the 1D helium atom (solid) and anharmonic Hooke's atom (dotted).

is related to the KS current $j_s(z, t)$ by

$$j_s(z, t)/n(z, t) = \frac{\hbar}{m} \partial_z \alpha(z, t). \quad (4.1)$$

As a consequence of the reduced dimensionality, density and KS current are directly connected by the 1D continuity equation,

$$\partial_t n(z, t) = -\partial_z j_s(z, t), \quad (4.2)$$

and the phase $\alpha(z, t)$ is completely determined by the density. Thus for the whole TDKS system we have an explicit formulation just in terms of the density. As the TDKS density does by definition agree with the exact one, also the exact and the KS currents are identical in 1D by virtue of equation (4.2)^{42,48,89}. This connection is crucial for the calculation of TDKS quantities from the TDSE solution as discussed in the next section.

A further important feature of the 1D two-electron singlet system is the simplicity of the exchange potential: As only two identical orbitals are present v_x just cancels the unphysical self-interaction of this orbital, which means that $v_x = -(1/2)v_h$. Consequently the only unknown is the correlation potential. If the latter is neglected the KS system becomes identical to the Hartree-Fock case. This allows for easy comparison with the uncorrelated Hartree-Fock approach. More importantly this means that for the two-electron singlet system memory is an exclusive feature of the correlation potential or kernel.

Finally the two-electron singlet character is also manifest in the QFD formulation of the noninteracting particle problem (cf. *Pub2*). Due to the two identical orbitals the transformation of the TDKS systems into hydrodynamic equations works similar to the

Madelung derivation for a single particle. This means that we end up with the equations

$$(\partial_t + u\partial_z)n = -n\partial_z u \quad (4.3)$$

and

$$m(\partial_t + u\partial_z)u = -\frac{1}{n}\partial_z p - \partial_z(v_{\text{hx}} + v_{\text{ext}}), \quad (4.4)$$

where $v_{\text{hx}}(z, t) = v_{\text{h}}(z, t) + v_{\text{x}}(z, t)$ and $u(z, t) = (\hbar/m)\partial_z\alpha(z, t)$ is the KS velocity. $u(z, t)$ is identical to the exact velocity in 1D. Instead of the stress tensor we now have a generalized scalar pressure

$$p = p_{\text{s},0} + p_{\text{c}} \quad (4.5)$$

with the explicitly density-dependent noninteracting pressure⁷⁰

$$p_{\text{s},0} = \frac{\hbar^2}{4m} \left(\frac{(\partial_z n)^2}{n} - \partial_z^2 n \right), \quad (4.6)$$

and the unknown correlation pressure defined by the constitutive relation $p_{\text{c}}[n]$. The latter can be split up into an adiabatic part $p_{\text{c},0}$ and a nonadiabatic part $p_{\text{c},\text{mem}}$ which incorporates the memory effects. We find that the density-dependence of $p_{\text{c},\text{mem}}$ can be rewritten as a dependence on gradients of the velocity. As we will see in section 5.2 this result is crucial for the interpretation of memory effects in the QFD picture (*Pub2*).

4.2 Numerical aspects

In order to study memory in v_{xc} we need both the adiabatically exact TDKS results and an exact benchmark solution for comparison. The latter is readily available for the 1D two-electron singlet system, where the TDSE can be solved on a desktop computer even for strong field processes. From the time-dependent wave function one can also obtain the exact density and current. As explained above those quantities agree with their TDKS counterparts, which in turn are all that is needed to define the exact TDKS orbital φ . Based on φ one can obtain also the exact v_{s} by inversion of the TDKSE. This approach is used to construct a numerical representation of the exact v_{xc} according to equation (3.19)^{42,89}.

To obtain the adiabatically exact xc potential for a given density $n(z, t)$ we need to construct $v_{\text{xc},0}$ (see section 3.3.4). Its numerical representation follows from the other ground state potentials according to equation (3.11). The Hartree-exchange contribution can be computed directly and $v_{\text{s},0}$ can be obtained by an inversion of the KSE that is especially simple for the two-electron singlet^{42,89}. But what about $v_{\text{ext},0}$? This is the local external potential which yields the given density as the ground state solution of the interacting SE. However there is no explicit expression that determines $v_{\text{ext},0}$ in terms of the density.

It has been shown in *Pub1* that the inversion of the SE can indeed be performed with an iterative scheme. Thus we are really in a position to compare v_{xc} and $v_{\text{xc},0}$ for an

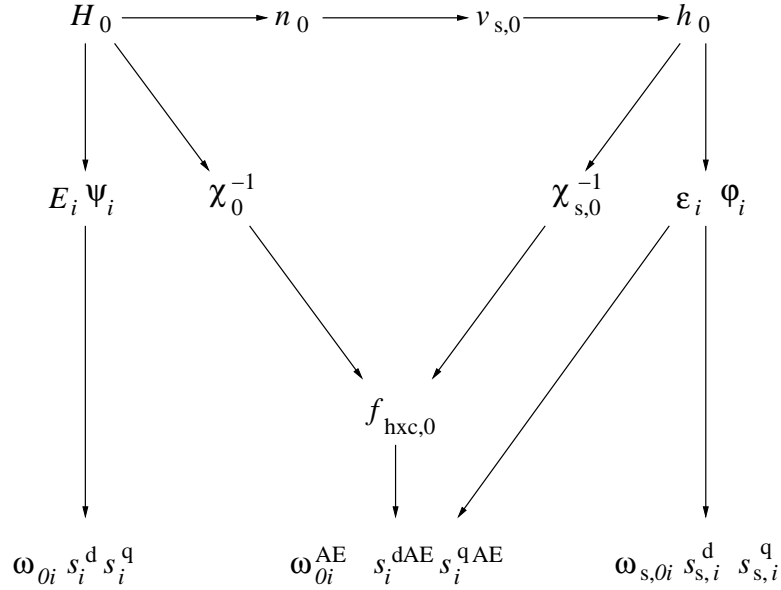


Figure 4.3: Schematic visualization of different routes to obtain transition energies and oscillator strengths within linear density response theory (see text).

where the \mathbf{x}^i are the eigenvectors of the AE Casida matrix. Transitions to an excited state of even symmetry can be analyzed analogously. In spite of the 1D character of the system we stick to the usual notation and denote these excitations as quadrupole (q) transitions.

These quantities can then be compared to the bare single particle KS results $\omega_{s,0i} = (\varepsilon_i - \varepsilon_0)/\hbar$ etc. and to the exact quantities, which are readily available as the lower eigenstates (including wave functions) of both the SE and the KSE can be computed. The possible comparisons are summarized in figure 4.3.

As mentioned in section 3.3.3 there is also an alternative way based on real-time propagation to compute the linear density response. This approach is also available in our case as it just requires to apply the TDSE and AE-TDKSE schemes of figure 4.2 to the case of a weak external perturbation. The resulting exact or AE density can then be used to compute, e.g., the corresponding time-dependent dipole moments. Their spectra in frequency space then show peaks at the transition frequencies of dipole active excitations (cf. *Pub3*).

5 The role of memory effects

Memories are made of this.

Dean Martin et al.

With the 1D two-electron singlet system, for which almost all wave function and TDDFT properties can be computed we now have everything in place to investigate the influence of memory effects in various regimes. In the following I pick some exemplary results out of those contained in *Pub1-Pub4*. Finally I will try to link these results in a short summary.

5.1 Validity of the adiabatic approximation for typical strong-field applications

At first we consider the regime of typical strong field interactions, i. e., the 1D helium atom is exposed to laser pulses of 780 nm wavelength at intensities in the range of 10^{14} W/cm². These parameters are in the established regime for the 1D investigation of double ionization phenomena^{38,42}. For this system we perform both exact TDSE and AE-TDKSE calculations (cf. figure 4.2).

We record the evolution of the total ionization $N_b(0) - N_b(t)$, where

$$N_b(t) = \int_{-a}^a n(z, t) dz, \quad (5.1)$$

with $|z| \leq a = 5$ Bohr. This observable is a measure of the average number of electrons that have escaped from the bound region close to the nucleus. It is essential for interpreting the double ionization process as the corresponding yields depend crucially on it^{62,90,91}. This observable has the additional benefit of being an explicit functional of the density, i. e., no further approximations enter through the specific observable. We study $N_b(t)$ both for the exact and the AE density (cf. figure 4.2). As shown in figure 5.1 the results agree perfectly.

These results together with further studies at different frequencies and intensities show that in the usual regime of atom strong-field interaction memory effects in v_{xc} are negligible. This is an important guidepost for future functional development: To overcome previous deficiencies of TDDFT in this regime it is not necessary to deal with the memory effects in v_{xc} . Instead it is of predominant importance to correctly take into account the spatial nonlocality. First steps in this direction have already been taken^{42,90}.

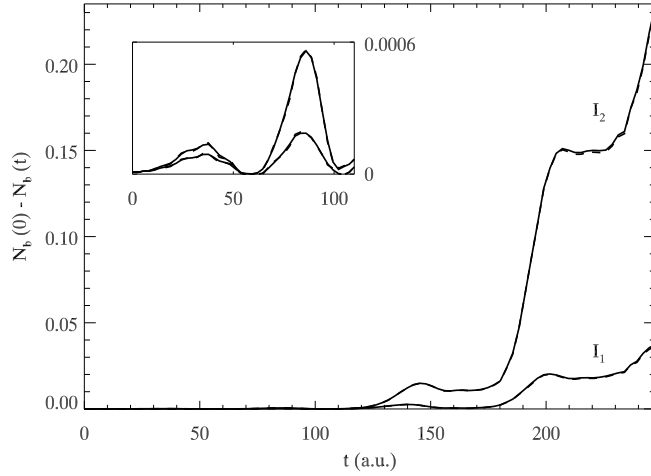


Figure 5.1: Total ionization during the interaction of the two-electron atom with a laser pulse of maximum intensity $I_1 = 4 \cdot 10^{14}$ W/cm² (lower two curves) and $I_2 = 7 \cdot 10^{14}$ W/cm² (upper two curves). Solid curves: exact TDSE calculation; dashed curves: AE-TDKSE scheme. The curves are virtually indistinguishable. The inset magnifies the evolution at early times (from *Pub1*).

5.2 Hydrodynamic interpretation of memory effects

It is good news that the adiabatically exact approximation holds well in the typical strong field scenario. However, there are of course other situations when memory can be found to play a significant role and the AE approximation breaks down. To obtain a better understanding of the conditions for the breakdown of the adiabatically exact approximations we investigate the QFD formulation of the 1D two-electron singlet system (cf. section 4.1).

In the QFD formulation the velocity u is an important dynamical quantity. This is why we have tracked both the density and the velocity for two different processes: One where the AE approximation holds and one where it is found to break down. Here the validity of the AE approximation for a specific process has been determined by comparing the TDSE and AE-TDKSE solutions. Typical situations during the studied two processes are shown in figure 5.2 for the TDSE solution of the anharmonic Hooke's atom. As we see the behavior of the density is qualitatively not very different. The velocity field however is almost flat for the adiabatic process while it develops strong gradients in the nonadiabatic one.

This behavior can be understood in the context of the QFD equations (4.3) and (4.4) of the 1D two-electron singlet system: In the adiabatic approximation we have $p_c = p_{c,0}$, i. e., the correlation pressure depends only on the instantaneous density. As a consequence equation (4.4) resembles the Euler equation of classical fluid dynamics.

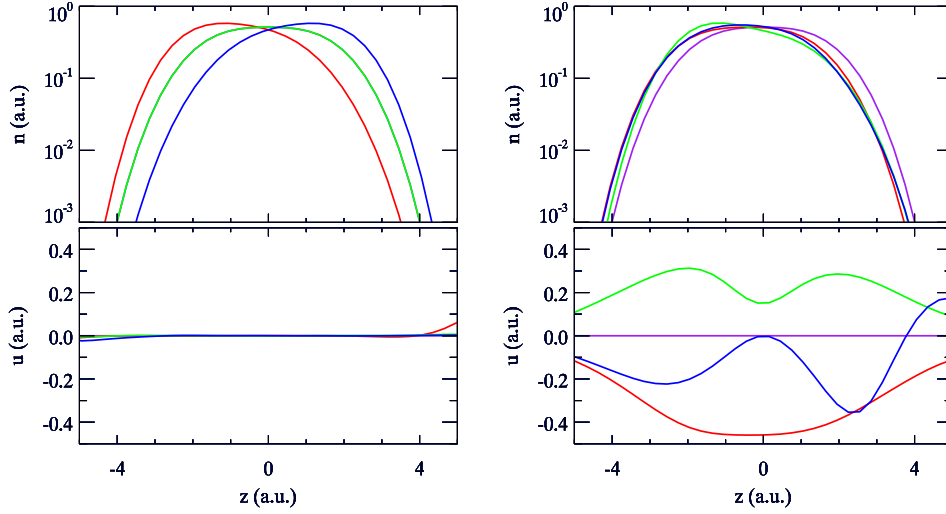


Figure 5.2: Snapshots of typical densities and velocities during an adiabatic (left) and a nonadiabatic (right) process for the anharmonic Hooke's atom (adapted from *Pub2*).

This means that the electron fluid flows without internal friction. On the other hand the exact QFD equations include a further correlation contribution $p_{c,\text{mem}}$, which depends on the gradient of the velocity field. Thus the exact momentum equation is closer to the Navier-Stokes equation of viscous flow. Now, whenever velocity gradients build up due to the nonlinear term $u\partial_z u$, the $p_{c,\text{mem}}$ term has to balance them through dissipative effects. As a consequence AE calculations, which fail to reproduce this damping effect, yield wrong results when velocity gradients appear.

Strong gradients of the velocity correspond to rapid and strong deformations of the electronic density. This means that the dynamics are far from the translational character of motion according to the HPT (see section 3.3.2). On the other hand in the limit of HPT motion the density is rigidly transported and the velocity gradients vanish. It thus makes sense that the AE approximation holds when the velocity profiles are flat.

Based on these findings we can formulate a criterion which provides an approximate upper bound for an ongoing process to be still within the adiabatic regime. In this way we have a warning signal whenever the applicability of the AE approximation is no longer justified (*Pub2*).

5.3 Memory effects and double excitations

After investigating strong field processes we now turn to the linear response regime. Here we consider the time-dependent density response to small perturbations of the external potential. The perturbed exact and AE densities are once again obtained with

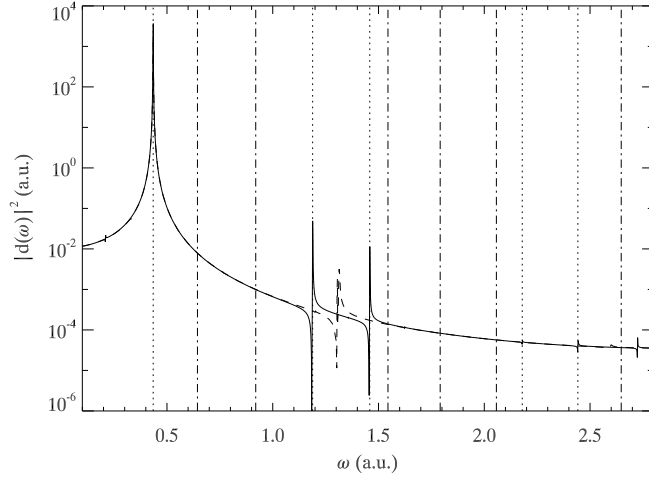


Figure 5.3: Dipole power spectrum for anharmonic Hooke's atom obtained from TDSE (solid line) and AE-TDKSE (dashed line). Vertical lines indicate transition energies of the ground state to singlet states of odd (dotted) and even parity (dotted-dashed) obtained from the exact eigenstates of the SE. The 2nd and 3rd dipole transitions possess significant double excitation character (from *Pub3*).

the help of the TDSE solution and the AE-TDKSE scheme. From the densities we derive the spectral information as detailed in sections 3.3.3 and 4.2. As an example we show the dipole power spectrum of the anharmonic Hooke's atom in figure 5.3.

We find that instead of the correct second and third dipole transition in the regime $\omega = 1 - 1.5$ a.u., the AE-TDKSE scheme only reproduces one peak at about 1.3 a.u. In this situation memory effects do clearly lead to transitions missing from the AE spectrum as discussed in the context of the Casida formulation (3.27) on the level of the xc kernel.

If we want to relate this effect to double excitations we need to project the exact correlated excited states $\psi_n(z_1, z_2)$ on product wave functions Φ_{ij} of the KS orbitals, where

$$\Phi_{ij}(z_1, z_2) = \begin{cases} \varphi_i(z_1)\varphi_j(z_2), & i = j \\ \frac{1}{\sqrt{2}} (\varphi_i(z_1)\varphi_j(z_2) + \varphi_j(z_1)\varphi_i(z_2)), & i \neq j \end{cases} \quad (5.2)$$

Doing this we find that the first correctly reproduced dipole transition has only 8% double excitation character whereas to the second and third transition double excitations contribute 56 and 36%.

For the 1D helium atom all excitations up to the energies that can be resolved by the numerical accuracy of the AE-TDKSE scheme are found to be of single excitation type. Thus it might not be surprising that the AE-TDKSE scheme yields excellent results for these excitations (*Pub3*). The autoionizing double excitations in helium cannot be

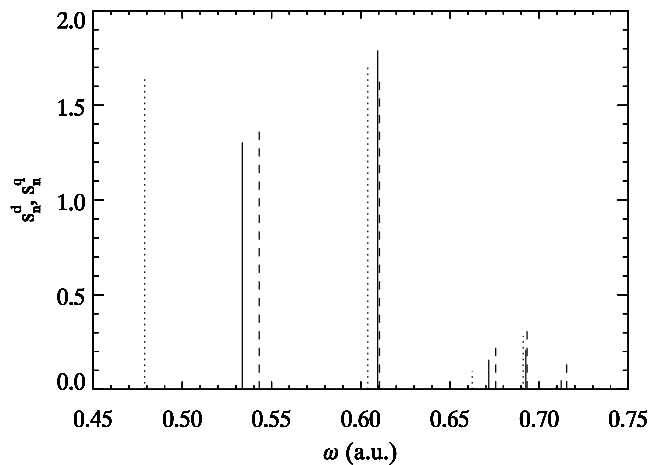


Figure 5.4: Oscillator strengths of transition energies obtained from the bare KS values (dotted), AE-Casida (dashed), and from the exact eigenstates (solid) for helium (adapted from *Pub4*).

resolved by the present techniques.

These findings indicate that there really is a connection between the failure of the AE approximation to reproduce a specific transition and its double excitation character. However it turns out that it is not straightforward to relate qualitative (missing peaks) and quantitative (shifts in energy) errors of the AE results to the magnitude of the double excitation contribution (*Pub3*).

5.4 Adiabatic approximation of the xc kernel

Up to now we have exclusively used the AE-TDKSE scheme based on the static xc potential, which has provided information on the nonlinear and linear regime. However the more common approach to linear response is based on the xc kernel. As mentioned before we can also reconstruct a numerical representation of the static xc kernel $f_{xc,0}$ (cf. section 4.2). $f_{xc,0}$ provides the adiabatically exact approximation of the frequency-dependent kernel.

We use $f_{xc,0}$ to obtain the AE excitation energies and oscillator strengths from the Casida matrix (3.27). The results for the 1D helium atom are shown in figure 5.4. Here we compare the bare KS values, the response results obtained with $f_{xc,0}$ and the exact quantities as indicated in figure 4.3. We can see clearly how the kernel corrects the bare KS values towards the exact ones.

This shows that for the lower single excitations the corrections due to exchange and correlation effects are significant. Remaining discrepancies with respect to the results of *Pub3* are a consequence of the finite basis of KS orbitals used in equation (3.27), which does not properly take into account the continuum part of the spectrum (*Pub4*). Here

the AE-TDKSE approach based on $v_{xc,0}$ performs much better as it does not involve any basis set issues. This agrees with the finding that the kernel and the potential results coincide for a system without continuum such as the anharmonic Hooke's atom (*Publ*₄).

5.5 Summary and outlook

In this thesis we have investigated the role of memory in the TDDFT description of correlated electron dynamics in weak and strong fields. This analysis has revealed that

- memory can be neglected in the strong field regime relevant for many typical applications.
- memory is important for electronic transitions of double excitation character.
- memory is related to dissipative effects within the electron fluid.

Especially the hydrodynamic picture of many-body quantum mechanics has turned out to be extremely helpful for the interpretation of memory effects. It suggests that for an ongoing process memory effects become important as soon as gradients in the electron velocity build up. Although it is difficult to know a priori whether a specific type of external perturbation at a given forcing frequency ω_f and intensity I will bring about such a situation, we can at least say something about certain limits. For $\omega_f \rightarrow 0$ memory effects will of course vanish because we approach a static situation, where the velocity goes to zero. There is also good reason to believe that the adiabatic approximation will hold in the limit of very large ω_f ¹. This seems counterintuitive but when the external field oscillates too fast it will no longer transfer enough momentum to the density distribution to make it move. As a result the velocity will also be zero. On the other hand for a fixed ω_f the density will always get deformed more violently when the intensity of the perturbation grows. Hence velocity gradients should become more important for increasing intensity.

Altogether the picture for a given type of system and external perturbation could look a bit like figure 5.5. In agreement with several recent findings on hydrodynamic approaches to the electron liquid^{13,26,70,75–78,82,83,88} this picture is reminiscent of the behavior of a viscoelastic fluid. If the latter is perturbed very slowly or very fast it behaves elastic or solid-like and there is no internal friction. But in between it will behave like a viscous fluid so that dissipative effects and thus memory become important.

There are various consequences of the obtained results. First of all we can now be confident that recent progress in the modeling of the spatial nonlocality in v_{xc} for strong field processes^{42,90} is on a promising route as memory effects do not contribute here. Hence there is good hope that in the near future TDDFT will be able to properly describe strong field interaction with atoms and molecules. Secondly, the relation between memory and double excitation has been clarified further. Last but not least the QFD

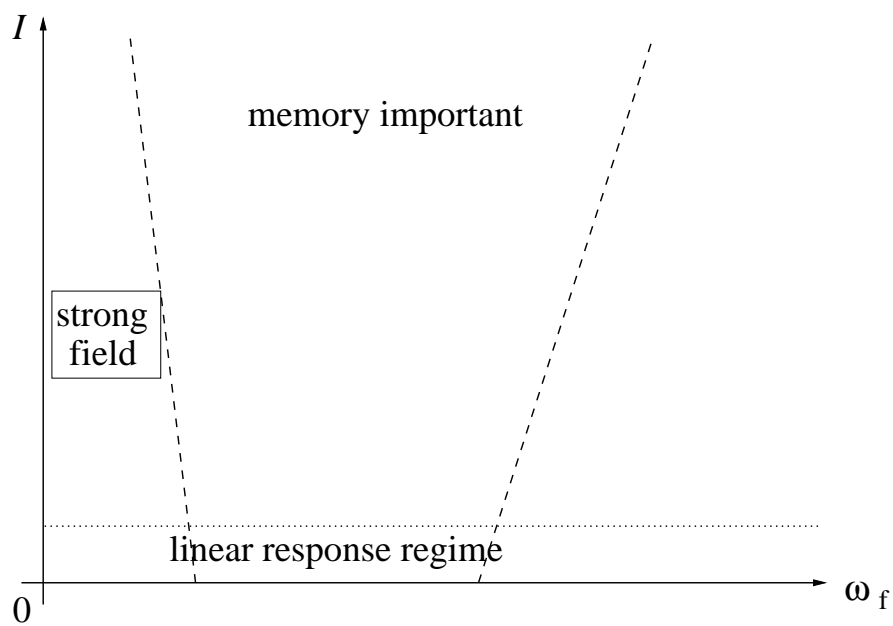


Figure 5.5: Schematic picture of the regime where memory is important (between dashed lines) for a fixed system and perturbation type (e. g., dipole field).

point of view can now provide guidance for the understanding and incorporation of memory effects in TDDFT.

Bibliography

- [1] Baer, R., 2008, [arXiv:0808.3848v1](https://arxiv.org/abs/0808.3848v1) [`cond-mat.other`].
- [2] Batani, D. (ed.), 2001, *Atoms, solids and plasmas in super-intense laser fields* (Kluwer Academic/Plenum Publishers, New York).
- [3] Bauer, D., 1997, Phys. Rev. A **56**(4), 3028.
- [4] Becker, A., and F. H. M. Faisal, 1996, J. Phys. B **29**, L197.
- [5] Becker, A., and F. H. M. Faisal, 1999, Phys. Rev. A **59**(3), R1742.
- [6] Bohm, A., 1986, *Quantum Mechanics: Foundations and Applications* (Springer, New York).
- [7] Broglia, R. A., G. Coló, G. Onida, and H. E. Roman, 2004, *Solid state physics of finite systems* (Springer, Berlin).
- [8] Bushong, N., Y. Pershin, and M. Di Ventra, 2007, Phys. Rev. Lett. **99**, 226802.
- [9] Calvayrac, F., P. G. Reinhard, and E. Suraud, 1997, Ann. Phys. (N.Y.) **255**(1), 125.
- [10] Calvayrac, F., P. G. Reinhard, E. Suraud, and C. A. Ullrich, 2000, Phys. Rep. **337**(6), 493.
- [11] Casida, M. E., 1995, in *Recent advances in density functional methods, part I*, edited by D. P. Chong (World Scientific Publishing, Singapore), pp. 155–192.
- [12] Chu, S.-I., 2005, J. Chem. Phys. **123**(6), 062207.
- [13] Conti, S., and G. Vignale, 1999, Phys. Rev. B **60**(11), 7966.
- [14] Corkum, P. B., 1993, Phys. Rev. Lett. **71**(13), 1994.
- [15] Corkum, P. B., and F. Krausz, 2007, Nature Phys. **3**(6), 381.
- [16] D’Agosta, R., and M. Di Ventra, 2006, J. Phys.: Condens. Matter **18**, 11059.
- [17] D’Agosta, R., and M. Di Ventra, 2008, J. Phys.: Condens. Matter **20**, 374102.
- [18] Delone, N. B., and V. P. Krainov, 1994, *Multiphoton processes in atoms* (Springer-Verlag, Berlin).

- [19] Di Ventra, M., 2008, *Electrical transport in nanoscale systems* (Cambridge University Press, Cambridge).
- [20] Dobson, J. F., 1994, Phys. Rev. Lett. **73**(16), 2244.
- [21] Dundas, D., K. T. Taylor, J. S. Parker, and E. S. Smyth, 1999, J. Phys. B **32**, L231.
- [22] Fano, U., 1961, Phys. Rev. **124**(6), 1866.
- [23] Friedrich, H., 2006, *Theoretical atomic physics* (Springer, Heidelberg).
- [24] Gavrilu, M. (ed.), 1992, *Atoms in intense laser fields* (Academic Press, Inc., San Diego).
- [25] Ghosh, S. K., and B. M. Deb, 1982, Phys. Rep. **92**(1), 1.
- [26] Giuliani, G., and G. Vignale, 2005, *Quantum theory of the electron liquid* (Cambridge University Press, Cambridge).
- [27] Görling, A., 1996, Phys. Rev. A **54**(5), 3912.
- [28] Gross, E. K. U., J. F. Dobson, and M. Petersilka, 1996, in *Density Functional Theory*, edited by R. F. Nalewajski (Springer, Berlin), pp. 81–172.
- [29] Gross, E. K. U., and W. Kohn, 1985, Phys. Rev. Lett. **55**(26), 2850.
- [30] Haan, S. L., and R. Grobe, 1998, Laser Phys. **8**, 885.
- [31] Haan, S. L., R. Grobe, and J. H. Eberly, 1994, Phys. Rev. A **50**(1), 378.
- [32] Hessler, P., N. T. Maitra, and K. Burke, 2002, J. Chem. Phys. **117**(1), 72.
- [33] Hohenberg, P., and W. Kohn, 1964, Phys. Rev. **136**, B864.
- [34] Kan, K.-K., and J. J. Griffin, 1977, Phys. Rev. C **15**(3), 1126.
- [35] Kling, M. F., and M. J. J. Vrakking, 2008, Annu. Rev. Phys. Chem. **59**, 463.
- [36] Kohn, W., and L. J. Sham, 1965, Phys. Rev. **140**, A1133.
- [37] Krausz, F., and M. Ivanov, 2009, Rev. Mod. Phys. **81**(1), 163.
- [38] Lappas, D. G., and R. van Leeuwen, 1998, J. Phys. B **31**, L249.
- [39] Lappas, D. G., A. Sanpera, J. B. Watson, K. Burnett, P. L. Knight, R. Grobe, and J. H. Eberly, 1996, J. Phys. B **29**, L619.
- [40] van Leeuwen, R., 1999, Phys. Rev. Lett. **82**(19), 3863.
- [41] Lein, M., E. K. U. Gross, and V. Engel, 2000, Phys. Rev. Lett. **85**(22), 4707.

-
- [42] Lein, M., and S. Kümmel, 2005, Phys. Rev. Lett. **94**, 143003.
- [43] Lindgren, I., and J. Morrison, 1986, *Atomic many-body theory* (Springer, Berlin).
- [44] Liu, W.-C., J. H. Eberly, S. L. Haan, and R. Grobe, 1999, Phys. Rev. Lett. **83**(3), 520.
- [45] Madden, R. P., and K. Codling, 1963, Phys. Rev. Lett. **10**, 516.
- [46] Madelung, E., 1926, Z. Phys. **40**, 322.
- [47] Madroñero, J., and A. Buchleitner, 2008, Phys. Rev. A **77**(5), 053402.
- [48] Maitra, N., K. Burke, H. Appel, E. Gross, and R. van Leeuwen, 2002, in *Ten topical questions in time-dependent density functional theory*, edited by K. D. Sen (World Scientific, Singapore), pp. 1186–1225.
- [49] Maitra, N. T., K. Burke, and C. Woodward, 2002, Phys. Rev. Lett. **89**(2), 023002.
- [50] Maitra, N. T., F. Zhang, R. J. Cave, and K. Burke, 2004, J. Chem. Phys. **120**(3), 5932.
- [51] Marques, M., A. Castro, G. Bertsch, and A. Rubio, 2003, Comput. Phys. Commun. **151**(1), 60.
- [52] Marques, M., C. Ullrich, F. Nogueira, A. Rubio, K. Burke, and E. Gross (eds.), 2006, *Time-dependent Density Functional Theory* (Springer, Berlin).
- [53] Moshhammer, R., B. Feuerstein, W. Schmitt, A. Dorn, C. D. Schröter, J. Ullrich, H. Rottke, C. Trump, M. Wittmann, G. Korn, K. Hoffmann, and W. Sandner, 2000, Phys. Rev. Lett. **84**(3), 447.
- [54] Mundt, M., and S. Kümmel, 2007, Phys. Rev. B **76**(3), 035413.
- [55] Onida, G., L. Reining, and A. Rubio, 2002, Rev. Mod. Phys. **74**(2), 601.
- [56] Orestes, E., K. Capelle, A. B. F. da Silva, and C. A. Ullrich, 2007, J. Chem. Phys. **127**(12), 124101.
- [57] Panfili, R., and W.-C. Liu, 2003, Phys. Rev. A **67**(4), 043402.
- [58] Parker, J. S., B. J. S. Doherty, K. T. Taylor, K. D. Schultz, C. I. Blaga, and L. F. DiMauro, 2006, Phys. Rev. Lett. **96**(13), 133001.
- [59] Parr, R. G., and W. Yang, 1989, *Density-Functional Theory of Atoms and Molecules* (Oxford University Press, Oxford).
- [60] Perdew, J. P., R. G. Parr, M. Levy, and J. L. Balduz, 1982, Phys. Rev. Lett. **49**(23), 1691.

- [61] Petersilka, M., U. Gossmann, and E. K. U. Gross, 1996, *Phys. Rev. Lett.* **76**(8), 1212.
- [62] Petersilka, M., and E. K. U. Gross, 1999, *Laser Phys.* **9**(1), 105.
- [63] Prauzner-Bechcicki, J. S., K. Sacha, B. Eckhardt, and J. Zakrzewski, 2007, *Phys. Rev. Lett.* **98**(20), 203002.
- [64] Püttner, R., B. Grémaud, D. Delande, M. Domke, M. Martins, A. S. Schlachter, and G. Kaindl, 2001, *Phys. Rev. Lett.* **86**(17), 3747.
- [65] Ruggenthaler, M., S. V. Popruzhenko, and D. Bauer, 2008, *Phys. Rev. A* **78**(3), 033413.
- [66] Runge, E., and E. K. U. Gross, 1984, *Phys. Rev. Lett.* **52**(12), 997.
- [67] Saalman, U., and R. Schmidt, 1996, *Z. Phys. D* **38**, 153.
- [68] Stapelfeldt, H., and T. Seideman, 2003, *Rev. Mod. Phys.* **75**(2), 543.
- [69] Tanner, G., K. Richter, and J.-M. Rost, 2000, *Rev. Mod. Phys.* **72**(2), 497.
- [70] Tao, J., G. Vignale, and I. V. Tokatly, 2008, *Phys. Rev. Lett.* **100**(20), 206405.
- [71] Taylor, K. T., J. S. Parker, K. J. Meharg, and D. Dundas, 2003, *Eur. Phys. J. D* **26**, 67.
- [72] Tokatly, I. V., 2005, *Phys. Rev. B* **71**(16), 165104.
- [73] Tokatly, I. V., 2005, *Phys. Rev. B* **71**(16), 165105.
- [74] Tokatly, I. V., 2006, in *Time-dependent Density Functional Theory*, edited by M. Marques, C. Ullrich, F. Nogueira, A. Rubio, K. Burke, and E. Gross (Springer, Berlin), pp. 123–136.
- [75] Tokatly, I. V., 2007, *Phys. Rev. B* **75**(12), 125105.
- [76] Ullrich, C. A., and K. Burke, 2004, *J. Chem. Phys.* **121**(1), 28.
- [77] Ullrich, C. A., and I. V. Tokatly, 2006, *Phys. Rev. B* **73**, 235102.
- [78] Ullrich, C. A., and G. Vignale, 1998, *Phys. Rev. B* **58**(23), 15756.
- [79] Ullrich, J., and V. P. Schevelko (eds.), 2003, *Many-Particle Dynamics in Atomic and Molecular Fragmentation* (Springer-Verlag, Berlin).
- [80] Vignale, G., 1995, *Phys. Rev. Lett.* **74**(16), 3233.
- [81] Vignale, G., 1995, *Phys. Lett. A* **209**, 206.

- [82] Vignale, G., and W. Kohn, 1996, Phys. Rev. Lett. **77**(10), 2037.
- [83] Vignale, G., C. A. Ullrich, and S. Conti, 1997, Phys. Rev. Lett. **79**(24), 4878.
- [84] Walker, B., B. Sheehy, L. F. DiMauro, P. Agostini, K. J. Schafer, and K. C. Kulander, 1994, Phys. Rev. Lett. **73**(9), 1227.
- [85] Wasserman, A., N. T. Maitra, and E. J. Heller, 2008, Phys. Rev. A **77**(4), 042503.
- [86] Weber, T., H. Giessen, M. Weckenbrock, G. Urbasch, A. Staudte, L. Spielberger, O. Jagutzki, V. Mergel, M. Vollmer, and R. Dörner, 2000, Nature (London) **405**, 658.
- [87] Weber, T., M. Weckenbrock, A. Staudte, L. Spielberger, O. Jagutzki, V. Mergel, F. Afaneh, G. Urbasch, M. Vollmer, H. Giessen, and R. Dörner, 2000, Phys. Rev. Lett. **84**(3), 443.
- [88] Wijewardane, H. O., and C. A. Ullrich, 2005, Phys. Rev. Lett. **95**, 086401.
- [89] de Wijn, A. S., S. Kümmel, and M. Lein, 2007, J. Comput. Phys. **226**, 89.
- [90] de Wijn, A. S., M. Lein, and S. Kümmel, 2008, Europhys. Lett. **84**(4), 43001.
- [91] Wilken, F., and D. Bauer, 2006, Phys. Rev. Lett. **97**, 203001.
- [92] Yabana, K., and G. F. Bertsch, 1996, Phys. Rev. B **54**(7), 4484.
- [93] Zangwill, A., and P. Soven, 1980, Phys. Rev. A **21**(5), 1561.

Acknowledgment

'Listen, Ford,' said Zaphod, 'everything's cool and froody.'
'You mean everything's under control.'
'No,' said Zaphod, 'I do not mean everything's under control.
That would not be cool and froody.'

'The restaurant at the end of the universe'
by Douglas Adams

I am grateful to a lot of people who have supported and accompanied me while I was working for and writing up this thesis. Especially I want to thank

Stephan Kümmel who has supervised this thesis. His enthusiasm for physics, his scientific expertise and his personality were and are a great inspiration to me. He has also shown great patience with respect to all my side-projects from hydrodynamics to graduation parties.

the members and alumni of the Kümmel-group: Monika Birkelbach, Anne Klimach, Linn Leppert, Rickard Armiento, Dirk Hofmann, Andreas Karolewski, Thomas Körzdörfer, Michael Mundt and Sebastian Wüstner. They and many others in the department have contributed to a friendly atmosphere both for work and also for private activities.

Rickard Armiento, who shared office with me for more than two years. He has been a great vis-a-vis for physics discussions, life-saving computer support and all kinds of nonsense from Becke-meter to Candy mountain.

Linn, Rickard and the great Hollemann for their diligent reading and checking of the manuscript.

my parents, who have given lots of support and advice for this project while the intervals between my visits have become longer and longer.

Monika Steghöfer for her love, care and support during all the ups and downs of this thesis and life in general.



“Head ’em up, move ’em out. Power stride and ready to ride!”

Erklärung

Hiermit erkläre ich, dass ich die vorliegende Arbeit selbständig verfasst und keine anderen als die angegebenen Quellen und Hilfsmittel verwendet habe.

Bayreuth, 28. Mai 2009

Mark Thiele

Part II

Publications

List of included publications as referred to in this thesis:

- Pub1* *Adiabatic Approximation in Nonperturbative Time-dependent Density-Functional Theory*, M. Thiele, E. K. U. Gross and S. Kümmel, Phys. Rev. Lett. **100**, 153004 (2008).
- Pub2* *Hydrodynamic perspective on memory in time-dependent density-functional theory*, M. Thiele and S. Kümmel, Phys. Rev. A **79**, 052503 (2009).
- Pub3* *Photoabsorption spectra from adiabatically exact time-dependent density-functional theory in real time*, M. Thiele and S. Kümmel, Phys. Chem. Chem. Phys. **11**, 4631 (2009).
- Pub4* *Reconstructing the adiabatic exchange-correlation kernel of time-dependent density-functional theory*, M. Thiele and S. Kümmel, Phys. Rev. A **80**, 012514 (2009).

Other publications not related to this thesis:

- Scaling and energy transfer in rotating turbulence*, W.-C. Müller and M. Thiele, Europhys. Lett. **77**, 34003 (2007).
- Structure and decay of rotating homogeneous turbulence*, M. Thiele and W.-C. Müller, accepted for publication in J. Fluid Mech. (2009).

Publication 1

*Adiabatic Approximation in
Nonperturbative Time-dependent Density-Functional Theory*

M. Thiele, E. K. U. Gross and S. Kümmel,
Phys. Rev. Lett. **100**, 153004 (2008).

Copyright 2008 by the American Physical Society.
<http://link.aps.org/doi/10.1103/PhysRevLett.100.153004>

Adiabatic Approximation in Nonperturbative Time-Dependent Density-Functional Theory

M. Thiele,¹ E. K. U. Gross,² and S. Kümmel¹

¹*Physikalisches Institut, Universität Bayreuth, D-95440 Bayreuth, Germany*

²*Theoretische Physik, Freie Universität Berlin, D-14195 Berlin, Germany*

(Received 22 November 2007; published 18 April 2008)

We construct the exact exchange-correlation potential of time-dependent density-functional theory and the approximation to it that is adiabatic but exact otherwise. For the strong-field double ionization of the Helium atom these two potentials are virtually identical. Thus, memory effects play a negligible role in this paradigm process of nonlinear, nonperturbative electron dynamics. We identify the regime of high-frequency excitations where the adiabatic approximation breaks down and explicitly calculate the nonadiabatic contribution to the exchange-correlation potential.

DOI: [10.1103/PhysRevLett.100.153004](https://doi.org/10.1103/PhysRevLett.100.153004)

PACS numbers: 31.15.ee, 31.70.Hq, 32.80.Rm

Progress in laser technology has provided the experimental tools to study and manipulate electron dynamics on atomic scales [1]. On the theoretical side, this strong-field regime can in principle be accessed by solving the many-electron time-dependent Schrödinger equation (TDSE). In practice, however, a first-principles approach in this vein is ruled out by the tremendous computational cost of solving the TDSE for more than two electrons in three dimensions. Time-dependent density-functional theory (TDDFT) [2] offers a computationally attractive approach to strong-field electron dynamics [3,4] which is in principle exact, but in practice requires approximations for the time-dependent exchange-correlation (xc) potential $v_{xc}(\mathbf{r}, t)$.

Up to now applications of TDDFT almost exclusively rely on “adiabatic approximations” [e.g., the adiabatic local density approximation (ALDA)], which are obtained by plugging the time-dependent density into one of the existing ground-state density functionals for v_{xc} . Approaches of this type have also been used to calculate the double ionization (DI) of the helium atom, one of the most prominent effects in the regime of strong-field electron dynamics. Its importance as a benchmark for theoretical many-body methods stems from the fact that DI yields in the low-intensity regime are found to be substantially increased due to pronounced electron correlation effects [5,6]. As a result of this “nonsequential ionization” (NSI), the famous “knee” structure appears in the double-ionization probability as a function of intensity. A combination of theoretical [7–12] and experimental [13–15] studies has by now established the recollision model as the mechanism responsible for NSI. But most attempts based on adiabatic TDDFT have failed completely to even qualitatively describe NSI [16–19]. It has been argued [20] that this failure may be due to a missing particle number discontinuity [21] in the commonly used ground-state functionals for v_{xc} .

A priori there is little reason to believe that any ground-state functional can yield reliable results for a process like DI, because it is known that nonadiabatic effects in v_{xc} can play an important role [22–28]. It is a natural and common

assumption that these effects should be particularly important in nonlinear, nonperturbative processes that take a system far away from its ground-state, as, e.g., in strong-field ionization.

In this Letter we explore the adiabatic approximation beyond the linear response regime. For the hallmark example of a strong-field process, the helium DI, we compare the exact time-dependent xc potential to the xc potential (defined in detail below) that is an adiabatic approximation but is exact otherwise. This adiabatically exact approximation is local in time, i.e., shows no memory effects, but is fully nonlocal in space, i.e., the multiplicative potential $v_{xc}(\mathbf{r})$ depends not only on the density n at \mathbf{r} , but also on n at all other points of space. Our calculations reveal that for the intensities and frequencies that are usually considered in the context of strong-field electron dynamics, and specifically for the helium DI, the adiabatic approximation works extremely well. Thus, an accurate description requires nonlocality in space more than nonlocality in time.

For the definition of the “adiabatically exact approximation” one should recall that, for the initial state being the ground state, the exact xc potential shows “memory” as at any given time t it is a nonlocal functional of the exact time-dependent density n at all previous times, i.e., $v_{xc}^{\text{ex}}(\mathbf{r}, t) = v_{xc}^{\text{ex}}[n(\mathbf{r}', t')](\mathbf{r}, t)$ where $t' \leq t$. By definition it is related to the exact Kohn-Sham (KS) potential $v_s^{\text{ex}}[n(\mathbf{r}', t')](\mathbf{r}, t)$ by

$$v_{xc}^{\text{ex}}(\mathbf{r}, t) = v_s^{\text{ex}}(\mathbf{r}, t) - v_h(\mathbf{r}, t) - v_{\text{ext}}(\mathbf{r}, t), \quad (1)$$

where v_{ext} is the external potential and v_h is the Hartree potential, which is a functional of the density only at $t' = t$. By virtue of the Runge-Gross theorem, the potential v_s^{ex} corresponding to the exact time-dependent density is unique, and it can be shown to exist [29].

The adiabatic approximation is defined by treating the time-dependent density at a fixed time $t = t_0$ as a ground-state density, i.e., $n_0(\mathbf{r}) = n(\mathbf{r}, t_0)$. Consequently, the adiabatically exact KS potential $v_s^{\text{adia,ex}}(\mathbf{r})$ is the local potential which yields $n_0(\mathbf{r})$ as the solution of the *noninteracting*,

single-particle Schrödinger equation. The correspondence between n_0 and $v_s^{\text{adia,ex}}$ is unique according to Hohenberg and Kohn [30]. Following standard ground-state DFT, the xc contribution to $v_s^{\text{adia,ex}}(\mathbf{r})$ is given by

$$v_{\text{xc}}^{\text{adia,ex}}(\mathbf{r}) = v_s^{\text{adia,ex}}(\mathbf{r}) - v_h(\mathbf{r}, t_0) - v_{\text{ext},0}(\mathbf{r}), \quad (2)$$

i.e., this defines the adiabatically exact xc potential at $t = t_0$. Here, v_h is again the Hartree potential corresponding to the given density n_0 and $v_{\text{ext},0}(\mathbf{r})$ is the local external potential which yields n_0 as the solution of the *interacting* many-particle Schrödinger equation. Also the mapping between n_0 and $v_{\text{ext},0}(\mathbf{r})$ is unique according to Hohenberg and Kohn. Therefore, $v_{\text{xc}}^{\text{adia,ex}}(\mathbf{r})$ is uniquely defined by Eq. (2) and is a numerical representation of the unknown exact ground-state xc potential functional. The existence of the ground-state potentials is also guaranteed [31]. Comparing $v_{\text{xc}}^{\text{ex}}$ and $v_{\text{xc}}^{\text{adia,ex}}$ will directly reveal the nonadiabatic effects.

Using these definitions in practice requires the exact time-dependent density as an input. For the helium atom the latter can be calculated at bearable computational cost from the solution of the TDSE by using a one-dimensional model which reproduces the essential features of the DI process [10,11,16,17,32]. In this model, the helium atom in a time-dependent external potential $v_{\text{ext}}(z, t)$ is described by the Hamiltonian

$$H = \sum_{j=1,2} \left(\frac{p_j^2}{2m} + v_{\text{ext}}(z_j, t) \right) + W(z_1 - z_2) \quad (3)$$

with electron coordinates z_1, z_2 , momenta p_1, p_2 , electron mass m and the soft-core interaction $W(z) = e^2/\sqrt{z^2 + 1}$. The external potential $v_{\text{ext}}(z, t) = -2W(z) - ezE(t)$ contains the electron-nucleus interaction and the potential of the time-dependent electrical field $E(t)$. Taking the spatial wave function to be symmetric under exchange of electrons, the time-dependent Schrödinger equation $i\hbar\partial_t\psi = H\psi$ is solved numerically. The two-electron wave function obtained in this way allows to calculate the exact time-dependent density $n(z, t) = 2 \int |\psi(z, z', t)|^2 dz'$ and, via the inversion of the time-dependent KS equation (TDKS) [20,33], the exact time-dependent KS potential v_s^{ex} . From the latter, the exact correlation potential $v_c^{\text{ex}} = v_{\text{xc}}^{\text{ex}} - v_x$ follows by Eq. (1), as for a two-electron singlet system $v_{\text{hx}} := v_h + v_x = 1/2v_h$ with $v_h(z, t) = \int n(z', t)W(z - z')dz'$.

Thus, $v_{\text{xc}}^{\text{ex}}$ can readily be calculated. However, obtaining $v_{\text{xc}}^{\text{adia,ex}}$ is a formidable task even in the one-dimensional model. Calculating the adiabatically exact total KS potential is still easy: Making the above described identification $n_0(z) = n(z, t_0)$, the adiabatically exact total KS potential follows from the inversion of the static KS equation,

$$v_s^{\text{adia,ex}}(z) = \frac{\hbar^2}{m} \frac{1}{2\varphi(z)} \frac{d^2\varphi(z)}{dz^2} + \text{const.}, \quad (4)$$

where $\varphi(z) = \sqrt{n_0(z)}/2$. The challenge is posed by the exact xc part according to Eq. (2): finding $v_{\text{ext},0}(\mathbf{r})$ requires the inversion of the *interacting* static Schrödinger equation $H_0\psi_0 = E_0\psi_0$ (SE) for the ground state ψ_0 which satisfies the constraint $n_0(z) = 2 \int |\psi_0(z, z')|^2 dz'$. Here,

$$H_0 = \sum_{j=1,2} \left(\frac{p_j^2}{2m} + v_{\text{ext},0}(z_j) \right) + W(z_1 - z_2). \quad (5)$$

To find $v_{\text{ext},0}$ for a given n_0 we implemented a generalization of an iterative scheme [34]. Starting with an initial guess $v_{\text{ext},0}^{(1)}$ for $v_{\text{ext},0}$ we calculate [33] the corresponding ground-state wave function, which in turn yields the density $n_0^{(1)}$ corresponding to $v_{\text{ext},0}^{(1)}$. Then a new potential is constructed according to the rule

$$v_{\text{ext},0}^{(i)}(z) = v_{\text{ext},0}^{(i-1)}(z) + w(z)[n_0^{(i-1)}(z) - n_0(z)], \quad (6)$$

where $i = 2$ for the first step. $w(z) = \alpha|z|^\beta$ (with parameters $\alpha, \beta > 0$) is a weight function allowing to increase the contribution of the density-fall-off region. The thus obtained $v_{\text{ext},0}^{(2)}$ in turn leads to a $n_0^{(2)}$ via solution of the SE. These steps are iterated until the density $n_0^{(i)}$ has converged to n_0 according to the criterion

$$\int |n_0^{(i)}(z) - n_0(z)| dz \leq \Delta, \quad (7)$$

where Δ is a measure for the desired accuracy. Once we have obtained $v_{\text{ext},0}(z)$, the adiabatically exact correlation potential $v_c^{\text{adia,ex}}(z)$ follows from Eq. (2) with v_{hx} being identical for the time-dependent and static case.

In order to assess the validity of the adiabatic approximation, we solve the two-electron TDSE for given potentials $v_{\text{ext}}(z, t)$ representing paradigm cases of strong-field electron dynamics (discussed in detail below). At every time step t we then construct v_c^{ex} and $v_c^{\text{adia,ex}}$ according to the procedure described above.

In our first study we take $E(t)$ to be a dc electric field that is ramped up during 27 a.u. (0.65 fs) to a maximum value $E_0 = 0.141$ a.u. and held constant afterwards. Starting from the two-electron ground state this leads to field-induced ionization of the system with the electrons escaping to $z \rightarrow \infty$. To avoid numerical problems caused by strongly accelerated electrons, the interaction with the field is truncated at a distance of 35 a.u. from the nucleus [20]. The resulting time-evolution of the density and the potentials is shown in Fig. 1. v_s^{ex} and v_c^{ex} are defined only up to an additive time-dependent constant, which has been adjusted so that the boundary condition $v_c^{\text{ex}}(z, t) \rightarrow 0$ for $z \rightarrow \infty$ is fulfilled. The free additive constant in $v_s^{\text{adia,ex}}$ and $v_{\text{ext},0}$ cannot be fixed, thus all adiabatically exact potentials are shifted to match the exact ones at $z = 0$. As with other known density-inversion schemes, our procedures work accurately only in regions of space where a sufficient amount of density is located. As a rule of thumb, regions where $n(z) > 10^{-2}$ a.u. can safely be considered.

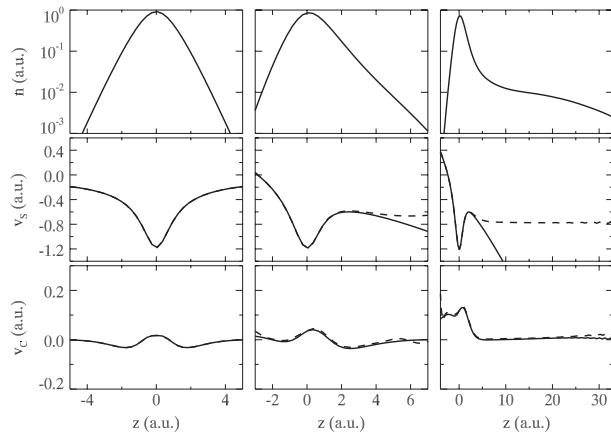


FIG. 1. Density, total KS potential, and correlation potential (from top to bottom) at the 3 times $t = 0, 21.5, 43.0$ a.u. (from left to right) during the interaction of the two-electron atom with a dc electric field. Solid curves: exact time-dependent v_s^{ex} and v_c^{ex} ; dashed curves: adiabatically exact $v_s^{\text{adia,ex}}$ and $v_c^{\text{adia,ex}}$ (Hartree units). Note the different scales in the plots and that v_c^{ex} and $v_c^{\text{adia,ex}}$ are very close, with deviations at the boundaries being a numerical consequence of low density; see text.

Restricting the analysis to regions of space where the density obtained with the iterative scheme also reproduces the one from the TDSE with high accuracy acts as a further safeguard against numerical artefacts.

Figure 1 shows that the exact and adiabatically exact versions of the total KS potential v_s differ substantially and qualitatively. This reflects the fact that the former corresponds to an excited density in the presence of the linear laser potential, and the latter to a bound ground state in a global potential minimum. However, the surprising result is that the lowest line of panels in Fig. 1 undoubtedly reveals that the correlation contributions to the potentials, i.e., $v_c^{\text{ex}}(z)$ and $v_c^{\text{adia,ex}}(z)$, agree extremely well at all times (also for times much longer than what is shown in Fig. 1). This indicates that memory effects in the correlation potential are practically negligible for this process. Also the buildup of a steplike structure in v_c at later times as identified in [20] is well reproduced by the adiabatically exact approximation.

To probe the regime where nonadiabatic effects manifest themselves in the correlation potential, we consider as our second study an external potential in which the density is deformed more rapidly than during the ramping process. Instead of adding an external laser field to the electron-nucleus interaction, we directly perturb the soft-core potential according to

$$v_{\text{ext}}(z, t) = -\frac{2e^2}{\sqrt{[z - (0.5 \text{ a.u.}) \sin(\omega t)]^2 + 1}}. \quad (8)$$

This forcing mimics an oscillatory motion of the nucleus. It has the benefit of keeping the density relatively well local-

ized, thus allowing for stable solutions in the TDKS-inversion-scheme. The chosen frequency $\omega \approx 0.9$ a.u. is close to the frequency range investigated in earlier work on two-electron systems in the nonadiabatic regime [25,26]. Figure 2 shows that for the external potential (8) the density gets rapidly and strongly deformed and does not return to its initial shape after a full cycle of the forcing. To contain such a density as a ground state, the adiabatically exact KS potential produces additional minima which are not present in its exact, nonadiabatic counterpart. The resulting $v_c^{\text{adia,ex}}$ displayed in the lowest line of Fig. 2 differs markedly from v_c^{ex} , showing that nonadiabatic effects become important.

Finally, in our third study we turn our attention to the practically most relevant case of strong, time-dependent external fields due to powerful laser pulses of the 780 nm wavelength that is typically used in strong-field experiments. The oscillation here is of moderate frequency but the density is strongly displaced from its initial position. This is a setup for which ALDA is known to fail badly [18]. The results shown below are obtained during a 4-cycle pulse with linear turn-on and -off for two cycles each. Our comparison now is done in the way that is most useful to assess the accuracy of the adiabatically exact approximation in practice: We propagate [33] the KS orbital while using at every time step the adiabatically exact approximation of v_c that is obtained self-consistently from the KS density [35].

The TDSE is solved as the exact reference and now is used only for that purpose. To compare the results of the adiabatically exact TDKS calculation to those of the TDSE, we focus on the number of bound electrons,

$$N_b(t) = \int_{-a}^a n(z, t) dz, \quad (9)$$

with $|z| \leq a = 5$ a.u. This is a decisive quantity for the

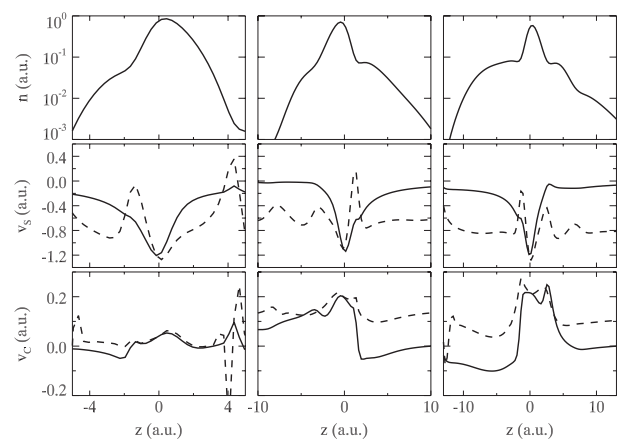


FIG. 2. Same as Fig. 1 but for the two-electron atom during high-frequency excitation according to (8) at $t = \frac{1}{2}T$, $t = T = 2\pi/\omega$ and $t = \frac{3}{2}T$ (from left to right). The initial situation at $t = 0$ is the same as in Fig. 1.

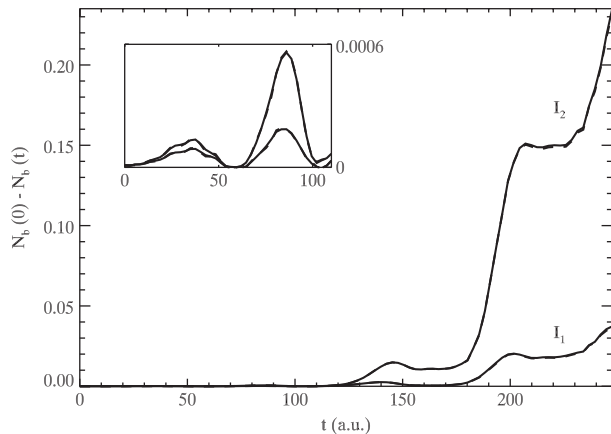


FIG. 3. Total ionization during the interaction of the two-electron atom with a laser pulse of maximum intensity $I_1 = 4 \times 10^{14}$ W/cm² (lower two curves) and $I_2 = 7 \times 10^{14}$ W/cm² (upper two curves). Solid curves: exact TDSE calculation; dashed curves: adiabatically exact TDKS scheme. The inset shows a magnification of the first part of the curve.

interpretation of the ionization results, as the DI yields depend crucially on it [18,19]. It is also well suited for the comparison, because it can be calculated directly from the density without making additional approximations. Figure 3 shows the time evolution of the total ionization, $N_b(0) - N_b(t)$, for two different maximum laser intensities typical of experimental conditions. The striking result is that the curves obtained from the adiabatically exact TDKS calculation lie virtually on top of the exact ones. Thus, the time evolution is not influenced by memory effects for the intensities within the crucial NSI region.

In summary, we calculated the adiabatic xc potential by inverting the interacting SE. Thus, we were able to visualize the nonadiabatic effects in $v_{xc}(\mathbf{r}, t)$ exactly, providing a procedure to directly track down this fundamental but elusive feature of TDDFT. As a test of immediate practical relevance we have performed a nonlinearized, nonperturbative Kohn-Sham calculation of strong-field ionization which consistently used the adiabatically exact approximation for v_{xc} . While memory effects in v_{xc} are known to be crucial for the description of phenomena like, e.g., double excitations, our results show that they are negligible for typical strong-field excitations, and, in particular, for the paradigm process of the helium DI. Here, the adiabatically exact TDDFT approach yields excellent results.

S.K. acknowledges support by the Deutsche Forschungsgemeinschaft.

- [1] P. B. Corkum and F. Krausz, *Nature Phys.* **3**, 381 (2007).
- [2] E. Runge and E. K. U. Gross, *Phys. Rev. Lett.* **52**, 997 (1984); E. K. U. Gross, J. F. Dobson, and M. Petersilka, in *Density Functional Theory*, edited by R. F. Nalewajski (Springer, Berlin, 1996), p. 81.
- [3] S.-I. Chu, *J. Chem. Phys.* **123**, 062207 (2005).
- [4] F. Calvayrac *et al.*, *Phys. Rep.* **337**, 493 (2000).
- [5] D. N. Fittinghoff *et al.*, *Phys. Rev. Lett.* **69**, 2642 (1992).
- [6] B. Walker *et al.*, *Phys. Rev. Lett.* **73**, 1227 (1994).
- [7] P. B. Corkum, *Phys. Rev. Lett.* **71**, 1994 (1993).
- [8] A. Becker and F. H. M. Faisal, *J. Phys. B* **29**, L197 (1996); *Phys. Rev. A* **59**, R1742 (1999).
- [9] D. Dundas *et al.*, *J. Phys. B* **32**, L231 (1999).
- [10] W.-C. Liu *et al.*, *Phys. Rev. Lett.* **83**, 520 (1999).
- [11] M. Lein, E. K. U. Gross, and V. Engel, *Phys. Rev. Lett.* **85**, 4707 (2000).
- [12] J. S. Prauzner-Bechcicki *et al.*, *Phys. Rev. Lett.* **98**, 203002 (2007).
- [13] R. Moshhammer *et al.*, *Phys. Rev. Lett.* **84**, 447 (2000).
- [14] T. Weber *et al.*, *Phys. Rev. Lett.* **84**, 443 (2000).
- [15] T. Weber *et al.*, *Nature (London)* **405**, 658 (2000).
- [16] D. Bauer, *Phys. Rev. A* **56**, 3028 (1997).
- [17] D. G. Lappas and R. van Leeuwen, *J. Phys. B* **31**, L249 (1998).
- [18] M. Petersilka and E. K. U. Gross, *Laser Phys.* **9**, 105 (1999).
- [19] F. Wilken and D. Bauer, *Phys. Rev. Lett.* **97**, 203001 (2006).
- [20] M. Lein and S. Kümmel, *Phys. Rev. Lett.* **94**, 143003 (2005); M. Mundt and S. Kümmel, *Phys. Rev. Lett.* **95**, 203004 (2005).
- [21] J. P. Perdew *et al.*, *Phys. Rev. Lett.* **49**, 1691 (1982).
- [22] M. Lein, E. K. U. Gross, and J. P. Perdew, *Phys. Rev. B* **61**, 13431 (2000).
- [23] I. V. Tokatly and O. Pankratov, *Phys. Rev. Lett.* **86**, 2078 (2001).
- [24] N. T. Maitra *et al.*, *J. Chem. Phys.* **120**, 5932 (2004).
- [25] C. A. Ullrich and I. V. Tokatly, *Phys. Rev. B* **73**, 235102 (2006); C. A. Ullrich, *J. Chem. Phys.* **125**, 234108 (2006).
- [26] P. Hessler, N. T. Maitra, and K. Burke, *J. Chem. Phys.* **117**, 72 (2002).
- [27] Y. Kurzweil and R. Baer, *Phys. Rev. B* **73**, 075413 (2006).
- [28] I. D'Amico and G. Vignale, *Phys. Rev. B* **59**, 7876 (1999).
- [29] R. van Leeuwen, *Phys. Rev. Lett.* **82**, 3863 (1999).
- [30] P. Hohenberg and W. Kohn, *Phys. Rev.* **136**, B864 (1964).
- [31] J. T. Chayes, L. Chayes, and M. B. Ruskai, *J. Stat. Phys.* **38**, 497 (1985).
- [32] D. G. Lappas *et al.*, *J. Phys. B* **29**, L619 (1996).
- [33] A. S. de Wijn, S. Kümmel, and M. Lein, *J. Comput. Phys.* **226**, 89 (2007).
- [34] K. Peirs, D. Van Neck, and M. Waroquier, *Phys. Rev. A* **67**, 012505 (2003).
- [35] A similar procedure has been used in H. O. Wijewardane and C. A. Ullrich, *Phys. Rev. Lett.* **100**, 056404 (2008).

Publication 2

*Hydrodynamic perspective on memory in
time-dependent density-functional theory*

M. Thiele and S. Kümmel,
Phys. Rev. A **79**, 052503 (2009).

Copyright 2009 by the American Physical Society.
<http://link.aps.org/doi/10.1103/PhysRevA.79.052503>

Hydrodynamic perspective on memory in time-dependent density-functional theory

M. Thiele and S. Kümmel

Physikalisches Institut, Universität Bayreuth, D-95440 Bayreuth, Germany

(Received 18 December 2008; published 7 May 2009)

The adiabatic approximation of time-dependent density-functional theory is studied in the context of nonlinear excitations of two-electron singlet systems. We compare the exact time evolution of these systems to the adiabatically exact one obtained from time-dependent Kohn-Sham calculations relying on the exact ground-state exchange-correlation potential. Thus, we can show under which conditions the adiabatic approximation breaks down and memory effects become important. The hydrodynamic formulation of quantum mechanics allows us to interpret these results and relate them to dissipative effects in the Kohn-Sham system. We show how the breakdown of the adiabatic approximation can be inferred from the rate of change of the ground-state noninteracting kinetic energy.

DOI: [10.1103/PhysRevA.79.052503](https://doi.org/10.1103/PhysRevA.79.052503)

PACS number(s): 31.15.ee, 31.70.Hq, 32.80.Rm

I. INTRODUCTION

Time-dependent density-functional theory (TDDFT) provides an attractive approach to treat electron dynamics in the nonlinear regime, where the solution of the many-electron time-dependent Schrödinger equation (TDSE) is not possible with the computational resources available today [1]. Important applications such as correlated electron dynamics in the presence of strong laser fields [2] crucially depend on methods like this. The benefit of TDDFT is mainly due to the fact that it is a rigorous reformulation of the quantum-mechanical many-body problem in terms of single-particle equations that can be integrated with moderate computational effort. The price to pay for this gain is the necessity to approximate the unknown but uniquely defined time-dependent exchange-correlation (xc) potential $v_{xc}(\mathbf{r}, t)$.

Most applications of TDDFT are based on an “adiabatic approximation” in which the exact $v_{xc}(\mathbf{r}, t)$ is replaced by an existing ground-state density functional. However, even if the exact ground-state xc potential is available for this procedure (adiabatically exact approximation), one would still introduce an error that will become important as soon as nonadiabatic or “memory” effects are non-negligible. The question of the breakdown of the adiabatic approximation is thus of major importance for any TDDFT application [3–9]. In practice, this problem is complicated further by the fact that the exact ground-state xc potential $v_{xc,0}$ is also unknown. Hence, in most situations, e.g., when using the adiabatic local density approximation (ALDA), it is difficult to tell apart the two possible sources of error: the adiabatic approximation of v_{xc} and the spatial approximation of $v_{xc,0}$. Finally, to be able to identify any introduced error, an exact reference solution is required.

It is exactly for these reasons that one-dimensional (1D) two-electron singlet systems provide an invaluable tool to study the validity range of any adiabatic approximation. Here, both the exact reference solution and the adiabatically exact approximation can be obtained [5,10,11]. Hence, we will focus on these systems to investigate the conditions for the breakdown of the adiabatic approximation. We find that nonadiabatic effects become important when the time-dependent density experiences rapid deformation. Based on

this observation we derive a simple criterion for the breakdown of the adiabatic approximation related to the ground-state noninteracting kinetic energy. Both the observations and the criterion can be very well interpreted when one is taking a hydrodynamic point of view on the two-electron system.

The hydrodynamic formulation of quantum mechanics or quantum fluid dynamics (QFD) dates back to Madelung’s reformulation of the single-particle TDSE in 1926 [12]. During the following years, further development of the theory with extensions to many-body systems has taken place mainly within condensed matter and nuclear physics (see, e.g., Refs. [13,14] and references therein). In the early 1980s QFD formulations [15] were among the immediate predecessors of TDDFT [16,17]. The latter finally provided rigorous existence and uniqueness proofs [16,18] both for TDDFT and QFD, i.e., the well-defined closure of the respective system of equations. Since then hydrodynamic concepts have proven very valuable to obtain a better understanding of collective electron dynamics (e.g., Refs. [19,20]) and even to find exact constraints on the properties of the exact xc potential (e.g., Ref. [21]). Many approaches to go beyond the adiabatic approximation mentioned earlier are based on hydrodynamical ideas, such as current density-functional theory [22,23] and TDDFT in a comoving Lagrangian reference frame [24–26]. Only recently, QFD for the general many-body problem has been cast in a very compact formulation for density and fluid velocity based on a rigorous microscopic expression of the exact stress tensor [24–26]. The latter approach has received much attention lately [27–29], providing a very intuitive way to assess many-electron phenomena. In this paper, we will argue that it is also suitable to analyze the role of memory effects and the validity regime of the adiabatic approximation in TDDFT.

It is found that the QFD formulation valid for the systems studied here is formally similar to well-known equations of classical hydrodynamics. This allows for a very intuitive explanation of the breakdown of the adiabatic approximation in TDDFT. Rapid density compression and rarefaction translate into strong gradients of the velocity field. The latter are linked to dissipative effects in the electron liquid, which are not correctly accounted for when memory effects are neglected. On the other hand, electron motion with no or slow

density deformation is properly described by the adiabatic approximation.

Our paper is organized as follows. In Sec. II we provide the basic theory for the 1D two-electron singlet system within Schrödinger quantum mechanics and TDDFT, define the adiabatic approximation, and list the required inversion concepts. We introduce the hydrodynamic point of view in Sec. III with further details provided in Appendixes A–C. In Sec. IV we present our results for the breakdown of the adiabatic approximation and its relation to dissipative effects before finally offering a summary and conclusions in Sec. V.

II. QUANTUM MECHANICS OF THE TWO-ELECTRON SYSTEM

A. Governing equations

The ground state $\psi_0(\mathbf{r}_1, \mathbf{r}_2)$ of the two-electron singlet system follows from the solution of the interacting static Schrödinger equation (SE) $H_0\psi_0 = E_0\psi_0$, with the Hamilton operator

$$H_0 = \sum_{j=1,2} \left(-\frac{\hbar^2}{2m} \nabla_j^2 + v_{\text{ext},0}(\mathbf{r}_j) \right) + V_{\text{ee}}(|\mathbf{r}_1 - \mathbf{r}_2|). \quad (1)$$

Here $v_{\text{ext},0}(\mathbf{r}_j)$ is the external potential and the symmetric electron-electron interaction is given by $V_{\text{ee}}(|\mathbf{r}_1 - \mathbf{r}_2|)$. The time evolution of a general symmetric wave function $\psi(\mathbf{r}_1, \mathbf{r}_2, t)$ on the other hand is obtained from the solution of the TDSE, $i\hbar \partial_t \psi = H\psi$, governed by

$$H = \sum_{j=1,2} \left(-\frac{\hbar^2}{2m} \nabla_j^2 + v_{\text{ext}}(\mathbf{r}_j, t) \right) + V_{\text{ee}}(|\mathbf{r}_1 - \mathbf{r}_2|) \quad (2)$$

with the time-dependent external potential v_{ext} . The exact electron density, e.g., in the time-dependent case, can be obtained by

$$n(\mathbf{r}, t) = 2 \int |\psi(\mathbf{r}, \mathbf{r}', t)|^2 d^3r'. \quad (3)$$

For the one-dimensional case, i.e., $\psi(z, z', t)$, the TDSE can be integrated numerically at bearable cost. To avoid the Coulomb singularity in 1D we employ the soft-core interaction $W(z) = e^2 / \sqrt{z^2 + 1}$ for V_{ee} (always) and for the electron-nucleus interaction if we are dealing specifically with the helium atom. This approximation has been shown to reproduce the essential features of correlated electron dynamics [30–35]. It is also possible in one dimension to numerically invert the SE [11] to find $v_{\text{ext},0}(z)$ for a given ground-state density $n_0(z)$. This will be useful for the reconstruction of certain quantities relevant in the context of TDDFT (see below).

The standard Kohn-Sham (KS) density-functional theory (DFT) representation of the two-electron singlet system consists of two noninteracting particles in the same spatial orbital $\varphi(\mathbf{r})$. For the ground state this orbital is the lowest eigenstate φ_0 of the stationary Kohn-Sham equation (KSE),

$$\left(-\frac{\hbar^2}{2m} \nabla^2 + v_{s,0}(\mathbf{r}) \right) \varphi_i(\mathbf{r}) = \varepsilon_i \varphi_i(\mathbf{r}), \quad (4)$$

where the effective potential $v_{s,0}$ is a unique functional of the density $n_0(\mathbf{r}) = 2|\varphi_0(\mathbf{r})|^2$ by virtue of the Hohenberg-Kohn theorem [36]. Similarly the time-dependent Kohn-Sham equation (TDKSE),

$$i\hbar \partial_t \varphi(\mathbf{r}, t) = \left(-\frac{\hbar^2}{2m} \nabla^2 + v_s(\mathbf{r}, t) \right) \varphi(\mathbf{r}, t), \quad (5)$$

governs the evolution of a general orbital $\varphi(\mathbf{r}, t)$. Here the unique relation between v_s and $n(\mathbf{r}, t) = 2|\varphi(\mathbf{r}, t)|^2$ is established by the Runge-Gross theorem [16]. Naturally, it is possible to calculate eigenstates of the KSE and to integrate the TDKSE. Furthermore, both equations can be inverted. This is especially straightforward for the KSE where, for any given density $n(\mathbf{r}, t)$,

$$v_{s,0}(\mathbf{r}, t) = \frac{\hbar^2}{m} \left[\frac{1}{4} \frac{\nabla^2 n(\mathbf{r}, t)}{n(\mathbf{r}, t)} - \frac{1}{8} \left(\frac{\nabla n(\mathbf{r}, t)}{n(\mathbf{r}, t)} \right)^2 \right]. \quad (6)$$

As this rule to construct $v_{s,0}$ relies only on the instantaneous density, t just takes the role of a parameter here. On the other hand the inversion of the TDKSE [37,38] works according to

$$\begin{aligned} v_s(\mathbf{r}, t) &= \frac{\hbar^2 \nabla^2 \varphi(\mathbf{r}, t)}{m 2\varphi(\mathbf{r}, t)} + i\hbar \frac{\dot{\varphi}(\mathbf{r}, t)}{\varphi(\mathbf{r}, t)} \\ &= \frac{\hbar^2}{m} \left\{ \frac{1}{4} \frac{\nabla^2 n(\mathbf{r}, t)}{n(\mathbf{r}, t)} - \frac{1}{8} \left[\frac{\nabla n(\mathbf{r}, t)}{n(\mathbf{r}, t)} \right]^2 \right\} \\ &\quad - \hbar \left\{ \dot{\alpha}(\mathbf{r}, t) + \frac{\hbar}{2m} [\nabla \alpha(\mathbf{r}, t)]^2 \right\} \\ &= v_{s,0}(\mathbf{r}, t) - \hbar \left\{ \dot{\alpha}(\mathbf{r}, t) + \frac{\hbar}{2m} [\nabla \alpha(\mathbf{r}, t)]^2 \right\}, \quad (7) \end{aligned}$$

i.e., it requires both density and phase information of $\varphi(\mathbf{r}, t) = \sqrt{n(\mathbf{r}, t)/2} e^{i\alpha(\mathbf{r}, t)}$.

B. xc potential of TDDFT

The xs potential of TDDFT is related to the xc potential v_{xc} according to

$$v_s(\mathbf{r}, t) = v_{\text{ext}}(\mathbf{r}, t) + v_h(\mathbf{r}, t) + v_{\text{xc}}(\mathbf{r}, t) \quad (8)$$

or, for the ground-state situation (where t is again just a parameter),

$$v_{s,0}(\mathbf{r}, t) = v_{\text{ext},0}(\mathbf{r}, t) + v_h(\mathbf{r}, t) + v_{\text{xc},0}(\mathbf{r}, t), \quad (9)$$

where $v_h(\mathbf{r}, t) = \int n(\mathbf{r}', t) V_{\text{ee}}(|\mathbf{r} - \mathbf{r}'|) d^3r'$ is the Hartree potential, which is a local-in-time functional of the density. For the two-electron singlet system the exchange contribution to v_{xc} simplifies to $v_x = -\frac{1}{2}v_h$ so that in the following we will often consider v_c separately from $v_{\text{hx}} = v_h + v_x = \frac{1}{2}v_h$. When the initial state is the ground state, the xc potential at any given time t is a nonlocal functional of the exact time-dependent density n at all previous times, i.e., $v_{\text{xc}}(\mathbf{r}, t) = v_{\text{xc}}[n(\mathbf{r}', t')](\mathbf{r}, t)$ where $t' \leq t$. This dependency on the history of the density is usually referred to as “memory effects” in the xc potential [1,39].

Most TDDFT applications rely on the adiabatic approximation, which is defined by treating the time-dependent density at a fixed time $t=t_0$ as a ground-state density, i.e., $n(\mathbf{r}, t_0)=n_0(\mathbf{r})$. Then, in the TDKSE $v_{xc}(\mathbf{r}, t_0)$ is substituted by one of the existing approximations of the ground-state xc potential. This procedure does not only lead to the loss of any memory effects but is also approximate with respect to the spatial nonlocality of the xc potential.

To treat the full spatial nonlocality exactly one needs to replace these approximations for $v_{xc}(\mathbf{r}, t_0)$ by the exact $v_{xc,0}[n_0(\mathbf{r}')](\mathbf{r})$ of ground-state DFT. This defines the adiabatically exact approximation which exclusively neglects the memory effects. Only recently it has become possible to construct this approximation for 1D two-electron systems [11]. In this approach a numerical representation of the exact and fully nonlocal $v_{xc,0}$ is obtained from Eq. (9) using the above-mentioned KSE- and SE-inversion schemes to calculate $v_{s,0}$ and $v_{ext,0}$ of the ground-state systems corresponding to n_0 .

Thus, in the following, we can propagate the TDKSE in the adiabatically exact approximation using at every time step the $v_{xc,0}$ self-consistently obtained from the calculated density (AE-TDKSE scheme). The resulting observables can then be compared to their exact counterparts provided by the solution of the TDSE for the same process allowing us to assess the validity of the adiabatically exact approximations.

C. Exact properties of v_{xc}

Several properties of the exact v_{xc} have been derived over the years. One of them is the zero-force theorem [40],

$$\int n(\mathbf{r}, t) \nabla v_{xc}(\mathbf{r}, t) d^3r = 0, \quad (10)$$

which states that, as a consequence of Newton's third law, the net xc force exerted on the system as a whole is zero. This is automatically fulfilled for the adiabatically exact v_{xc} , which is at any time t the exact ground-state xc potential corresponding to the instantaneous density. For the two-electron singlet system studied here, the zero-force theorem holds also separately for both the Hartree-type exchange and the correlation part of v_{xc} .

Another important constraint is provided by the harmonic potential theorem (HPT) [21] for interacting electron dynamics in a parabolic potential with a time-dependent dipole perturbation, i.e., $v_{ext}(\mathbf{r}, t)=(k/2)r^2+\mathbf{E}(t)\cdot\mathbf{r}$. It can be shown that for this v_{ext} and any number of electrons N , the electron density is rigidly translated according to $n(\mathbf{r}, t)=n_0(\mathbf{r}-\mathbf{X}(t))$. Here, $\mathbf{X}(t)=(1/N)\int \mathbf{r}n(\mathbf{r}, t)d^3r$ is the center-of-mass coordinate obeying

$$m\ddot{\mathbf{X}}(t) = -k\mathbf{X}(t) - \mathbf{E}(t). \quad (11)$$

Thus, for $k/m =: \omega_0^2$ and, e.g., $\mathbf{E}(t)=\mathbf{E}_0 \sin(\omega_f t)$ and with $\mathbf{X}(0)=\dot{\mathbf{X}}(0)=0$,

$$\mathbf{X}(t) = \mathbf{E}_0 \frac{1}{\omega_0^2 - \omega_f^2} \left(\frac{\omega_f}{\omega_0} \sin(\omega_0 t) - \sin(\omega_f t) \right). \quad (12)$$

For TDDFT to satisfy the HPT, the xc potential needs to rigidly follow the rigidly translated density, a feature also

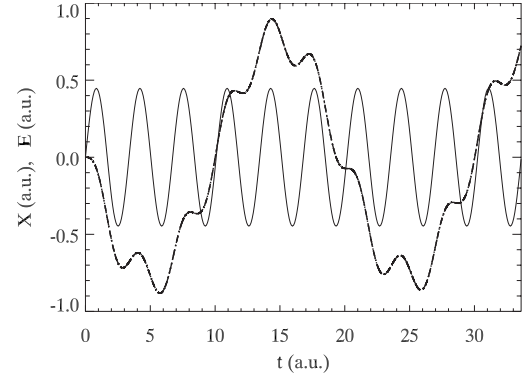


FIG. 1. Time evolution of $X(t)$ for the 1D two-electron Hooke's atom with $v_{ext}(z)=(k/2)z^2+E_0z \sin(\omega_f t)$, where $k=0.1$ a.u., $E_0=0.447$ a.u., and $\omega_f=1.870$ a.u. The TDSE (dashed) and AE-TDKSE (dotted-dashed) curves both lie on top of the dotted one given by Eq. (12). For comparison, we also show $E(t)=E_0 \sin(\omega_f t)$ (thin solid line).

termed generalized translational invariance [40]. When the initial state of the system is the ground state, this means that $v_{xc,0}$ is rigidly translated with the density, i.e., the adiabatically exact v_{xc} is valid exactly for HPT motion. Later on, when we want to establish a criterion for the validity regime of the adiabatic approximation, the fact that HPT motion always should fulfill this criterion will be of importance.

To shortly illustrate the important concept of HPT motion and to test the accuracy of the numerical realization of the AE-TDKSE scheme, we have performed calculations for a 1D Hooke's atom. We show in Fig. 1 how theory [Eq. (12)] and numerical results both from the exact TDSE and the AE-TDKSE schemes provide exactly the same evolution of $X(t)$. This shows that the AE-TDKSE scheme, which by definition should be able to reproduce HPT motion, is working very accurately. It should also be noted that the HPT theorem is valid not only in the linear regime but also for strong perturbation amplitudes E_0 , as used in the test calculation on which Fig. 1 is based.

In the following, we will consider three different 1D bound systems: the "anharmonic Hooke's atom" characterized by $v_{ext,0}(z)=(k/2)(z^2+\tilde{k}z^6)$ (A6-Hooke) or $v_{ext,0}(z)=(k/2)(z^2+\tilde{k}z^4)$ (A4-Hooke) with $k=0.1$ a.u. and $\tilde{k}=0.01$ a.u. [41] (we use Hartree atomic units unless stated otherwise). The anharmonic term has been introduced to deliberately avoid HPT motion when the dipole field $e\mathbf{z}E(t)$ is applied [5]. The third system studied is the soft-core helium atom [11,30,34,35] characterized by the ground-state potential $v_{ext,0}(z)=-2W(z)$. The different systems are summarized in Table I. The initial state for any time-dependent process is the ground state of the particular system.

III. HYDRODYNAMICS OF THE TWO-ELECTRON SYSTEM

After the inspection of the relevant equations of quantum mechanics we will now turn to their hydrodynamic formulation. For our purposes it will suffice to deal with the nonin-

TABLE I. Ground state properties of 1D two-electron singlet systems studied in this paper. The ground-state noninteracting kinetic energy $T_{s,0}$ is defined in Eq. (23). The lowest KS excitation frequency $\omega_{s,1}$ is determined from the 1D version of Eq. (4). The breakdown threshold $\dot{T}_{s,0}^{\text{crit}}$ is defined in Eq. (25). All values are in Hartree atomic units.

System	$v_{\text{ext,gs}}(z)$	$\omega_{s,1}$	$T_{s,0}(0)$	$\dot{T}_{s,0}^{\text{crit}}$
A6-Hooke	$k/2(z^2 + \tilde{k}z^6)^a$	0.267	0.156	0.007
A4-Hooke	$k/2(z^2 + \tilde{k}z^4)^a$	0.192	0.108	0.003
Helium	$-2W(z)$	0.479	0.277	0.021

^a $k=0.1$, $\tilde{k}=0.01$.

interacting TDKSE system, which for the exact v_{xc} produces the same density as the interacting TDSE system. The QFD formulation of the TDKSE presented in the following allows for a more intuitive interpretation of the adiabatic approximation guided by well-known concepts of classical fluid dynamics. A short review of the classical theory is provided in Appendix A.

A. Governing equations

As mentioned before, the single-particle KS wave function $\varphi(\mathbf{r}, t) = \sqrt{n(\mathbf{r}, t)}/2e^{i\alpha(\mathbf{r}, t)}$ is completely determined by the density n and the phase α . This means that we can transform the KSE system into a set of hydrodynamic equations for the density n and the KS velocity field,

$$\mathbf{u}_s(\mathbf{r}, t) = \mathbf{j}_s(\mathbf{r}, t)/n(\mathbf{r}, t) = \frac{\hbar}{m} \nabla \alpha(\mathbf{r}, t), \quad (13)$$

where \mathbf{j}_s is the KS current [42] by noting that \mathbf{u}_s contains the same information as α . The transformation closely follows the one given by Madelung for the single-particle Schrödinger equation [12,43]. The details are provided in Appendix B. Finally, one arrives at the hydrodynamic set of equations consisting of the continuity equation

$$D_t n = -n \nabla \cdot \mathbf{u}_s, \quad (14)$$

the momentum equation

$$m D_t \mathbf{u}_s = -\frac{1}{n} \partial_i (P_{sij} + \delta_{ij} p_c) - \partial_j (v_{\text{hx}} + v_{\text{ext}}) \quad (15)$$

(we use the Einstein convention of implicit sums $\sum_{i=1}^3$ over products with the same index i), and the Poisson equation

$$\Delta v_{\text{hx}} = -2\pi e^2 n. \quad (16)$$

Here $D_t = \partial_t + \mathbf{u}_s \cdot \nabla$ is the convective derivative and

$$P_{sij} = \frac{\hbar^2}{4m} \left(\frac{(\partial_i n)(\partial_j n)}{n} - \delta_{ij} \nabla^2 n \right) \quad (17)$$

is the noninteracting stress tensor [24–26]. The correlation contribution p_c is defined by $\nabla p_c = n \nabla v_c$. The formal closure of the hydrodynamic set of equations is proven by the Runge-Gross theorem [16], which implies that p_c exists and

is uniquely defined by the density n , i.e., we have an unknown but well-defined constitutive relation $p_c[n]$.

The equations for the two-electron singlet system closely resemble those derived by Madelung [12] for the single particle. Also P_{sij} has the same form as the quantum stress tensor of single-particle QFD [14,28]. This is a consequence of the singlet property of the system leading to two spatially identical KS orbitals. The only differences are due to the appearance of the correlation contribution p_c and the Hartree-exchange potential v_{hx} .

For the 1D situation that we study, where u_s denotes the z coordinate of the KS velocity, one arrives at

$$D_t n = -n \partial_z u_s \quad (18)$$

and

$$m D_t u_s = -\frac{1}{n} \partial_z p - \partial_z (v_{\text{hx}} + v_{\text{ext}}), \quad (19)$$

where $D_t = \partial_t + u_s \partial_z$. Now, $v_{\text{hx}}(z, t) = 1/2 \int n(z', t) W(|z - z'|) dz'$ and the tensor in Eq. (15) has collapsed into a generalized scalar pressure

$$p = p_{s,0} + p_c \quad (20)$$

with the noninteracting pressure [29]

$$p_{s,0} = \frac{\hbar^2}{4m} \left(\frac{(\partial_z n)^2}{n} - \partial_z^2 n \right). \quad (21)$$

Note that $\partial_z p_{s,0} = -n \partial_z u_{s,0}$.

At this point it is instructive to pause for a moment and have a look at the derived three-dimensional (3D) and 1D QFD equations. They are exact reformulations of the TDKSE, i.e., when the exact v_c is available, they will have the exact time-dependent density as solution. The latter is of course also provided by the QFD equations for the interacting system, which can be derived from the TDSE [24–26]. However, the exact KS velocity \mathbf{u}_s and the exact interacting velocity \mathbf{u} do not necessarily agree in three dimensions. This is a consequence of the open question whether KS and interacting current are identical [42]. Of course in one dimension the relation $u_s = u$ holds, allowing us for the time-dependent process at hand to identify u from the TDSE with the exact u_s . The latter can then be compared with the adiabatically exact u_s stemming from the corresponding AE-TDKSE calculation.

B. Contributions to the generalized pressure

Looking at Eqs. (18) and (19) we notice a strong structural similarity to the 1D versions of the classical hydrodynamic equations reviewed in Appendix A. To push the analogy even further we recall that the classical stress tensor (Appendix A) contains a (hydro)static density-dependent pressure part and a dynamic velocity-dependent viscous contribution. As we will show in the following, the same classification holds for the generalized pressure of Eq. (20).

We start by splitting up the correlation pressure according to $p_c = p_{c,0} + p_{c,\text{mem}}$, where the former part stems from the adiabatically exact $v_{c,0}$ while the latter includes all the

TABLE II. Time-dependent processes of the A6-Hooke and A4-Hooke systems as given in Table I with $v_{\text{ext}}(z,t)=v_{\text{ext,gs}}(z)+ezE_0 \sin(\omega_f t)$. Intensity I in W/cm^2 ; E_0 and ω_f in Hartree atomic units. The memory character of a process follows from the deviation of the TDSE- and AE-TDKSE-solutions in time (see text).

Process	I	E_0	ω_f	Memory
A6-Hooke I	7×10^{14}	0.141	0.029	No
A6-Hooke II	7×10^{15}	0.447	1.870	Yes
A4-Hooke I	7×10^{14}	0.141	0.029	No
A4-Hooke II	7×10^{15}	0.447	1.870	Yes
A4-Hooke III	7×10^{15}	0.447	0.935	Yes

memory effects with respect to n . While $p_{s,0}$ and $p_{c,0}$ exclusively depend on the instantaneous density (nonlocal in space and local in time), the situation for $p_{c,\text{mem}}$ requires a closer inspection.

Due to the relation between KS velocity and density as provided by Eq. (14) the nonlocal-in-time relation to the density in $p_{c,\text{mem}}[n]$ can be re-expressed in terms of a dependency on the initial state density n_{gs} and on the history of the KS velocity u_s . This follows from a ‘‘kinematic’’ solution of Eq. (14), where from a prescribed velocity field $u_s(z,t')$ for $0 \leq t' \leq t$ one can always reconstruct $\dot{n}(z,t')$ on the same interval. Together with $n_{\text{gs}}(z)$ this fixes $n(z,t')$ and hence $p_{c,\text{mem}}$ for $0 \leq t' \leq t$. As a consequence $p_{c,\text{mem}}[n]$ is replaced by $\hat{p}_{c,\text{mem}}[n_{\text{gs}}, u_s]$, which is a functional of n_{gs} (nonlocal in space) and velocity u_s (nonlocal in space and time).

The HPT motion mentioned earlier has a very intuitive form in the hydrodynamic picture: rigid motion of the density corresponds to purely advective motion without deformation, i.e., a continuity equation with vanishing right-hand side (rhs) or $\partial_z u_s = 0$ (see Appendix A). Thus, the velocity is constant in space following $u_s = \dot{X}(t)$. In the momentum equation the nonlinear term of the convective derivative disappears and the xc pressure is replaced by its adiabatically exact contribution. This means that $\hat{p}_{c,\text{mem}}[n_{\text{gs}}, u_s] = 0$ here, telling us that $\hat{p}_{c,\text{mem}}$ is in fact a functional of $\partial_z u_s$, i.e., we actually have $\tilde{p}_{c,\text{mem}}[n_{\text{gs}}, \partial_z u_s]$. The latter observation is a consequence of the Galilean invariance of the stress tensor [23,44], of which p is the scalar ‘‘leftover’’ in one dimension.

Thus $p_{s,0}$ and $p_{c,0}$ clearly provide the ground-state contribution or hydrostatic pressure [29] in Eq. (20) (recall also that $\partial_z p_{s,0} = -n \partial_z v_{s,0}$), while the dynamical component can only stem from $\tilde{p}_{c,\text{mem}}$.

IV. BREAKDOWN OF THE ADIABATIC APPROXIMATION

It has already been shown that for certain time-dependent processes, the exact and adiabatically exact xc potentials corresponding to a given exact density will be different [11]. To demonstrate that these memory effects have an observable influence on the dynamics, we have performed self-consistent AE-TDKSE calculations for several processes with and without nonadiabatic effects. The obtained results can then be compared with the exact TDSE solution. We concentrate on the anharmonic Hooke system (cf. Table II),

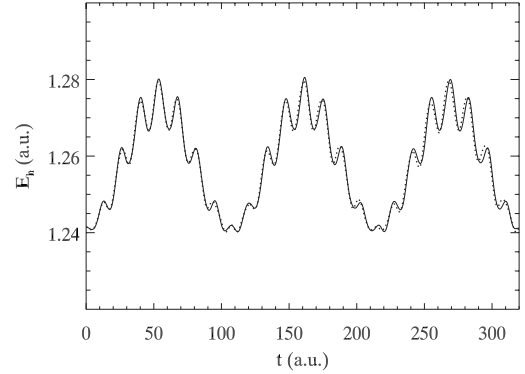


FIG. 2. Time evolution of E_h for A6-Hooke I system calculated with TDSE (solid line) and AE-TDKSE (dotted line).

which is especially suitable to analyze deviations from HPT motion while still profiting from the localization of the density due to the strong confinement provided by the parabolic potential.

A. A6-Hooke process without memory

We start with the A6-Hooke I process, for which the driving field intensity and frequency are in the range of typical strong laser processes (cf. Table II). Figures 2 and 3 show the evolution of the Hartree energy $E_h(t) = 1/2 \int n(z,t) v_h(z,t) dz$ and of the ground-state noninteracting kinetic energy $T_{s,0}(t)$ for both the TDSE and AE-TDKSE calculations. We choose these observables for monitoring memory because of their direct scalar dependence on the density [5]. $T_{s,0}(t)$ is defined as

$$T_{s,0}(t) = \frac{\hbar^2}{m} \int [\partial_z \varphi_0(z,t)]^2 dz, \quad (22)$$

where $\varphi_0(z,t) = \sqrt{n(z,t)}/2$ and thus,

$$T_{s,0}(t) = \frac{\hbar^2}{8m} \int \frac{[\partial_z n(z,t)]^2}{n(z,t)} dz, \quad (23)$$

with similar relations for the 3D case. The good agreement of the TDSE and AE-TDKSE results indicates that the adia-

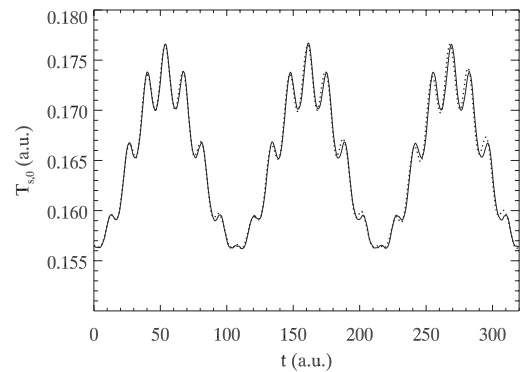


FIG. 3. Time evolution of $T_{s,0}$ for A6-Hooke I system calculated with TDSE (solid line) and AE-TDKSE (dotted line).

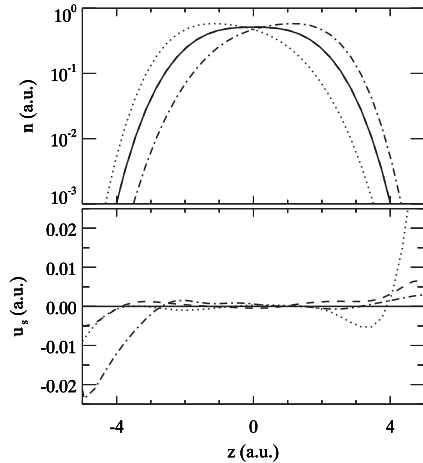


FIG. 4. Snapshots of exact density n and velocity u_s during A6-Hooke I process. According to Eq. (13) the velocity increases as the density drops (e.g., around $z=4$ a.u.). The resulting velocity gradients in regions of very low density are discussed further below.

batically exact approximation is valid here. Figure 4 shows snapshots of typical densities and velocities during this process. Although there is not only bulk motion but also some density deformation going on, it apparently happens on a slow enough time scale for the adiabatic approximation to remain valid. The slowness of the density deformation corresponds to almost flat velocity profiles according to Eq. (18), indicating that the instantaneous velocity is a more suitable quantity in this context than the instantaneous density deformation. Note that in the 1D situation studied in this paper density deformation always corresponds to density compression on the one hand and rarefaction on the other as at least two dimensions are required for a finite fluid volume to deform its shape while conserving its volume.

B. A6-Hooke process with memory

Now we turn our attention to a process at higher intensity and frequency (A6-Hooke II process) and repeat the analysis with respect to the energies. Figures 5 and 6 show the evo-

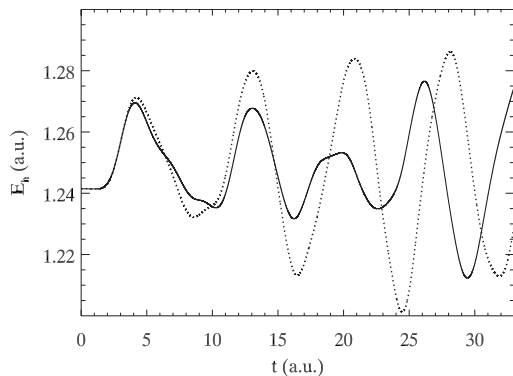


FIG. 5. Time evolution of E_h for A6-Hooke II system calculated with TDSE (solid line) and AE-TDKSE (dotted line).

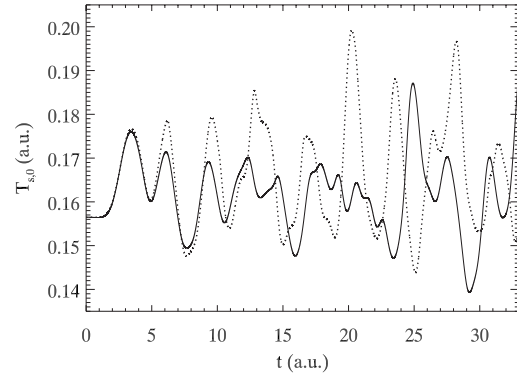


FIG. 6. Time evolution of $T_{s,0}$ for A6-Hooke II system calculated with TDSE (solid line) and AE-TDKSE (dotted line).

lution of E_h and $T_{s,0}$ for both the TDSE and AE-TDKSE calculations. In striking contrast to the situation before, we can see that around $t \approx 3.5$ a.u. the solutions start to differ.

The different density evolutions in the two calculations indicate the insufficiency of the adiabatic approximation for this process. To analyze the conditions of the breakdown, it is instructive to compare the evolution of the density and velocity field for TDSE and AE-TDKSE calculations during the time interval where the energies start to deviate (Figs. 7–9). As in the A6-Hooke I process, the density gets deformed compared to HPT motion. But now this deformation is happening more rapidly, i.e., strong gradients appear in the velocity. This is a situation that is completely unlike the HPT motion described earlier as it leads to regions of either rapid density compression or rarefaction. Such behavior has been discussed in several earlier works: strong velocity gradients were shown to lead to the breakdown of the approximation of Vignale, Ullrich, and Conti [23] for the description of collective intersubband transitions in quantum wells [45] and of $s \rightarrow p$ transitions in atomic systems [46]. Similarly, it has been observed that rapid and strong density deformation

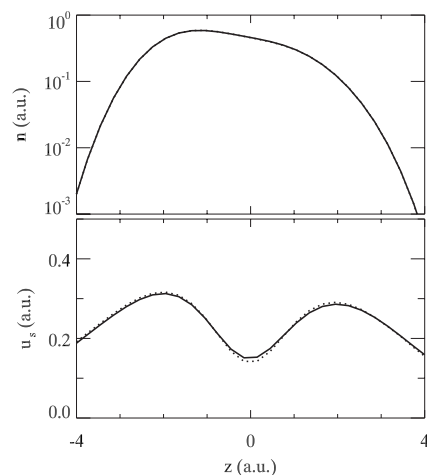


FIG. 7. Comparison of densities and velocities from TDSE (solid line) and AE-TDKSE (dotted line) schemes at $t=3.36$ a.u. for A6-Hooke II system.

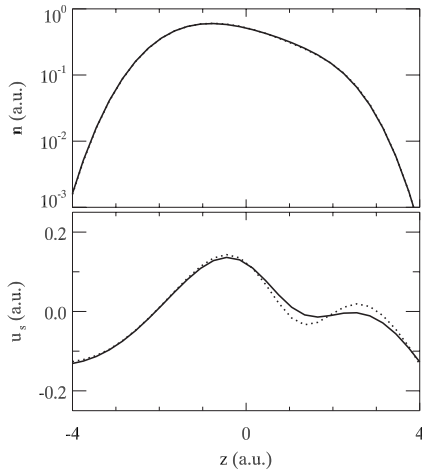


FIG. 8. Comparison of densities and velocities from TDSE (solid line) and AE-TDKSE (dotted line) schemes at $t=4.20$ a.u. for A6-Hooke II system.

leads to failure of the ALDA [7] and the time-dependent Krieger-Li-Iafraite approximations [9] in simple model systems. However, all these approaches are approximate not only in their nonlocal-in-time dependency on the density but also with respect to nonlocality in space. The adiabatically exact approximation which we use here allows us to investigate the exclusive relation between strong density deformation and memory effects while treating the nonlocality in space exactly.

The appearance of strong gradients in the velocity field has been related to a transition of the system from mostly collective toward single-particle-like motion [7,45]. However, for the two-electron singlet case this concept has to be refined as the motion here is always collective in the sense that only two equivalent orbitals exist and evolve exactly in the same way. Hence the velocity gradients cannot arise from differences in the single-particle currents, which were iden-

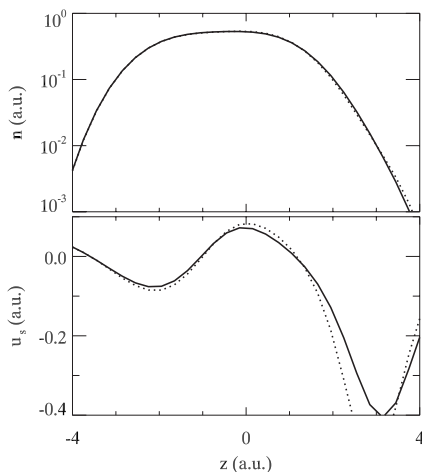


FIG. 9. Comparison of densities and velocities from TDSE (solid line) and AE-TDKSE (dotted line) schemes at $t=5.46$ a.u. for A6-Hooke II system.

tified to be a reason for noncollective motion in systems with more electrons [47]. So, for the two-electron singlet system, it might be more appropriate to regard velocity gradients as a deviation from rigid “bulk motion” of the density distribution.

So why and how are strong velocity gradients related to the breakdown of the adiabatic approximation? It is instructive to now look back at the essential features of the hydrodynamic equations derived above. In the adiabatic approximation, where $\tilde{p}_{c,mem}[n_{gs}, \partial_z u_s]=0$, we are dealing with a momentum equation that strongly resembles the Euler equation, i.e., no velocity-dependent components appear on the rhs as would be the case for, e. g., the Navier-Stokes equation. Thus, it is immediately clear that as soon as strong velocity gradients develop, the nonlinear term $u_s \partial_z u_s$ on the left-hand side will become dominant for the time evolution because there is no term $\tilde{p}_{c,mem}[n_{gs}, \partial_z u_s]$ on the rhs, which could balance it. Hence, one should indeed expect that the solutions of calculations with and without $\tilde{p}_{c,mem}[n_{gs}, \partial_z u_s]$ start to deviate in such a situation.

From the analogy of $\tilde{p}_{c,mem}[n_{gs}, \partial_z u_s]$ to the viscous stress contributions in classical hydrodynamics it follows that its reaction to strong velocity gradients is, at least to leading order, of dissipative nature. Here, the term dissipation specifically refers to the dissipation of classical (collective) kinetic energy through a diffusive term in the momentum equation, i.e., the nonadiabatic term, $\tilde{p}_{c,mem}$, can lead to dissipation of the velocity field’s kinetic energy. The latter does not disappear from the system but can be transferred to other internal energy components. It should be mentioned that further contributions to $\tilde{p}_{c,mem}[n_{gs}, \partial_z u_s]$ may also lead to energy injection. Nonadiabatic effects of velocity-dependent contributions have also been shown to be connected to entropy production and irreversible relaxation in infinite systems [48].

Generally, there seems to be a tendency of the AE-TDKSE solution to lead to more pronounced gradients than the TDSE (cf. Figs. 8 and 9). This appears quite reasonable, as it is well known that due to the nonlinear convective term $u_s \partial_z u_s$, the 1D Euler equation can build up discontinuities in the velocity field [49]. This effect can be balanced by a dissipative velocity-dependent term on the rhs, as frequently studied in one dimension in the context of the viscous Burgers’ equation [49]. However, due to the nature of the adiabatic approximation, any velocity-dependent term on the rhs of Eq. (19) is excluded. Thus, a “smoothing” or damping effect on the buildup of velocity gradients is not available in this situation. The absence of such a mechanism does generally not pose a problem for a quantum system, as discontinuities in the (not observable) velocity just signal kinks in the phase [cf. Eq. (13)]. But here, it will clearly make the phase of the adiabatically exact system start to differ from that of the exact system, leading to a different time evolution of the whole process and thus to the breakdown of the adiabatic approximation.

We have seen that the development of strong gradients in the velocity will threaten the validity of the adiabatic approximation. One should also note that the main effect of this feature on the observable quantity of interest, namely, the density n , is due to the rhs of the continuity equation [Eq.

(18)]. This indicates that the effect is weighted by the density ($n\partial_z u_s$), showing that the strong gradients might be less important in regions where the density is small. Note that in the limit of vanishing density the definition of the velocity breaks down anyway [28]. In a way, one could also regard those parts of the flow where the rhs of Eq. (18) vanishes due to vanishing n and/or $\partial_z u_s$ as approximately incompressible and hence not problematic for the adiabatic approximation. In these regions the density is just advected by the velocity field as a whole without any deformation happening (cf. Appendix A). An important limiting case is of course electron motion according to the harmonic potential theorem, where $\partial_z u_s$ vanishes exactly and, as stated above, the adiabatic approximation is exactly valid.

C. Breakdown criterion

While the obtained results and the hydrodynamic argument provide us with a good qualitative understanding of the adiabatic approximation, the appearance of strong velocity gradients does not offer a very practical criterion to determine when its breakdown will actually occur. Ideally one would like to infer already from the type, frequency, and strength of the applied perturbation whether an adiabatic approach is justified. However, facing the whole scope of possible strong field excitations, it seems too ambitious to predict the appearance of strong density gradients just from looking at $v_{\text{ext}}(z, t)$. Instead, we will in the following present a simple criterion that will tell us, for an ongoing time-dependent KS calculation, when the adiabatic approximation is most certainly breaking down and the density evolution will start to differ from the exact one.

A suitable criterion that is based on the density should be sensitive to its rapid deformation, which, as shown above, corresponds to strong velocity gradients in regions of finite n . To this end, we turn back to $T_{s,0}$, which basically provides an integral measure of the curvature and hence the deformation of the instantaneous density. As we are not interested in the absolute deformation of the density but rather how rapidly it changes in time, it is advantageous to look at

$$\begin{aligned}\dot{T}_{s,0} &= - \int j_s \partial_z v_{s,0} dz \\ &= - \int n u_s \partial_z v_{s,0} dz \\ &= \int u_s \partial_z p_{s,0} dz \\ &= - \int p_{s,0} \partial_z u_s dz.\end{aligned}\quad (24)$$

There are several additional reasons why this quantity might be suitable for a memory criterion: it has been shown [5] that time derivatives of energy components can indicate memory effects. Additionally, $\dot{T}_{s,0}$ is based on just the orbitals, i.e., it is always available in any time-dependent KS scheme. Furthermore, we see that $\dot{T}_{s,0}$ provides an integral measure of the velocity gradient $\partial_z u_s$ weighted with the noninteracting pres-

sure $p_{s,0}$. The latter quantity vanishes in regions where the density falls off to zero and hence ensures that velocity gradients in regions of low density will contribute less to $\dot{T}_{s,0}$. Finally, $T_{s,0}$ can be regarded as a quantity intimately related to the ground-state character of a given density. The latter is expected to change rapidly in any nonadiabatic process.

Another attractive feature of $\dot{T}_{s,0}$ is that in the limit of HPT motion without deformation, $\dot{T}_{s,0}$ vanishes exactly as $\partial_z u_s = 0$ in Eq. (24). Note that this property is shared by, e.g., \dot{E}_h , but the latter is much more sensitive to the density distribution in space than to its deformation.

In the following we will define an approximate upper bound for $|\dot{T}_{s,0}(t)|$ of an ongoing time-dependent process that is still adiabatic. This bound is provided by the ratio

$$\dot{T}_{s,0}^{\text{crit}} = \frac{T_{s,0}(t=0)}{\tau^{\text{mem}}}, \quad (25)$$

where $T_{s,0}(t=0)$ is the initial value of the ground-state noninteracting kinetic energy of the system under study. τ^{mem} is the memory time scale defined in the following way: as soon as a process is happening on the time scale τ^{mem} (or on shorter time scales), it is expected to be no longer adiabatic. To fix τ^{mem} we consider the limit of the linear response of the system. Here memory is known to become important as soon as the considered process takes place at a frequency ω at which the xc kernel, $\partial v_{\text{xc}}[n]/\partial n$, shows significant frequency dependence [1,4]. As the xc kernel is composed of the inverse response functions of the interacting and the noninteracting systems, it will “inherit” their frequency dependence. This means that a good estimate for an upper bound for the frequency range where the xc kernel is almost independent of ω is provided by the lowest occurring transition frequency [50]. For the systems studied here this is the lowest KS transition energy $\omega_{s,1} = (\varepsilon_1 - \varepsilon_0)/\hbar$ (cf. Table I). Thus it makes sense to define $\tau^{\text{mem}} = 2\pi/\omega_{s,1}$. Consequently an approximate upper bound for the validity of the adiabatic approximation for a specific process is provided by $|\dot{T}_{s,0}(t)| < \dot{T}_{s,0}^{\text{crit}}$. The possibility to extend this criterion to the case of more than two electrons in three dimensions is discussed in Appendix C.

Figure 10 shows the exact evolution of $\dot{T}_{s,0}(t)$ for the two A6-Hooke systems together with the upper bound for $|\dot{T}_{s,0}(t)|$ according to Eq. (25). $\dot{T}_{s,0}(t)$ differs strongly for both processes and the proposed criterion clearly separates both regimes.

Figure 11 shows $\dot{T}_{s,0}(t)$ for a larger data set of TDSE calculations for the A6-Hooke system (cf. Table III), where the memory character of each process has been determined by comparing v_c and $v_{c,0}$ obtained from the inversion schemes. Although the applied dipole fields vary strongly with respect to E_0 and ω_f , the criterion seems to hold in a large part of the parameter space. Note that the procedure used here to determine memory effects is not completely equivalent to the approach presented before. Therefore, the data shown in Fig. 11 should be seen more as a trend for the applicability of the adiabatic approximation with respect to the parameters E_0 and ω_f for a given system. These results

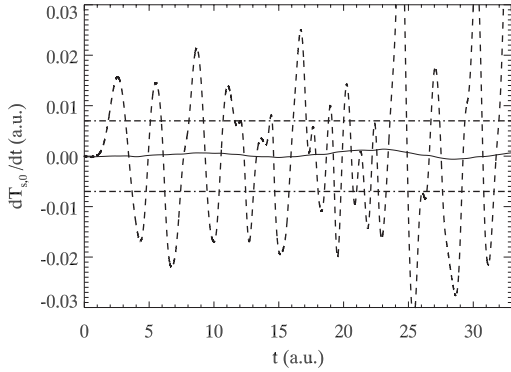


FIG. 10. Exact evolution of $\dot{T}_{s,0}$ for A6-Hooke systems I (without memory, solid line) and II (with memory, dashed line). The dotted-dashed line represents the memory criterion according to Table I and formula (25).

also indicate that $\dot{T}_{s,0}^{\text{crit}}$ provides an upper bound for (and not the maximum of) the $|\dot{T}_{s,0}(t)|$ that can occur during a still adiabatic process. On the other hand with $|\dot{T}_{s,0}| \geq \dot{T}_{s,0}^{\text{crit}}$ the adiabatic approximation is certainly breaking down.

To show the applicability of the criterion to different systems we consider the A4-Hooke I–III processes. Figure 12 shows the exact evolution of $\dot{T}_{s,0}(t)$ for the three processes together with the appropriate criterion. Here again, $|\dot{T}_{s,0}(t)| > \dot{T}_{s,0}^{\text{crit}}$ correctly indicates memory effects for A4-Hooke III process. The regime $|\dot{T}_{s,0}(t)| < \dot{T}_{s,0}^{\text{crit}}$ covers both the adiabatic A4-Hooke I process at almost vanishing $|\dot{T}_{s,0}|$ and the non-adiabatic A4-Hooke II process with relatively high $|\dot{T}_{s,0}|$. These findings highlight once more that $\dot{T}_{s,0}^{\text{crit}}$ has the character of an approximate upper bound for the adiabatic regime.

For completeness we also show in Fig. 13 three different processes in the helium atom studied previously [11]. Although the helium system differs qualitatively from the anharmonic Hooke case and the studied processes are of different types the criterion works similarly well here.

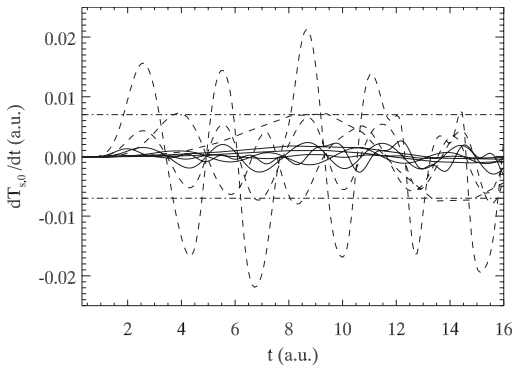


FIG. 11. Exact evolution of $\dot{T}_{s,0}$ for A6-Hooke processes described in Table III (without memory: solid lines; with memory: dashed line). The dotted-dashed line represents the memory criterion according to Table I and formula (25).

TABLE III. Time-dependent processes of A6-Hooke in a dipole field according to $v_{\text{ext}}(z,t) = v_{\text{ext,gs}}(z) + e z E_0 \sin(\omega_f t)$. Intensity I in W/cm^2 ; E_0 and ω_f in Hartree atomic units. The memory character of a process follows from the deviation of v_c and $v_{c,0}$ corresponding to the exact time-dependent density.

I	E_0	ω_f	Memory
1×10^{14}	0.053	0.117	No
1×10^{14}	0.053	0.935	No
7×10^{14}	0.141	0.058	No
7×10^{14}	0.141	0.117	Yes
7×10^{14}	0.141	0.935	Yes
7×10^{14}	0.141	1.870	No
1×10^{15}	0.169	3.740	No
2×10^{15}	0.239	1.870	Yes
2×10^{15}	0.239	2.805	No
7×10^{15}	0.447	1.870	Yes

V. CONCLUSION

We have studied the conditions for the breakdown of the adiabatic approximation in TDDFT. To allow for a numerically exact analysis of this problem we focused on 1D two-electron singlet systems where both exact and adiabatically exact calculations are possible. To interpret the results and proceed toward a quantitative criterion for the breakdown, we have transformed the governing equations into a hydrodynamic formulation based on the density n and the KS velocity u_s .

The breakdown of the adiabatic approximation was found to be related to the appearance of strong velocity gradients corresponding to rapid compression and rarefaction of the density. Within the hydrodynamic picture these features can be clearly linked to dissipative effects in the KS system that are missed whenever the adiabatic approximation is used. Guided by this observation we derived a criterion for the breakdown of the adiabatic approximation based on the rate of change of the ground-state noninteracting kinetic energy.

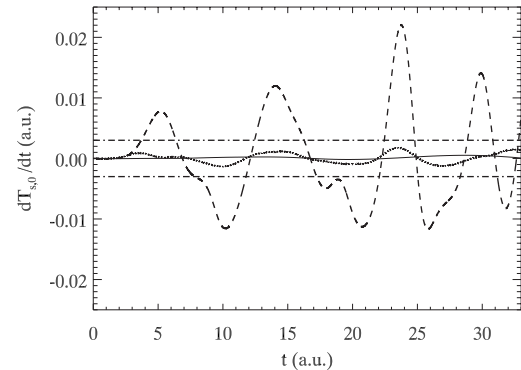


FIG. 12. Exact evolution of $\dot{T}_{s,0}$ for A4-Hooke systems I (without memory, solid line), II (with memory, dotted line), and III (with memory, dashed line). The dotted-dashed line represents the memory criterion according to Table I and formula (25).

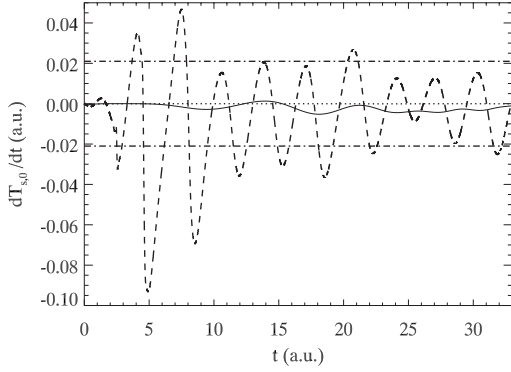


FIG. 13. Exact evolution of $\dot{T}_{s,0}$ for helium systems ramp (without memory, solid line), pulse with $I=7 \times 10^{14}$ W/cm² (without memory, dotted line), and oscillating nucleus (with memory, dashed line) as investigated in Ref. [11]. The dotted-dashed line represents the memory criterion according to Table I and formula (25). For the pulse $\dot{T}_{s,0}$ is reaching finite amplitudes at later times but not exceeding 40% of $\dot{T}_{s,0}^{\text{crit}}$.

The latter provides an integral measure of strong velocity gradients in regions of finite density. We showed that this criterion provides an approximate upper bound for the validity of the adiabatic approximation for a given time-dependent process.

The evaluation of the criterion for different processes indicates that memory effects generally become more important for growing strength of the external perturbation. However, for forcing frequencies that are very low the adiabatic approximation is found to hold even at strong perturbation amplitudes. In the opposite limit of very high frequencies there are also indications for the applicability of the adiabatic approximation in agreement with recent analytical findings [51]. This behavior agrees with the analogy between the electron liquid and a viscoelastic material [23]: in the nonadiabatic regime, the electronic system behaves fluidlike and internal friction leads to dissipative effects. The opposing regime is characterized by solidlike elastic behavior as for HPT motion or in the limiting case of infinite frequency. The effects that are crucial in the latter regime are thus mainly incorporated into the exact ground state $v_{xc,0}$. Hence, the adiabatic approximation works well in the elastic regime.

The small perturbation limit also leads to the linear response regime of TDDFT. Here memory effects are known to be crucial for the correct representation of double and multiple excitations [4,8]. Investigating these questions using the adiabatically exact approximation has been the topic of a recent study [52]. Earlier studies [46] have already established a connection between dissipative effects and nonadiabatic corrections to linear response quantities.

Of course the ultimate goal is the development of xc functionals that are applicable both in the adiabatic and nonadiabatic regimes. Currently, there is a lot of progress going on in this direction [23,53–58] with most of these approaches drawing from hydrodynamic concepts. The present work shows that both the QFD approach and the 1D two-electron singlet system as a benchmark case can provide important guidance on this route.

ACKNOWLEDGMENTS

M.T. is grateful for stimulating discussions with Hans Schamel, Wolf-Christian Müller, and Ralf Kaiser. S.K. and M.T. acknowledge support by the Deutsche Forschungsgemeinschaft.

APPENDIX A: CLASSICAL FLUID DYNAMICS

In classical fluid dynamics (cf., e.g., Refs. [49,59]), the flow of a medium is described in terms of the density field $n(\mathbf{r}, t)$, the velocity field $\mathbf{u}(\mathbf{r}, t)$, and the stress tensor $\Pi(\mathbf{r}, t)$. The first governing equation is the continuity equation,

$$D_t n = -n \nabla \cdot \mathbf{u}, \quad (\text{A1})$$

where the material or convective derivative $D_t = \partial_t + \mathbf{u} \cdot \nabla$ describes the rate of change following the fluid. An important special case is provided by incompressible flow corresponding to $\nabla \cdot \mathbf{u} = 0$. In this case the rhs of the continuity equation vanishes and the density is just transported or advected with the flow, i.e., no compression and rarefaction takes place.

To determine the velocity field a second evolution equation is required; the momentum balance

$$m D_t \mathbf{u} = \frac{1}{n} \nabla \cdot \Pi - \nabla v_{\text{ext}}. \quad (\text{A2})$$

Here, the divergence of the stress tensor Π represents internal forces whereas $\nabla v_{\text{ext}}(\mathbf{r}, t)$ describes external body forces acting on the fluid. $\Pi_{ij} = -p \delta_{ij} + \sigma_{ij}$ contains the scalar hydrostatic pressure $p(\mathbf{r}, t)$, a nonideal contribution, and the viscous shear-stress tensor $\sigma_{ij}(\mathbf{r}, t)$. These quantities have to be determined from constitutive equations, which formally close the system of equations. For a classical Newtonian fluid,

$$\sigma_{ij} = \eta \left[\partial_j u_i + \partial_i u_j - \frac{2}{3} \delta_{ij} \nabla \cdot \mathbf{u} \right] + \zeta \delta_{ij} \nabla \cdot \mathbf{u}, \quad (\text{A3})$$

where η and ζ are the shear and the bulk viscosity of the liquid. These material properties and an equation of state for the pressure p are required as further input into the theory. For constant η and ζ Eq. (A2) turns into the famous Navier-Stokes equation.

Obviously σ depends on spatial derivatives of the velocity field and accounts for viscous effects in the fluid. It is set to zero for an inviscid flow for which the Navier-Stokes equation reduces to the Euler equation,

$$m D_t \mathbf{u} = -\frac{1}{n} \nabla p - \nabla v_{\text{ext}}. \quad (\text{A4})$$

The absence of dissipation in the latter equation is the reason for major differences to the Navier-Stokes equation: flow governed by the Euler equation can build up shocks that would otherwise be attenuated by dissipation. Furthermore, viscous effects are crucial in the context of turbulence, which is the prevalent flow state of most classical fluids. These phenomena are all related to the intrinsic nonlinearity of both the Euler and Navier-Stokes equations, which is provided by the term $\mathbf{u} \cdot \nabla \mathbf{u}$ in the convective derivative.

We conclude this short review with the 1D version of the Navier-Stokes equation for the z component u ,

$$mD_t\mu = \frac{1}{n}\partial_z\tilde{p} - \partial_z v_{\text{ext}}, \quad (\text{A5})$$

where the stress-tensor Π has taken the form of a generalized pressure \tilde{p} . Naturally the latter still contains the hydrostatic pressure p and dynamical contributions from σ_{zz} .

APPENDIX B: QUANTUM FLUID DYNAMICS

While the classical hydrodynamic equations just represent a continuum approximation to the classical mechanics of point particles, many-body quantum mechanics based on the continuous wave function can be exactly transformed into quantum fluid dynamics (QFD) [28].

The derivation for a single-particle wave function $\varphi(\mathbf{r}, t)$ [12] starts by inserting $\varphi(\mathbf{r}, t) = R(\mathbf{r}, t)e^{i\alpha(\mathbf{r}, t)}$ with R and α real into

$$i\hbar\partial_t\varphi(\mathbf{r}, t) = \left(-\frac{\hbar^2}{2m}\nabla^2 + v_{\text{ext}}(\mathbf{r}, t)\right)\varphi(\mathbf{r}, t). \quad (\text{B1})$$

Separating real and imaginary parts of the equation, realizing that $R^2 = |\varphi|^2 = n$, and defining $\mathbf{u} = \frac{\hbar}{m}\nabla\alpha$ one arrives at

$$D_t n = -n\nabla\cdot\mathbf{u} \quad (\text{B2})$$

and

$$mD_t u_j = -\frac{1}{n}\partial_i P_{ij} - \partial_j v_{\text{ext}}, \quad (\text{B3})$$

where

$$P_{ij} = \frac{\hbar^2}{4m}\left(\frac{(\partial_i n)(\partial_j n)}{n} - \delta_{ij}\nabla^2 n\right) \quad (\text{B4})$$

is the quantum stress tensor [14,24,28]. The obtained equations show a strong analogy to the continuity and Navier-Stokes equations for classical fluids as presented before.

The QFD equations for the time-dependent two-electron singlet KS system can be derived in the same way using $R^2 = |\varphi|^2 = n/2$ and v_s instead of v_{ext} or by evaluating the general many-particle form of the noninteracting stress tensor P_{sij} [24–26] for the time-dependent singlet KS wave function. After all factors of 2 have canceled out, we are left with

$$D_t n = -n\nabla\cdot\mathbf{u}_s \quad (\text{B5})$$

and

$$mD_t u_{sj} = -\frac{1}{n}\partial_i P_{sij} - \partial_j v_s, \quad (\text{B6})$$

where P_{sij} is given by Eq. (B4). Consequently the only difference to the one particle case is that the effective potential v_s still contains two density-dependent contributions v_{hx} and

v_c . The most appropriate way to deal with v_{hx} is via a separate Poisson equation,

$$\Delta v_{\text{hx}} = -2\pi e^2 n, \quad (\text{B7})$$

as in the theory of conducting fluids [60]. On the other hand the unknown v_c is clearly related to internal forces within the system. In analogy with Eq. (A2) it thus makes sense to define the correlation contribution to the stress tensor according to

$$\nabla p_c = n\nabla v_c \quad (\text{B8})$$

and group it together with P_{sij} so that [29]

$$mD_t u_{sj} = -\frac{1}{n}\partial_i(P_{sij} + \delta_{ij}p_c) - \partial_j(v_{\text{hx}} + v_{\text{ext}}). \quad (\text{B9})$$

It is also interesting to note that the QFD point of view opens up connections to other fields of physics. The Madelung fluid concept [12] for instance is also employed in the study of solitary waves and the nonlinear Schrödinger equation [43].

APPENDIX C: BEYOND THE 1D TWO-ELECTRON SYSTEM

The basic structure of the QFD equations is not modified for systems of more than two electrons in three dimensions. Thus the adiabatic approximation can still be interpreted as neglecting xc contributions that depend on gradients of the velocity field.

We have seen that in 1D velocity gradients can occur only for compressive flow, which leads to dissipation of classical kinetic energy and can be detected by the proposed criterion. In three dimensions shear flow is another possible source of dissipation through internal friction. Quite appropriately $T_{s,0}$ is governed by

$$\dot{T}_{s,0}(t) = -\int (\partial_j u_{si})P_{s,0ji}d^3r, \quad (\text{C1})$$

which means that it is not only sensitive to compression, where $\nabla\cdot\mathbf{u}_s \neq 0$ ($i=j$), but also to shear velocity gradients ($i \neq j$) multiplied by off-diagonal elements of $P_{s,0ji}$. As the time-scale argument based on the xc kernel does also remain valid the criterion can thus be formulated as in one dimension.

Of course the presence of more than two particles means that different single-particle currents can contribute to the total current. Whether this will lead to additional nonadiabatic effects that are not detected by the proposed criterion cannot be established at present. However the violation of the breakdown criterion should still provide a definitive warning signal for an ongoing TDKS calculation.

- [1] *Time-Dependent Density Functional Theory*, edited by M. Marques, C. Ullrich, F. Nogueira, A. Rubio, K. Burke, and E. Gross (Springer, Berlin, 2006).
- [2] P. B. Corkum and F. Krausz, *Nat. Phys.* **3**, 381 (2007).
- [3] M. Lein, E. K. U. Gross, and J. P. Perdew, *Phys. Rev. B* **61**, 13431 (2000).
- [4] N. T. Maitra, F. Zhang, R. J. Cave, and K. Burke, *J. Chem. Phys.* **120**, 5932 (2004).
- [5] P. Hessler, N. T. Maitra, and K. Burke, *J. Chem. Phys.* **117**, 72 (2002).
- [6] H. O. Wijewardane and C. A. Ullrich, *Phys. Rev. Lett.* **95**, 086401 (2005).
- [7] C. A. Ullrich and I. V. Tokatly, *Phys. Rev. B* **73**, 235102 (2006).
- [8] C. A. Ullrich, *J. Chem. Phys.* **125**, 234108 (2006).
- [9] H. O. Wijewardane and C. A. Ullrich, *Phys. Rev. Lett.* **100**, 056404 (2008).
- [10] I. D'Amico and G. Vignale, *Phys. Rev. B* **59**, 7876 (1999).
- [11] M. Thiele, E. K. U. Gross, and S. Kümmel, *Phys. Rev. Lett.* **100**, 153004 (2008).
- [12] E. Madelung, *Z. Phys.* **40**, 322 (1926).
- [13] K.-K. Kan and J. J. Griffin, *Phys. Rev. C* **15**, 1126 (1977).
- [14] S. K. Ghosh and B. M. Deb, *Phys. Rep.* **92**, 1 (1982).
- [15] B. M. Deb and S. K. Ghosh, *J. Chem. Phys.* **77**, 342 (1982).
- [16] E. Runge and E. K. U. Gross, *Phys. Rev. Lett.* **52**, 997 (1984).
- [17] E. K. U. Gross, J. F. Dobson, and M. Petersilka, in *Density Functional Theory*, edited by R. F. Nalewajski (Springer, Berlin, 1996), pp. 81–172.
- [18] R. van Leeuwen, *Phys. Rev. Lett.* **82**, 3863 (1999).
- [19] S. Kümmel, K. Andrae, and P.-G. Reinhard, *Appl. Phys. B: Lasers Opt.* **73**, 293 (2001).
- [20] K. Capelle, *J. Chem. Phys.* **119**, 1285 (2003).
- [21] J. F. Dobson, *Phys. Rev. Lett.* **73**, 2244 (1994).
- [22] G. Vignale and W. Kohn, *Phys. Rev. Lett.* **77**, 2037 (1996).
- [23] G. Vignale, C. A. Ullrich, and S. Conti, *Phys. Rev. Lett.* **79**, 4878 (1997).
- [24] I. V. Tokatly, *Phys. Rev. B* **71**, 165104 (2005).
- [25] I. V. Tokatly, *Phys. Rev. B* **71**, 165105 (2005).
- [26] I. V. Tokatly, in *Time-Dependent Density Functional Theory*, edited by M. Marques, C. Ullrich, F. Nogueira, A. Rubio, K. Burke, and E. Gross (Springer, Berlin, 2006), pp. 123–136.
- [27] R. D'Agosta and M. Di Ventra, *J. Phys.: Condens. Matter* **18**, 11059 (2006).
- [28] R. D'Agosta and M. Di Ventra, *J. Phys.: Condens. Matter* **20**, 374102 (2008).
- [29] J. Tao, G. Vignale, and I. V. Tokatly, *Phys. Rev. Lett.* **100**, 206405 (2008).
- [30] D. Bauer, *Phys. Rev. A* **56**, 3028 (1997).
- [31] D. G. Lappas, A. Sanpera, J. B. Watson, K. Burnett, P. L. Knight, R. Grobe, and J. H. Eberly, *J. Phys. B* **29**, L619 (1996).
- [32] D. G. Lappas and R. van Leeuwen, *J. Phys. B* **31**, L249 (1998).
- [33] W.-C. Liu, J. H. Eberly, S. L. Haan, and R. Grobe, *Phys. Rev. Lett.* **83**, 520 (1999).
- [34] M. Lein, E. K. U. Gross, and V. Engel, *Phys. Rev. Lett.* **85**, 4707 (2000).
- [35] S. L. Haan and R. Grobe, *Laser Phys.* **8**, 885 (1998).
- [36] P. Hohenberg and W. Kohn, *Phys. Rev.* **136**, B864 (1964).
- [37] M. Lein and S. Kümmel, *Phys. Rev. Lett.* **94**, 143003 (2005).
- [38] A. S. de Wijn, S. Kümmel, and M. Lein, *J. Comput. Phys.* **226**, 89 (2007).
- [39] N. T. Maitra, K. Burke, and C. Woodward, *Phys. Rev. Lett.* **89**, 023002 (2002).
- [40] G. Vignale, *Phys. Rev. Lett.* **74**, 3233 (1995).
- [41] This choice of parameters leads to density distributions that can be well represented on the used numerical grid.
- [42] N. Maitra, K. Burke, H. Appel, E. Gross, and R. van Leeuwen, in *Ten Topical Questions in Time-Dependent Density Functional Theory*, edited by K. D. Sen (World Scientific, Singapore, 2002), pp. 1186–1225.
- [43] R. Fedele and H. Schamel, *Eur. Phys. J. B* **27**, 313 (2002).
- [44] G. Giuliani and G. Vignale, *Quantum Theory of the Electron Liquid* (Cambridge University Press, Cambridge, 2005).
- [45] C. A. Ullrich and G. Vignale, *Phys. Rev. B* **58**, 15756 (1998).
- [46] C. A. Ullrich and K. Burke, *J. Chem. Phys.* **121**, 28 (2004).
- [47] F. Calvayrac, P. G. Reinhard, E. Suraud, and C. A. Ullrich, *Phys. Rep.* **337**, 493 (2000).
- [48] R. D'Agosta and G. Vignale, *Phys. Rev. Lett.* **96**, 016405 (2006).
- [49] D. Acheson, *Elementary Fluid Dynamics* (Clarendon, Oxford, 1990).
- [50] It appears highly unlikely that the frequency dependence of the inverse interacting and noninteracting response functions directly cancels at the lowest transition frequency.
- [51] R. Baer, e-print arXiv:0808.3848, *J. Mol. Struct.: THEOCHEM* (in press).
- [52] M. Thiele and S. Kümmel, *Phys. Chem. Chem. Phys.* (in press).
- [53] Y. Kurzweil and R. Baer, *Phys. Rev. B* **72**, 035106 (2005).
- [54] Y. Kurzweil and R. Baer, *Phys. Rev. B* **73**, 075413 (2006).
- [55] E. Orestes, K. Capelle, A. B. F. da Silva, and C. A. Ullrich, *J. Chem. Phys.* **127**, 124101 (2007).
- [56] J. F. Dobson, M. J. Bünner, and E. K. U. Gross, *Phys. Rev. Lett.* **79**, 1905 (1997).
- [57] C. A. Ullrich, U. J. Gossmann, and E. K. U. Gross, *Phys. Rev. Lett.* **74**, 872 (1995).
- [58] I. V. Tokatly, *Phys. Rev. B* **75**, 125105 (2007).
- [59] G. K. Batchelor, *An Introduction to Fluid Dynamics* (Cambridge University Press, Cambridge, 1967).
- [60] J. Goedbloed and S. Poedts, *Principles of Magnetohydrodynamics* (Cambridge University Press, Cambridge, 2004).

Publication 3

*Photoabsorption spectra from adiabatically exact
time-dependent density-functional theory in real time*

M. Thiele, S. Kümmel,
Phys. Chem. Chem. Phys. **11**, 4631 (2009).

Reproduced by permission of The Royal Society of Chemistry.
<http://www.rsc.org/Publishing/Journals/CP/article.asp?doi=b902567g>

Photoabsorption spectra from adiabatically exact time-dependent density-functional theory in real time

Mark Thiele and Stephan Kümmel*

Received 6th February 2009, Accepted 23rd March 2009

First published as an Advance Article on the web 22nd April 2009

DOI: 10.1039/b902567g

Photoabsorption spectra for 2-electron singlet systems are obtained from the real-time propagation of the time-dependent Kohn–Sham equations in the adiabatically exact approximation. The latter is provided by the exact ground state exchange–correlation potential corresponding to the instantaneous density. The results are compared to exact data obtained from the solution of the interacting Schrödinger equation. We find that the adiabatically exact approximation provides very good results for transitions of genuinely single excitation character but yields incorrect results if double excitations contribute substantially. However, the extent of the error can vary: some double excitations are just shifted in energy whereas others are missed completely. These situations are analyzed with the help of transition densities.

I. Introduction

The importance of time-dependent linear response theory for the study of electronic matter can hardly be overestimated. From the calculation of dynamic polarizabilities, van der Waals coefficients and frequency-dependent dielectric constants to excitation spectra, linear response theory has a broad range of applications for atoms, molecules, clusters, and solid-state systems.^{1–6}

For the treatment of electrical response in the absence of magnetic fields time-dependent density-functional response theory is by now the most important method available. Its first application to the calculation of photoabsorption cross-sections of atoms⁷ even predates its formal foundation within the framework of time-dependent density functional theory (TDDFT).⁸ TDDFT in the time-dependent Kohn–Sham (TDKS) framework maps the interacting many-electron problem onto a system of non-interacting particles which yield the same time-dependent density $n(\mathbf{r}, t)$. The evolution of the corresponding single-particle Schrödinger equations is governed by an effective potential incorporating all non-classical many-body effects into an exchange correlation (xc) contribution $v_{xc}(\mathbf{r}, t)$. The xc potential is a well-defined but generally unknown functional of the time-dependent density that needs to be approximated in TDDFT applications.

A rigorous method to calculate excitation energies^{9–11} within linear response is based on the time-dependent exchange correlation kernel

$$f_{xc}[n](\mathbf{r}, t, \mathbf{r}', t') = \left. \frac{\delta v_{xc}[n](\mathbf{r}, t)}{\delta n(\mathbf{r}', t')} \right|_{n_0}, \quad (1.1)$$

i.e. the functional derivative of the xc potential taken at the ground state density $n_0(\mathbf{r})$. It is the crucial ingredient of the systematic way to derive the excitation energies of the exact

system from the Kohn–Sham (KS) eigenvalues and orbitals of static density functional theory (DFT). This approach, which is most frequently used in the matrix formulation of Casida,¹¹ thus relies crucially on the density-functional approximations for the exact ground state xc-potential and for the time- or frequency-dependent f_{xc} . The latter is, by rigorous definition, just the functional derivative given in eqn (1.1), but in practice is frequently treated as a quantity that is approximated independently. It is usually applied in the adiabatic approximation where the frequency dependence or memory effects of f_{xc} , *i.e.*, its nonlocal-in-time relation to the density, are neglected. This approximation is not able to reproduce all of the transition energies of the exact spectrum.¹² The missing energy differences have been found to be connected to transitions to states with significant double or multiple excitation character.^{12–17}

A second way of calculating excitation energies is provided by the propagation (real-time solution) of the TDKS equations. Here the photoabsorption spectrum is obtained from time-dependent dipole^{18–21} or higher order moments²² of an initially perturbed electronic configuration. Beside an accurate initial state this method requires an approximation of the exact time-dependent v_{xc} . Once again, most available approximations are adiabatic, *i.e.*, neglecting memory effects in v_{xc} , so the problem with respect to states of multiple excitation character persists.

Consequently, the shortcomings of the adiabatic approximation to f_{xc} or v_{xc} that are responsible for the missing multiply excited states are attracting considerable attention.^{12,23} However, the issue is an involved one as basically all available approximations are not only adiabatic in time but also lack the correct spatially nonlocal dependency on the density. Thus, errors due to missing temporal nonlocality and incorrect spatial nonlocality are indistinguishably entangled in these approximations. In order to rigorously determine the consequences of the adiabatic approximation one needs to compare exact excitation energies to those obtained with the adiabatically exact f_{xc} or v_{xc} , *i.e.*, functionals

Physikalisches Institut, Universität Bayreuth, D-95440, Bayreuth, Germany. E-mail: stephan.kuettel@uni-bayreuth.de

that are adiabatic in time but have the fully correct spatial dependency on the density.

A reliable scheme which allows to numerically construct the adiabatically exact (AE) approximation for v_{xc} has recently been developed for the propagation approach.²⁴ Its basic idea is to replace the time-dependent v_{xc} by the exact ground-state xc-potential $v_{xc,0}$ corresponding to the instantaneous density. In order to perform the desired comparison, one needs to resort to simple systems like the 2-electron singlet in one dimension, where both the exact and the adiabatically exact real-time propagations are possible.^{24–27} Previous studies of these model systems have concentrated on the regime of strong, nonperturbative, nonlinear excitations. In this article we will extend the developed methods to the real-time calculation of linear response photoabsorption spectra. The exact quantities as obtained from the propagation of the interacting time-dependent Schrödinger equation (TDSE) are compared to those stemming from the solution of the TDKS equations in the adiabatically exact approximation (AE-TDKSE).

This comparison reveals that some excitations are very accurately reproduced by the adiabatically exact approximation while others are found at wrong energies or are not present altogether. As we will see, the reproduced transitions can be related to single excitations and the failures to states having substantial double excitation character. We also demonstrate that transition densities can provide valuable additional and complementary information.

The article is organized as follows: in section two we introduce the governing equations of the studied systems and the boost-method used for the linear response calculations. Section three comprises our results including the spectra and transition densities before we provide a summary in section four.

II. Theoretical background

In the following section we introduce the governing equations of the 2-electron singlet system and the real-time formalism for linear response calculations. We will only consider the case of one spatial dimension, z .

A Governing equations for the 2-electron singlet system

The one-dimensional (1D) 2-electron system is described by the Hamiltonian operator

$$H_0 = \sum_{j=1,2} \left(-\frac{\hbar^2}{2m} \frac{d^2}{dz_j^2} + v_{\text{ext},0}(z_j) \right) + V_{\text{ee}}(|z_1 - z_2|), \quad (2.2)$$

where $v_{\text{ext},0}(z_j)$ is the external ground-state potential and $V_{\text{ee}}(|z_1 - z_2|)$ represents the symmetric electron–electron interaction. In order to deal with the Coulomb singularity in 1D we employ the soft-core interaction $W(z) = e^2/\sqrt{z^2 + 1}$ for V_{ee} (always) and for the external potential whenever we consider the helium atom. This 1D model system has been found to reproduce the essential features of correlated electron dynamics.^{28–36}

The eigenstates $\psi_i(z_1, z_2)$ of (2.2) are the solutions of the interacting static Schrödinger equation (SE)

$$H_0 \psi_i = E_i \psi_i \quad (2.3)$$

with eigenvalues E_i . Due to the reduced dimensionality of the problem it is possible to calculate the lower eigenvalues and eigenstates with moderate computational effort. In the present work the i th eigenstate is obtained by an imaginary time-propagation,³⁷ where any contributions of states ψ_j with $j < i$ are projected out. The eigenstates will always have definite parity

$$\psi_i(z_1, z_2) = \pm \psi_i(-z_1, -z_2) \quad (2.4)$$

and be (anti)symmetric with respect to exchange of the electrons, *i.e.* $\psi_i(z_1, z_2) = \pm \psi_i(z_2, z_1)$. As we are not interested in triplet states with parallel spins here, we exclude the antisymmetric spatial wave functions. The obtainable E_i will allow us to compare eigenvalue differences to the excitation energies found in the absorption spectra (see below). While the ground state ψ_0 provides the initial state for all time-dependent calculations, the eigenstates ψ_i can be used to construct the transition density

$$\rho_{if}(z) = 2 \int dz' \psi_i(z, z') \psi_f(z, z') \quad (2.5)$$

between the states i and f .

Finally, as a closing remark on the static equations presented so far, we note that it is an important aspect of our work that in 1D it is possible to numerically invert the SE²⁴ to find $v_{\text{ext},0}(z)$ for a given ground state density $n_0(z)$. This will also prove to be extremely useful in the (TD)DFT case which we discuss below.

The time-evolution of a general symmetric wave function $\psi(z_1, z_2, t)$ follows from the solution of the time-dependent Schrödinger equation, $i\hbar \partial_t \psi = H \psi$, governed by

$$H = \sum_{j=1,2} \left(-\frac{\hbar^2}{2m} \frac{d^2}{dz_j^2} + v_{\text{ext}}(z_j, t) \right) + V_{\text{ee}}(|z_1 - z_2|) \quad (2.6)$$

with the time-dependent external potential v_{ext} . The exact electron density can always be obtained through

$$n(z, t) = 2 \int |\psi(z, z', t)|^2 dz'. \quad (2.7)$$

Within standard KS-DFT the two-electron singlet system is mapped onto a system of two noninteracting particles in the same spatial orbital $\varphi(z)$. This means that we are only dealing with one occupied Kohn–Sham orbital. The stationary Kohn–Sham orbitals follow from the Kohn–Sham equation (KSE)

$$\left(-\frac{\hbar^2}{2m} \frac{d^2}{dz^2} + v_{s,0}(z) \right) \varphi_i(z) = \varepsilon_i \varphi_i(z). \quad (2.8)$$

The evolution of a general orbital $\varphi(z, t)$ is governed by the time-dependent Kohn–Sham equation (TDKSE)

$$i\hbar \partial_t \varphi(z, t) = \left(-\frac{\hbar^2}{2m} \frac{d^2}{dz^2} + v_s(z, t) \right) \varphi(z, t). \quad (2.9)$$

The effective potentials $v_{s,0}$ and v_s are unique functionals of the densities $n_0(z) = 2|\varphi_0(z)|^2$ and $n(z, t) = 2|\varphi(z, t)|^2$, respectively, by virtue of the Hohenberg–Kohn and the Runge–Gross theorem.^{8,38}

For our studies, it is a most relevant feature of the KSE that it can be inverted to obtain the $v_{s,0}(z, t_0)$ corresponding to a given density $n_0(z) = n(z, t_0)$ at a fixed time t_0 (*i.e.*, interpreting

$n(z, t_0)$ as a ground-state density). In this way the exact ground state xc potential can be obtained from

$$v_{s,0}(z, t_0) = v_{\text{ext},0}(z, t_0) + v_{\text{h}}(z, t_0) + v_{\text{xc},0}(z, t_0), \quad (2.10)$$

where $v_{\text{ext},0}$ follows from the SE inversion mentioned above and $v_{\text{h}}(z, t_0) = \int n(z', t_0) V_{\text{ee}}(|z - z'|) dz'$ is the Hartree potential. $v_{\text{xc},0}$ is thus a spatially nonlocal functional of the corresponding ground state density. For the two-electron singlet system the exchange contribution to v_{xc} is simply $v_{\text{x}} = -1/2v_{\text{h}}$ so that in the following $v_{\text{hx}} = v_{\text{h}} + v_{\text{x}} = 1/2v_{\text{h}}$ will often be separated from v_{c} .

On the other hand, the exact time-dependent quantities are related to v_{ext} of eqn (2.6) *via* the usual expression

$$v_{\text{s}}(z, t) = v_{\text{ext}}(z, t) + v_{\text{h}}(z, t) + v_{\text{xc}}(z, t). \quad (2.11)$$

When the initial state is the ground state, the xc potential at any given time t is a spatially nonlocal functional of the exact time-dependent density n at all previous times, *i.e.*, $v_{\text{xc}}(z, t) = v_{\text{xc}}[n(z', t')](z, t)$ where $t' \leq t$. The nonlocal dependency of v_{xc} on the density with respect to time is usually referred to as “memory effects” being present in the xc potential.³⁹

As mentioned above these memory effects of v_{xc} (or equivalently the frequency dependence of f_{xc}) are crucial for TDDFT to reproduce the complete spectrum of excitations. Hence it is of considerable interest to study the specific situation when only the memory effects are missed by the employed approximation while the spatial dependence is taken into account exactly. This can be realized by the adiabatically exact approximation which is defined by treating the time-dependent density at a fixed time $t = t_0$ as a ground state density, *i.e.*, $n(z, t_0) = n_0(z)$, and by replacing $v_{\text{xc}}(z, t_0)$ by the exact $v_{\text{xc},0}[n_0(z')](z)$ of ground state DFT. The latter quantity is generally unknown. However, it can be constructed numerically for 1D 2-electron singlet systems by using eqn (2.10).²⁴ This substitution ensures that the full spatial nonlocality of v_{xc} is treated exactly while memory effects are excluded. In this respect, the adiabatically exact approximation is fundamentally different from commonly used adiabatic approximations. It offers the chance to investigate exclusively the influence of memory effects on the excitation spectrum, allowing for unprejudiced insights into the nature of memory in v_{xc} .

B Excitation energies from real-time TDDFT

In order to obtain photoabsorption spectra from propagating the TDSE or AE-TDKSE we need to apply a small initial perturbation to the system. For the dipole response this is done by boosting the correlated wave function according to

$$\psi'(z_1, z_2) = \psi(z_1, z_2) e^{\frac{i}{\hbar} p_{\text{boost}}(z_1 + z_2)}, \quad (2.12)$$

(and similarly for the KS orbital), *i.e.*, giving the density distribution a spatially uniform initial velocity $u_0 = p_{\text{boost}}/m$ ^{18,20,22,40} with $p_{\text{boost}} = 0.01$ a.u. throughout. The boost parameter p_{boost} was chosen in such a way that the dipole response is first order in p_{boost} , *i.e.*, in the linear response regime. After that the system is propagated subject to the static external potential $v_{\text{ext},0}$ and the whole evolution of

the density $n(z, t)$ is recorded. From the latter we obtain the time-dependent dipole moment

$$d(t) = \int dz n(z, t) z. \quad (2.13)$$

In a similar way we obtain the quadrupole response by

$$\psi'(z_1, z_2) = \psi(z_1, z_2) e^{\frac{i}{\hbar} \eta_{\text{boost}}(z_1^2 + z_2^2)}, \quad (2.14)$$

corresponding to a linear initial velocity of $u_0 = (\eta_{\text{boost}}/m)z$ with $\eta_{\text{boost}} = 0.001$ a.u. throughout. In this case we track the quadrupole moment

$$q(t) = \int dz n(z, t) z^2. \quad (2.15)$$

Due to the one-dimensionality of the system both moments are just simple scalar expressions. As a consequence, the quadrupole moment can be viewed as rather similar to the monopole in our study. The Fourier transform of these quantities yields the dipole and quadrupole power spectra $|d(\omega)|^2$ and $|q(\omega)|^2$. We consider these quantities because they are numerically more stable than the dynamical polarizability and we are mainly interested in the positions and not the strengths of the single peaks.

The possibility to store the whole time-evolution of the density allows us to obtain the Fourier transform $\delta n(z, \omega)$ of the AE density fluctuation $\delta n(z, t)$. The former evaluated at the excitation frequency ω_{0f} is proportional to ρ_{0f} ,⁴¹ *i.e.*

$$\text{Im } \delta n(z, \omega_{0f}) \sim \rho_{0f}(z) \quad (2.16)$$

This allows us to qualitatively obtain the AE transition density ρ_{0f} from δn . The exact ρ_{0f} can of course be constructed from the eigenstates of the interacting SE, *cf.* eqn (2.5).

C Relation to the Casida matrix approach

A more common way to obtain linear response excitation energies within TDDFT is *via* the frequency-dependent xc kernel. The Casida equation¹¹ allows to derive the exact transition energies from (TD)DFT quantities. However, two density functionals are required as an input: first the ground state (DFT) $v_{\text{xc},0}$ is necessary to obtain the correct Kohn–Sham eigenvalues and eigenstates, secondly the frequency-dependent xc-kernel of TDDFT is needed to transform the KS eigenvalues into the exact excitation energies.

Another issue relevant for the Casida formulation is the error introduced by the truncation of the underlying infinite-dimensional matrix equation. It is reasonable to assume that this approximation will only affect the high transition energies. Naturally, a related problem occurs in real-time propagation, where excitations above a certain energy will no longer be represented on the chosen discrete time coordinate grid.

Finally, the Casida formalism requires diagonalization of the truncated matrix system. Here some approaches rely on the so-called single pole approximation.^{9,23} Obviously, questions related to the diagonalization are completely circumvented in the real-time propagation.

III. Results and discussion

In the following we investigate the spectra of characteristic 1D 2-electron systems: the soft-core helium atom^{24,30,31,34}

Table 1 Ground state properties of 1D 2-electron singlet systems studied in this article. All values are in Hartree atomic units

System	$v_{\text{ext,gs}}(z)$
Helium	$-2W(z)$
Hooke	$k/2z^{2a}$
A6-Hooke	$k/2(z^2 + \tilde{k}z^6)^a$

^a $k = 0.1$, $\tilde{k} = 0.01$.

characterized by the ground state potential $v_{\text{ext},0}(z) = -2W(z)$, “Hooke’s atom” with $v_{\text{ext},0}(z) = (k/2)z^2$ (Hooke) and the “anharmonic Hooke’s atom” characterized by $v_{\text{ext},0}(z) = (k/2)(z^2 + \tilde{k}z^6)$ (A6-Hooke) with $k = 0.1$ a.u. and $\tilde{k} = 0.01$ a.u.²⁷ (we use Hartree atomic units unless stated otherwise). The anharmonic term has been introduced to A6-Hooke to deliberately avoid the special properties of the harmonic system. The different systems are summarized in Table 1. The initial state for any time-dependent process is the ground state of the particular system. Quite generally, one should keep in mind that due to the finite numerical accuracy of the AE-TDKSE scheme, smaller spectral features should not be overinterpreted.

A Helium

The soft-core helium system has the typical features of an atomic system in the sense of decreasing energy level spacings up to the first ionization threshold followed by a continuous spectrum.^{28,31,33} This is reflected in the dipole and quadrupole power spectra shown in Fig. 1 and 2. The numerical reliability of the AE-TDKSE propagation results is restricted to the energy range below $\omega \approx 0.7$ a.u. In this regime, the inversion algorithms have converged sufficiently. The figures show that in the trust region the exact spectra are extremely well reproduced by the adiabatically exact ones. All transition peaks appear and are located almost at the exact energies. The latter were also calculated from the static SE (2.3) and agree with the values reported in Ref. 35. These findings imply that in this energy regime the xc kernel can only be weakly frequency dependent and the exact ground-state kernel is able

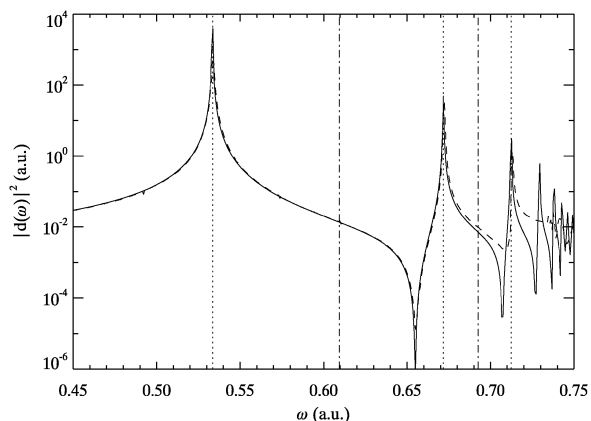


Fig. 1 Dipole power spectrum for helium obtained from TDSE (solid line) and AE-TDKSE (dashed line). Vertical lines indicate the first five transition energies from the ground state to singlet states of odd (dotted) and even parity (dotted-dashed) as obtained from eqn (2.3).

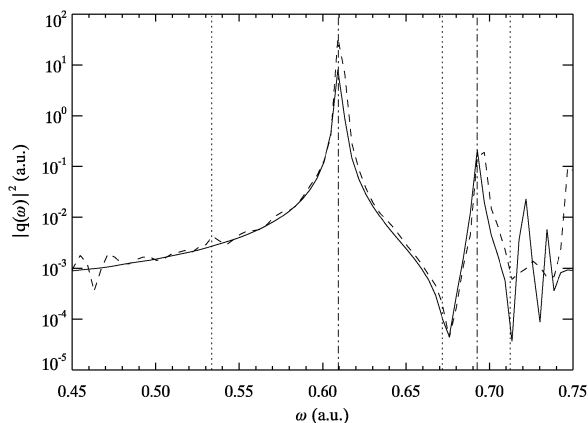


Fig. 2 Quadrupole power spectrum for helium obtained from TDSE (solid line) and AE-TDKSE (dashed line). Vertical lines indicate the first five transition energies from the ground state to singlet states of odd (dotted) and even parity (dotted-dashed) as obtained from eqn (2.3).

to reproduce all transitions correctly. Thus, for the helium atom the AE approximation is extremely powerful not only for strong, non-perturbative fields,²⁴ but also in the linear response regime.

In trying to understand the excellent performance of the AE approximation we now investigate the nature of the observed excitations. To this end we project the correlated final states ψ_f on symmetric KS product wave functions

$$\Phi_{ij}(z_1, z_2) = \begin{cases} \varphi_i(z_1)\varphi_j(z_2), & i = j \\ \frac{1}{\sqrt{2}}(\varphi_i(z_1)\varphi_j(z_2) + \varphi_j(z_1)\varphi_i(z_2)), & i \neq j \end{cases} \quad (3.17)$$

constructed from the exact occupied and unoccupied orbitals of eqn (2.8) for helium. In this way we can estimate the single and double excitation character of a correlated excited state with respect to the KS basis. Table 2 shows the overlap between the KS product states and the first six eigenstates of the helium Hamiltonian of eqn (2.2). States 1 to 5 are the final states of the transitions denoted with vertical lines in Fig. 1 and 2. Clearly they are completely dominated by states Φ_{ij} with single excitation character. This fits in with the general concept of energy levels in the helium atom where the single particle picture is known to work well.

Table 2 Projection amplitudes $|\langle \Phi_{ij} | \psi_f \rangle|^2$ of correlated singlet states ψ_f on KS product wave functions Φ_{ij} for the helium atom. Values less than 0.01 have been omitted

ij	f					
	0	1	2	3	4	5
00	0.99					
01		0.92		0.02		
02			0.97			
03		0.03		0.90		0.03
04					0.93	
05				0.05		0.82
06					0.04	
07						0.09
09						0.01
12		0.02				

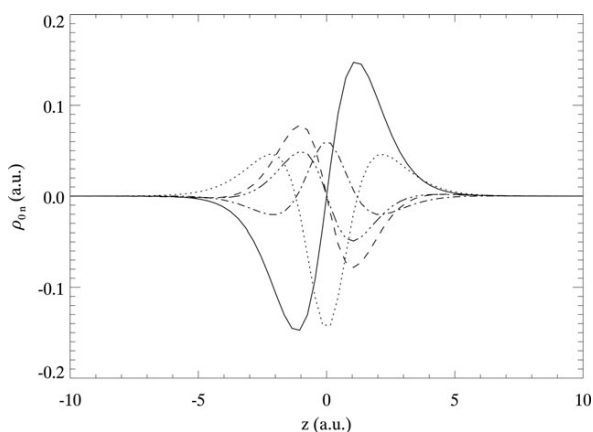


Fig. 3 Exact transition densities ρ_{0n} of helium excitations for $n = 1$ (solid), 2 (dotted), 3 (dashed) 4 (dotted-dashed) and 5 (triple-dotted-dashed).

The transition densities for helium are shown in Fig. 3. They can be interpreted as a momentary picture of the density redistribution during a transition: negative regions correspond to density removal while positive values signal density accumulation.^{42,43} As a consequence of symmetry, the transition density is always antisymmetric for dipole and symmetric for quadrupole excitations. For helium we find for the dipole transitions a purely left–right oscillation (sloshing mode) and for quadrupole transitions an inward–outward redistribution (breathing mode) of decreasing intensity for growing energy. These patterns provide a hydrodynamic interpretation of the electron motion during a transition.

The discussion so far and the excellent performance of the AE approximation begs the natural question: Where are the double excitations that are expected to be missed by the adiabatically exact approximation? Unfortunately (for our analysis), for the 1D helium atom they only appear above the first ionization threshold.^{28,44} The lowest double excitations are in fact embedded in the one particle ionization continuum and thus have the character of autoionizing or Fano resonances.^{45,46} They can only be expected at energies around 1.3 a.u.²⁸ which is far beyond the numerical accuracy of our AE-TDKSE scheme. Even if this regime could be reached, the peculiar degeneracy of a single and a double excitation which is characteristic of a Fano resonance would very likely complicate the analysis. Thus, we will now consider systems where the double excitations lie in the energy regime that can be resolved by the AE-TDKSE scheme.

To develop an intuition for what kind of systems one needs to study in order to find low-lying double-excitations, it is helpful to look at the problem from the KS perspective of independent particles. Due to the Coulombic asymptotics of the KS potential the single particle energy level spacing is quickly decreasing for growing energies (Rydberg series). This means that infinitely many single particle transitions are found at energies lower than one of the first double excitation. In order to circumvent this situation one needs a system with a more constant spacing of the energy levels. This requirement takes us to another typical 1D singlet system, namely Hooke's atom. Here the intuitive argument based on the KS transitions

implies that the excitation of two electrons to the first excited state (*i.e.*, a double excitation) will be roughly in the energy range of the transition of one electron to the second excited state (one of the lower single excitations).³⁶ As the energy spectrum of the harmonic external potential is completely discrete there is also no issue with Fano-type degeneracies.

B Hooke's atom

The dipole response of Hooke's atom is shown in Fig. 4. For this systems we found the AE-TDKSE results to be converged for $\omega < 1$ a.u. Here the power spectrum is more irregular with respect to the order of positive and negative parity than for helium. Clearly the dominant transition for dipole excitations is at the harmonic frequency $\omega_{01} = (k/m)^{\frac{1}{2}}$, which is well reproduced by the AE-TDKSE results. This agreement is a consequence of the fact that to first order linear response the dipole boost resembles an applied time-dependent dipole field. Thus the response to the latter in Hooke's atom is exactly reproduced by the adiabatically exact approximation due to the applicability of the harmonic potential theorem.^{27,47} The dominance of the harmonic frequency leads to suppression of higher dipole active transitions like $f = 4, 5$ in agreement with almost vanishing oscillator strengths of these excitations.⁴⁸

The quadrupole power spectrum (*cf.* eqn (2.14)) shown in Fig. 5 reveals that instead of the excitations $f = 2, 3$ there is only one transition at $\omega \approx 0.5$ a.u. in the AE approximation. Apparently we have finally encountered a situation where the adiabatically exact approximation does not yield the proper excitation frequency.

Consequently, we investigate once more the single particle character of the relevant excitations. The projections of the final states on the Hooke KS basis are shown in Table 3. We find that, in contrast to the helium atom, even the lower states have nonvanishing double excitation contributions. The transition $f = 1$, though, is still predominantly of single excitation character in agreement with the ability of the AE-TDKSE to reproduce the corresponding peak in the spectrum. For $f = 2, 3$ there is already a strong contribution

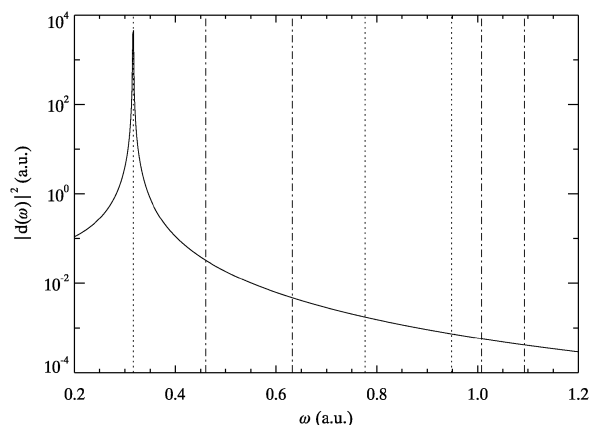


Fig. 4 Dipole power spectrum for Hooke's atom obtained from TDSE (solid line) and AE-TDKSE (dashed line directly on top). Vertical lines indicate transition energies of the ground state to singlet states of odd (dotted) and even parity (dotted-dashed).

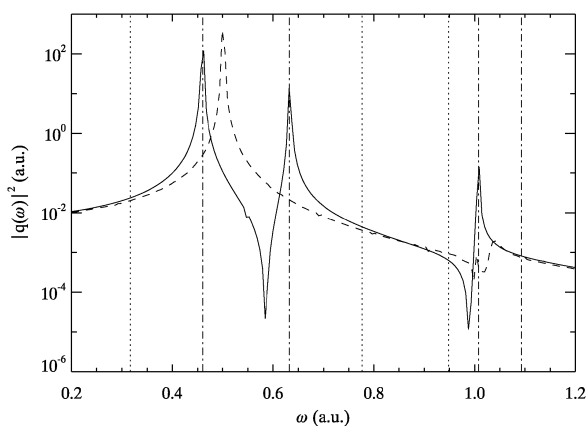


Fig. 5 Quadrupole power spectrum for Hooke's atom obtained from TDSE (solid line) and AE-TDKSE (dashed line). Vertical lines indicate transition energies of the ground state to singlet states of odd (dotted) and even parity (dotted-dashed).

Table 3 Projection amplitudes $|\langle \Phi_{ij} | \psi_f \rangle|^2$ of correlated singlet states ψ_f on KS product wave functions Φ_{ij} for Hooke. Values less than 0.01 have been omitted

ij	f						
	0	1	2	3	4	5	6
00	0.92		0.02	0.03			
01		0.81			0.10	0.05	
02			0.54	0.35			
03		0.03			0.72	0.18	
04				0.05			0.13
05						0.05	
11	0.07		0.43	0.40			
12		0.14			0.16	0.54	
13				0.02			0.49
14		0.01			0.02		
22				0.14			0.36
23						0.16	

of the Φ_{11} product state which can explain the failure of the AE-TDKSE in this energy regime.

To obtain a better understanding of the relevant excitations we once more look at the transition densities. For the first six excitations they are shown in Fig. 6 and 7. We find sloshing ($f = 1$) and breathing ($f = 2$) type excitations as in the helium atom but also higher order transitions ($f = 3-6$) that no longer show a structure which can easily be related to one of these two types.

The transition densities can further be used to sort out which excitation is reproduced by the AE approximation and which is not. Based on the structure of the transition density, one can identify which exact transition belongs to which (shifted) AE peak. The adiabatically exact transition densities obtained from the Fourier transform of the time-dependent density (see above) provide some evidence that the peak at $\omega \approx 0.5$ a.u. should correspond to the $f = 2$ excitation: as shown in Fig. 8 the structure of the first two transitions present in the AE spectrum closely resembles that of the exact excitations $f = 1, 2$. This means that the second transition is properly reproduced by the AE-TDKSE with respect to its breathing-type character but it is shifted to the wrong energy.

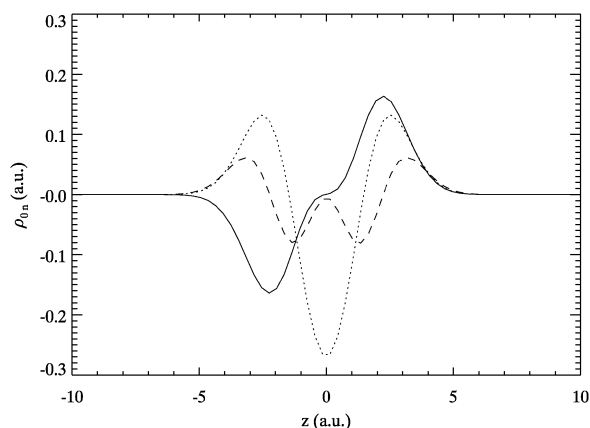


Fig. 6 Exact transition densities ρ_{0n} of Hooke excitations for $n = 1$ (solid), 2 (dotted) and 3 (dashed).

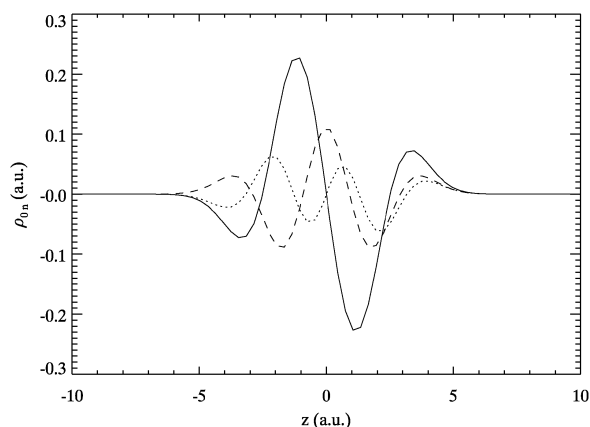


Fig. 7 Exact transition densities ρ_{0n} of Hooke excitations for $n = 4$ (solid), 5 (dotted) and 6 (dashed).

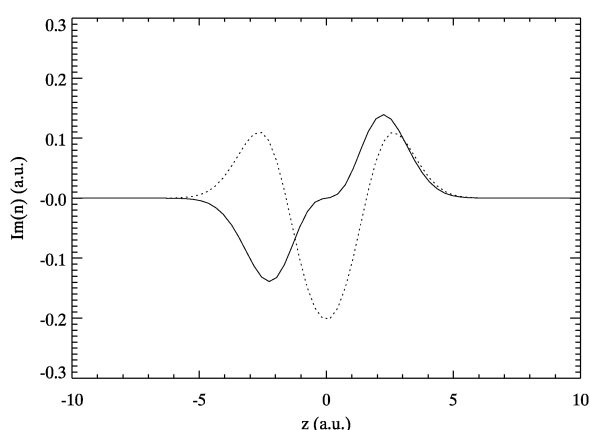


Fig. 8 Adiabatically exact transition densities of Hooke obtained from the Fourier transform of the time-dependent AE-TDKSE density (see text). The shown transition densities correspond to the adiabatically exact transitions found at $\omega \approx 0.32$ (solid) and 0.50 a.u. (dotted), cf. Fig. 4 and 5. All curves were scaled so that the peak heights are roughly the same to allow for better comparison with the exact transition densities of Fig. 6.

At the same time the $f = 3$ excitation is missed completely by the AE approximation. So despite the fact that in view of table 3 both the $f = 2$ and the $f = 3$ transitions could be termed “double excitations” the AE approximation treats them quite differently.

C Anharmonic Hooke’s atom

To obtain a more complex structure of the dipole response we finally turn to the anharmonic version of Hooke’s atom. The dipole power spectrum of A6-Hooke shown in Fig. 9 indicates that the first transition is well reproduced but the AE-TDKSE produces only one peak at $\omega \approx 1.3$ a.u. instead of the $f = 4$ and $f = 5$ excitations. These energies are still well within the numerical validity regime of the AE-TDKSE which extends up to $\omega \approx 1.8$ a.u. From the quadrupole power spectrum in Fig. 10 we can infer that the AE approximation produces a peak at $\omega \approx 0.77$ a.u. instead of the $f = 2$ and 3 peaks. By varying the boost parameter we found the peaks at $\omega \approx 0.88$ and 1.74 a.u. to be higher order effects that can be neglected in

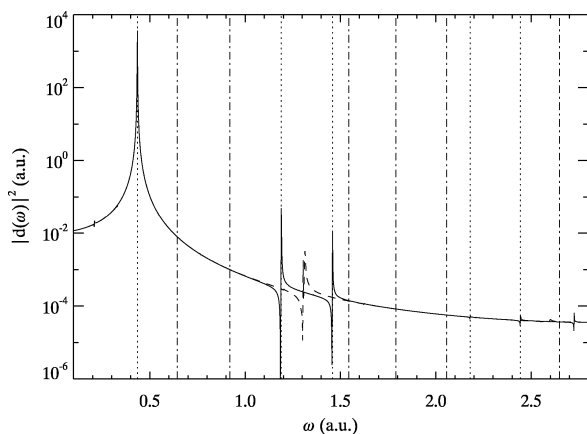


Fig. 9 Dipole power spectrum for A6-Hooke obtained from TDSE (solid line) and AE-TDKSE (dashed line). Vertical lines indicate transition energies of the ground state to singlet states of odd (dotted) and even parity (dotted-dashed).

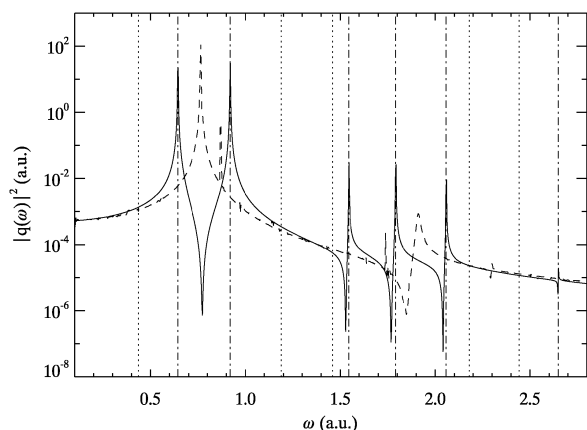


Fig. 10 Quadrupole power spectrum for A6-Hooke obtained from TDSE (solid line) and AE-TDKSE (dashed line). Vertical lines indicate transition energies of the ground state to singlet states of odd (dotted) and even parity (dotted-dashed).

our discussion of the linear response regime. The excitations to $f = 6,7$ are not present in the AE spectrum. One may speculate that the AE-TDKSE scheme might still be approximately valid around $\omega \approx 2$ a.u. and that thus the AE approximation reproduces only one peak ($\omega \approx 1.9$ a.u.) in the range of the $f = 6,7,8$ quadrupole triple. This would correspond to the AE-TDKSE producing only one peak among the quadrupole double $f = 2,3$ and the dipole double $f = 4,5$ respectively. In any case we have encountered two more situations where peaks are shifted to wrong energies or missing completely from the AE spectrum.

The projections for A6-Hooke are shown in Table 4. Again, a strong double excitation character is present for $f > 1$. One may wonder whether this difficulty is generally just a consequence of the chosen basis set. To check this we also used the single particle states corresponding to the $v_{\text{ext},0}$ of A6-Hooke as a basis (instead of the KS orbitals) and performed the overlap analysis once more. This leads to numbers quite similar to the ones reported in Table 4.

Once more the success for the $f = 1$ transition seems to be a consequence of the predominant single excitation character of ψ_1 . The failure for $f > 1$ is again a consequence of considerable double excitation contribution. It appears

Table 4 Projection amplitudes $|\langle \Phi_{ij} | \psi_f \rangle|^2$ of correlated singlet states ψ_f on KS product wave functions Φ_{ij} for A6-Hooke. Values less than 0.01 have been omitted

ij	f							
	0	1	2	3	4	5	6	7
00	0.95		0.03	0.02				
01		0.91			0.07			
02			0.31	0.63				0.03
03					0.36	0.61		
04								0.30
11	0.04		0.66	0.26				0.03
12		0.08			0.56	0.31		
13				0.02			0.32	0.43
14								
22				0.06			0.66	0.18
23						0.05		
33								0.02

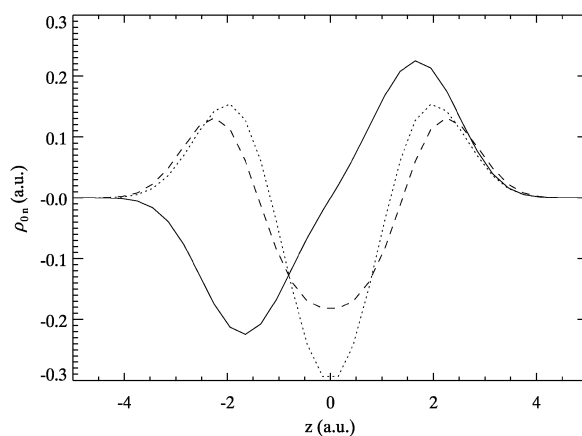


Fig. 11 Exact transition densities ρ_{0n} of A6-Hooke excitations for $n = 1$ (solid), 2 (dotted) and 3 (dashed).

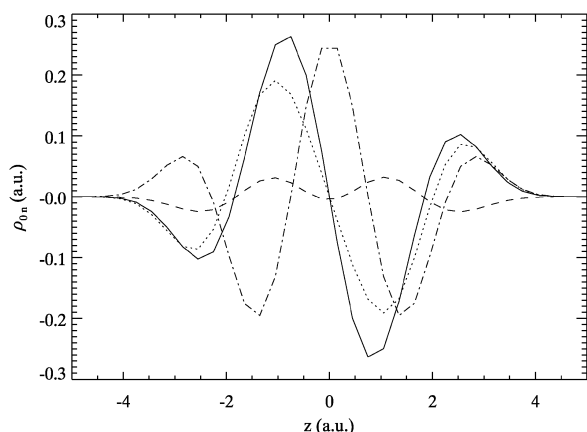


Fig. 12 Exact transition densities ρ_{0n} of A6-Hooke excitations for $n = 4$ (solid), 5 (dotted), 6 (dashed) and 7 (dotted-dashed).

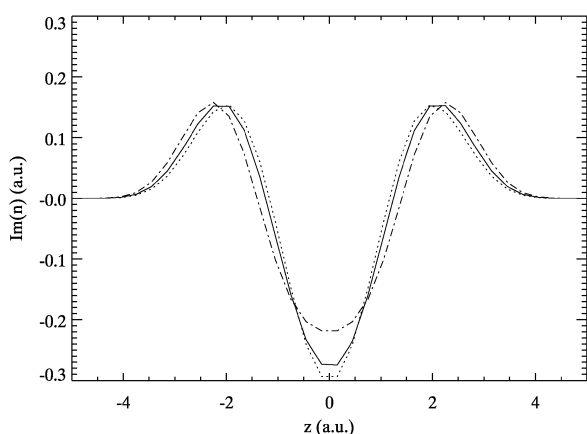


Fig. 13 AE transition density of A6-Hooke at $\omega \approx 0.77$ a.u. (solid) and the exact ρ_{0f} for $f = 2$ (dotted) and 3 (dotted-dashed). All curves were scaled to allow for better comparison.

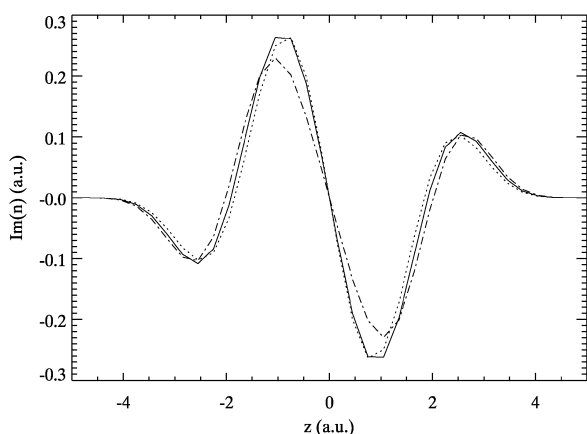


Fig. 14 AE transition density of A6-Hooke at $\omega \approx 1.3$ a.u. (solid) and the exact ρ_{0f} for $f = 4$ (dotted) and 5 (dotted-dashed). All curves were scaled to allow for better comparison.

especially plausible that $f = 6$ is missing as ψ_6 is exclusively of double excitation character.

The transition densities for A6-Hooke are shown in Fig. 11 to 12. Similar to Hooke's atom we only find exclusive sloshing and breathing signatures for the lowest transitions. The higher excitations show a variety of patterns.

For sorting out which AE excitation corresponds to which exact one the transition densities are again a helpful tool. Comparing the AE transition density at $\omega \approx 0.77$ to the ones for $f = 2$ and 3 in Fig. 13 shows that the AE excitation rather resembles $f = 2$. This implies that the latter transition is shifted to the wrong excitation energy while $f = 3$ is completely absent. This is noteworthy because ψ_3 has a smaller double excitation contribution than ψ_2 . A similar situation is found for $f = 4, 5$ as shown in Fig. 14.

IV. Summary and outlook

We have explored the performance of the adiabatically exact approximation—*i.e.*, no temporal nonlocality but full spatial nonlocality—for the linear response of 2-electron systems. It is known that this approximation is not able to generally provide the exact excitation energies. This property follows from the Casida equation in a formal way but one is only beginning to understand its practical consequences for the adiabatically exact spectrum.¹² In the present article we examine this relation more closely.

So far, it has commonly been assumed that adiabatic approximations are missing the transitions of double excitation character, or at least shift them to wrong energies. On the other hand they are expected to work for single excitations. We found that this concept generally applies to the AE approximation, but that the situation is involved when double excitations are present.

For the lower discrete part of the spectrum of the helium atom the transitions are of genuinely single excitation character and hence the AE-TDKSE reproduces all peaks of the exact spectrum. It even locates them at the virtually exact energies. These findings imply that the xc kernel in this energy regime is well represented by its $\omega \rightarrow 0$ limiting case, *i.e.*, the ground state kernel. This situation is a consequence of the special nature of the system. Here double excitations are to be expected only above the first ionization threshold where they take the form of autoionizing resonances embedded in the one particle continuum.

The situation is different in the Hooke-type systems that we studied. Here large parts of the spectrum are incorrectly predicted by the AE approximation, *i.e.*, peaks are shifted to wrong energies or missed completely. Already at the lower energies the double excitation character of a given transition is non-negligible. However, it is not straightforward to relate the failures for a specific transition to the corresponding magnitude of the double excitation contribution. Apparently it is not enough to consider the single particle character of an excitation to infer whether it will be missed or just shifted by the AE approximation.

We found transition densities to be a suitable tool to get deeper insight into the structure of specific excitations. Although they also do not provide a clear criterion to identify particularly nonadiabatic transitions, they allow for a better comparison of certain transitions and facilitate matching of

exact transitions to peaks that are incorrectly shifted in the AE spectrum.

Finally, the transition densities provide a route to a more intuitive hydrodynamic view of electronic excitations. Such a hydrodynamical perspective may be a new way to obtain an understanding of nonadiabatic effects.^{27,49}

Acknowledgements

We acknowledge financial support by the Deutsche Forschungsgemeinschaft.

References

- 1 J. F. Dobson and B. P. Dinte, *Phys. Rev. Lett.*, 1996, **76**, 1780.
- 2 G. F. Bertsch, J.-I. Iwata, A. Rubio and K. Yabana, *Phys. Rev. B*, 2000, **62**, 7998.
- 3 I. V. Tokatly and O. Pankratov, *Phys. Rev. Lett.*, 2001, **86**, 2078.
- 4 G. Onida, L. Reining and A. Rubio, *Rev. Mod. Phys.*, 2002, **74**, 601.
- 5 J. R. Chelikowsky, L. Kronik and I. Vasiliev, *J. Phys.: Condens. Matter*, 2003, **15**, R1517.
- 6 D. Rappoport and F. Furche, *J. Am. Chem. Soc.*, 2004, **126**, 1277.
- 7 A. Zangwill and P. Soven, *Phys. Rev. A*, 1980, **21**, 1561.
- 8 E. Runge and E. K. U. Gross, *Phys. Rev. Lett.*, 1984, **52**, 997.
- 9 M. Petersilka, U. Gossmann and E. K. U. Gross, *Phys. Rev. Lett.*, 1996, **76**, 1212.
- 10 E. K. U. Gross, J. F. Dobson and M. Petersilka, in *Density Functional Theory*, ed. R. F. Nalewajski, Springer, Berlin, 1996, pp. 81–172.
- 11 M. E. Casida, in *Recent Advances in Density Functional Methods, Part I*, ed. D. P. Chong, World Scientific Publishing, Singapore, 1995, pp. 155–192.
- 12 N. T. Maitra, F. Zhang, R. J. Cave and K. Burke, *J. Chem. Phys.*, 2004, **120**, 5932.
- 13 S. Hirata and M. Head-Gordon, *Chem. Phys. Lett.*, 1999, **302**, 375.
- 14 D. J. Tozer and N. C. Handy, *Phys. Chem. Chem. Phys.*, 2000, **2**, 2117.
- 15 R. J. Cave, F. Zhang, N. T. Maitra and K. Burke, *Chem. Phys. Lett.*, 2004, **389**, 39.
- 16 J. Neugebauer, E. J. Baerends and M. Nooijen, *J. Chem. Phys.*, 2004, **121**, 6155.
- 17 K. J. H. Giesbertz, E. J. Baerends and O. V. Gritsenko, *Phys. Rev. Lett.*, 2008, **101**, 033004.
- 18 K. Yabana and G. F. Bertsch, *Phys. Rev. B*, 1996, **54**, 4484.
- 19 U. Saalmann and R. Schmidt, *Z. Phys. D*, 1996, **38**, 153.
- 20 F. Calvayrac, P. G. Reinhard and E. Suraud, *Ann. Phys. (N.Y.)*, 1997, **255**, 125.
- 21 M. Marques, A. Castro, G. Bertsch and A. Rubio, *Comput. Phys. Commun.*, 2003, **151**, 60.
- 22 M. Mundt and S. Kümmel, *Phys. Rev. B*, 2007, **76**, 035413.
- 23 H. Appel, E. K. U. Gross and K. Burke, *Phys. Rev. Lett.*, 2003, **90**, 043005.
- 24 M. Thiele, E. K. U. Gross and S. Kümmel, *Phys. Rev. Lett.*, 2008, **100**, 153004.
- 25 I. D'Amico and G. Vignale, *Phys. Rev. B*, 1999, **59**, 7876.
- 26 P. Hessler, N. T. Maitra and K. Burke, *J. Chem. Phys.*, 2002, **117**, 72.
- 27 M. Thiele and S. Kümmel, *Phys. Rev. A*, 2009, submitted.
- 28 S. L. Haan, R. Grobe and J. H. Eberly, *Phys. Rev. A*, 1994, **50**, 378.
- 29 D. G. Lappas, A. Sanpera, J. B. Watson, K. Burnett, P. L. Knight, R. Grobe and J. H. Eberly, *J. Phys. B*, 1996, **29**, L619.
- 30 D. Bauer, *Phys. Rev. A*, 1997, **56**, 3028.
- 31 S. L. Haan and R. Grobe, *Laser Phys.*, 1998, **8**, 885.
- 32 D. G. Lappas and R. van Leeuwen, *J. Phys. B*, 1998, **31**, L249.
- 33 W.-C. Liu, J. H. Eberly, S. L. Haan and R. Grobe, *Phys. Rev. Lett.*, 1999, **83**, 520.
- 34 M. Lein, E. K. U. Gross and V. Engel, *Phys. Rev. Lett.*, 2000, **85**, 4707.
- 35 R. Panfili and W.-C. Liu, *Phys. Rev. A*, 2003, **67**, 043402.
- 36 E. Orestes, K. Capelle, A. B. F. da Silva and C. A. Ullrich, *J. Chem. Phys.*, 2007, **127**, 124101.
- 37 A. S. de Wijn, S. Kümmel and M. Lein, *J. Comput. Phys.*, 2007, **226**, 89.
- 38 P. Hohenberg and W. Kohn, *Phys. Rev.*, 1964, **136**, B864.
- 39 *Time-dependent Density Functional Theory*, ed. M. Marques, C. Ullrich, F. Nogueira, A. Rubio, K. Burke and E. Gross, Springer, Berlin, 2006.
- 40 M. Mundt, S. Kümmel, R. van Leeuwen and P.-G. Reinhard, *Phys. Rev. A*, 2007, **75**, 050501.
- 41 R. A. Broglia, G. Coló, G. Onida and H. E. Roman, *Solid State Physics of Finite Systems*, Springer, Berlin, 2004.
- 42 S. Kümmel, K. Andrae and P.-G. Reinhard, *Appl. Phys. B*, 2001, **73**, 293.
- 43 S. Tretiak and S. Mukamel, *Chem. Rev.*, 2002, **102**, 3171.
- 44 To the best of our knowledge this applies to all atomic systems.
- 45 U. Fano, *Phys. Rev.*, 1961, **124**, 1866.
- 46 H. Friedrich, *Theoretical Atomic Physics*, Springer, Heidelberg, 2006.
- 47 J. F. Dobson, *Phys. Rev. Lett.*, 1994, **73**, 2244.
- 48 The oscillator strengths $2|\langle\psi_0|z|\psi_j\rangle|^2\omega_{0j}$ can be computed directly from the exact eigenstates.
- 49 C. A. Ullrich and K. Burke, *J. Chem. Phys.*, 2004, **121**, 28.

Publication 4

*Reconstructing the adiabatic exchange-correlation kernel
of time-dependent density-functional theory*

M. Thiele, S. Kümmel,
Phys. Rev. A **80**, 012514 (2009).

Copyright 2009 by the American Physical Society.
<http://link.aps.org/doi/10.1103/PhysRevA.80.012514>

Reconstructing the adiabatic exchange-correlation kernel of time-dependent density-functional theory

M. Thiele and S. Kümmel

Physikalisches Institut, Universität Bayreuth, D-95440 Bayreuth, Germany

(Received 15 May 2009; published 24 July 2009)

The interacting and the Kohn-Sham static density-density response functions for different one-dimensional two-electron singlet systems are reconstructed numerically. From their inverse we obtain the exact static exchange-correlation kernel. This quantity represents the adiabatically exact approximation of the frequency-dependent exchange-correlation kernel that is crucial for time-dependent linear density-response theory. We investigate its performance for nonlocal perturbations and analyze its sum rule properties. We also compute the adiabatically exact transition energies that follow from the static kernel within linear-response theory.

DOI: [10.1103/PhysRevA.80.012514](https://doi.org/10.1103/PhysRevA.80.012514)

PACS number(s): 31.15.ee, 31.15.vj, 31.15.xp

I. INTRODUCTION

For the understanding of the electronic properties of a many-electron quantum system its transition energies are a valuable source of information. Experimentally, it is usually possible to determine these energies from photoabsorption spectra. On the theory side the ideal scenario would be to calculate the eigenvalues and eigenstates of the relevant Hamilton operator and to obtain the transition energies from eigenvalue differences. However, for many interacting electrons this is a prohibitively complicated task. Instead, one usually resorts to approximate linear-response methods that aim at excitation energies and oscillator strengths of the corresponding transitions.

A very common and successful approach along these lines is based on time-dependent density-functional theory (TDDFT) in the linear-response regime. This method does also depend on results of static density-functional theory (DFT). Within (TD)DFT the interacting many-electron problem is mapped onto the Kohn-Sham (KS) system of noninteracting particles, which reproduces the exact electronic density [1–3]. The price to pay for this gain in simplicity is the introduction of the exchange-correlation (xc) potential, which incorporates all nonclassical many-body effects. This quantity is well defined but needs to be approximated for practical applications.

The static xc potential, $v_{xc,0}(\mathbf{r})$, then allows to compute the eigenstates and eigenvalues of the noninteracting KS system. In a second step these quantities are transformed into the exact transition energies with the help of the Fourier transform of the xc kernel [4,5]. The latter is the functional derivative of the time-dependent xc potential evaluated at the ground-state density, i.e.,

$$f_{xc}(\mathbf{r}, \mathbf{r}', t - t') = \left. \frac{\delta v_{xc}(\mathbf{r}, t)}{\delta n(\mathbf{r}', t')} \right|_{n_0}, \quad (1)$$

and also needs to be approximated. Like v_{xc} the xc kernel is a unique functional of the density with a nonlocal dependency in space and time. The dependency on the density at earlier times is usually referred to as memory effects being present in f_{xc} .

Most applications of this linear-response approach rely on the adiabatic approximation, where f_{xc} is assumed to be local

in time and the memory effects are neglected. In principle this corresponds to using the static xc kernel $f_{xc,0}$, i.e., the functional derivative of $v_{xc,0}$. However as $f_{xc,0}$ is also generally unknown one is forced to make additional spatial approximations, e.g., the local density approximation, where f_{xc} is also local in space. This mix of different approximations prevents an unprejudiced assessment of the exclusive consequences of the adiabatic approximation. Nevertheless, there have been indications that the adiabatic approximation performs especially poor for the description of transitions of double excitation character [6–12].

Only recently it has become possible to disentangle spatial and temporal approximations for the two-electron singlet system [13–15]. In this case it is possible to obtain both the exact and adiabatically exact (AE) xc potentials so that the consequences of the adiabatic approximation can be directly assessed. This approach has been applied to the linear-response regime [12], which can also be tackled with real-time propagation methods [16–20]. The latter are based just on the time-dependent v_{xc} so that knowledge of f_{xc} is not necessary here. It has been shown that doubly excited states do indeed cause problems for the adiabatic approximation while transitions of single excitation character can be reproduced extremely well [12].

Although the linear-response effects of the adiabatic approximation can thus be analyzed on the level of the xc potential, it is still of great relevance to study these effects directly for the xc kernel. This is because it is quite common to approximate f_{xc} and use it for linear-response theory in the form which often is called “Casida matrix approach.” As a consequence some guidance with respect to memory effects at the level of the xc kernel would be a helpful addition to the ongoing exploration of f_{xc} [8,21–31]. Consequently, it is an intriguing question whether one can construct $f_{xc,0}$, i.e., the adiabatically exact xc kernel. In the present work we show that this is indeed possible for one-dimensional (1D) two-electron singlet systems.

This paper is organized in the following way: Sec. II comprises the relevant equations of linear density-response theory for the special case of a two-electron singlet system. In Sec. III we show how to reconstruct the density-density response functions of the exact and the KS system. Their numerical inversion is explained in Sec. IV, which also com-

prises response calculations based on the static xc kernel. The role of $f_{xc,0}$ in TDDFT is investigated in Sec. V, where it is used to compute the adiabatically exact transition frequencies and oscillator strengths. We conclude with a summary in Sec. VI.

II. THEORETICAL BACKGROUND

In this section we introduce the relevant formalism of linear density-response theory in the context of 1D two-electron singlet systems. The latter allow for an efficient numerical treatment of both the fully interacting and the KS systems while capturing important features of electronic correlation [32–38]. Furthermore we are able to compare our present findings with recent real-time studies based on the same systems [12].

We begin with the governing equations of the interacting and KS system emphasizing how they can be used to calculate the exact density response to a given ground-state (gs) potential perturbation. Then we define the response functions, their inverse counterparts, and most importantly the xc kernel. We also sketch the role of the xc kernel for the computation of the exact transition energies from linear-response theory. Next, we define the adiabatically exact approximation and its connection to the static xc kernel. This overview closes with a brief discussion of the relevant sum rules and symmetry properties.

A. Ground-state properties

The interacting 1D two-electron singlet system is governed by the static Schrödinger equation (SE), $H_0\psi_i = E_i\psi_i$, for the eigenvalues E_i and the correlated eigenstates $\psi_i(z_1, z_2)$. The latter are in our case real functions of definite parity that are symmetric under exchange of the two electrons. The Hamilton operator for the gs potential $v_{\text{ext},0}(z)$ is given by

$$H_0 = \sum_{j=1,2} \left[-\frac{\hbar^2}{2m} \frac{d^2}{dz_j^2} + v_{\text{ext},0}(z_j) \right] + V_{\text{ee}}(|z_1 - z_2|), \quad (2)$$

where the Coulomb singularity in 1D is avoided by using the soft-core interaction $W(z) = e^2 / \sqrt{z^2 + 1}$ for the electron-electron interaction V_{ee} and also for the external potential of the helium atom (see below).

The density response to a given perturbation $\delta v_{\text{ext},0}^{\text{exact}}(z)$ of the system's gs potential $v_{\text{ext,gs}}(z)$ can then be computed directly: First we calculate the ground state $\psi_0(z, z')$ of $H_0\psi_i = E_i\psi_i$, where $v_{\text{ext},0}(z) = v_{\text{ext,gs}}(z)$. In this way we obtain the unperturbed density

$$n_0(z) = 2 \int |\psi_0(z, z')|^2 dz'. \quad (3)$$

Then we repeat this procedure for $\tilde{v}_{\text{ext},0}(z) = v_{\text{ext,gs}}(z) + \delta v_{\text{ext},0}^{\text{exact}}(z)$, which provides us with $\tilde{n}_0(z)$, so that the density perturbation is given by

$$\delta n_0^{\text{exact}}(z) = \tilde{n}_0(z) - n_0(z). \quad (4)$$

Obviously, for the discussion of linear-response properties one needs to ensure that the potential perturbation is chosen such that $\delta n_0^{\text{exact}}(z)$ is sufficiently small.

The corresponding KS system is defined by the effective potential $v_{s,\text{gs}}(z)$ that follows from the exact density $n_0(z) = 2|\varphi_0(z)|^2$ through inversion of the static KS equation (KSE)

$$\left[-\frac{\hbar^2}{2m} \frac{d^2}{dz^2} + v_{s,0}(z) \right] \varphi_i(z) = \varepsilon_i \varphi_i(z) \quad (5)$$

for $i=0$ and $v_{s,0} = v_{s,\text{gs}}$ [15,39]. The uniqueness of this correspondence is established by the Hohenberg-Kohn theorem [40]. Note that for the two-electron singlet there is only one doubly occupied spatial KS orbital.

Similar to the interacting case the KS density response can be obtained from solving Eq. (5) for a perturbed $v_{s,0}$ and computing the difference of the corresponding ground-state density and n_0 . Equation (5) also provides the KS system's eigenvalues ε_i and eigenstates φ_i necessary to apply the TD-DFT response formalism introduced below.

B. Frequency-dependent linear density-response theory

Frequency-dependent linear-response theory states that for a small-amplitude frequency-dependent external perturbation $\delta v_{\text{ext}}^{\text{exact}}(z, \omega)$ the density response is given by

$$\delta n^{\text{resp}}(z, \omega) = \int \chi(z, z', \omega) \delta v_{\text{ext}}^{\text{exact}}(z', \omega) dz'. \quad (6)$$

Here, χ is the frequency-dependent density-density response or correlation function, which is also known as the susceptibility. The exact eigenstate or Lehmann representation of χ for the real eigenstates of the two-electron singlet system is given by

$$\chi(z, z', \omega) = \frac{1}{\hbar} \sum_{n>0} \left(\frac{\rho_{0n}(z)\rho_{0n}(z')}{\omega - \omega_{0n} + i\eta} - \frac{\rho_{0n}(z)\rho_{0n}(z')}{\omega + \omega_{0n} + i\eta} \right), \quad (7)$$

with the transition frequencies $\omega_{0n} = (E_n - E_0)/\hbar$ and the transition densities

$$\rho_{0n}(z) = 2 \int \psi_0(z, z') \psi_n(z, z') dz'. \quad (8)$$

The noninteracting KS system can be treated similarly resulting in

$$\chi_s(z, z', \omega) = \frac{1}{\hbar} \sum_{n>0} \left(\frac{\rho_{s,0n}(z)\rho_{s,0n}(z')}{\omega - \omega_{s,0n} + i\eta} - \frac{\rho_{s,0n}(z)\rho_{s,0n}(z')}{\omega + \omega_{s,0n} + i\eta} \right) \quad (9)$$

with

$$\rho_{s,0n}(z) = \varphi_0(z)\varphi_n(z) \quad (10)$$

and $\omega_{s,0n} = (\varepsilon_n - \varepsilon_0)/\hbar$.

The response equations, e.g., Eq. (6), can be Fourier transformed so that

$$\delta n^{\text{resp}}(z, t) = \int_0^t \int_{-\infty}^{+\infty} \chi(z, z', t - t') \delta v_{\text{ext}}^{\text{exact}}(z', t') dt' dz'. \quad (11)$$

Here it is important to recall that

$$\chi(z, z', t - t') = \left. \frac{\delta n(z, t)}{\delta v_{\text{ext}}(z', t')} \right|_{n_0} \quad (12)$$

is the functional derivative of the density with respect to the external potential evaluated at the ground-state density. Consequently we can also define the inverse response function

$$\chi^{-1}(z, z', t - t') = \left. \frac{\delta v_{\text{ext}}(z, t)}{\delta n(z', t')} \right|_{n_0}, \quad (13)$$

which allows to calculate the response of the potential to perturbations of the density. Analogous relations hold for the KS response function χ_s and its inverse χ_s^{-1} .

On this level we can finally build a bridge between the exact interacting system and the KS system: as the time-dependent potentials are related by

$$v_s(z, t) = v_{\text{ext}}(z, t) + v_h(z, t) + v_{\text{xc}}(z, t) \quad (14)$$

where $v_h(z, t) = \int n(z', t) V_{\text{ee}}(|z - z'|) dz'$ is the Hartree potential, the inverse response functions can be related by functional differentiation of Eq. (14). Back in frequency space this leads us to

$$\chi_s^{-1}(z, z', \omega) = \chi^{-1}(z, z', \omega) + V_{\text{ee}}(|z - z'|) + f_{\text{xc}}(z, z', \omega), \quad (15)$$

where $f_{\text{xc}}(z, z', \omega)$ is the xc kernel introduced above (we suppress the $|_{n_0}$ from now on). In real time it is given by the functional derivative of the xc potential

$$f_{\text{xc}}(z, z', t - t') = \frac{\delta v_{\text{xc}}(z, t)}{\delta n(z', t')}, \quad (16)$$

which means that f_{xc} is generally unknown and needs to be approximated. Note that for the two-electron singlet system $f_x(z, z') = -\frac{1}{2}f_h(z, z') = -\frac{1}{2}V_{\text{ee}}(|z - z'|)$, i.e., the exchange contribution is independent of time, thus strictly adiabatic. This is why we will sometimes consider $f_c = f_{\text{xc}} - f_x$ separately in the following.

The role of f_{xc} in linear-response TDDFT is twofold: on the one hand it determines the response of the xc potential to a perturbation of the ground-state density,

$$\delta v_{\text{xc}}^{\text{resp}}(z, \omega) = \int dz' f_{\text{xc}}(z, z', \omega) \delta n^{\text{exact}}(z', \omega), \quad (17)$$

i.e., it is the xc counterpart of the inverse response functions introduced above. On the other hand it is the crucial ingredient of the Casida matrix approach, a well established method to derive the exact transition frequencies from those of the KS system. It can be shown [4,5] that the exact excitation energies ω_{0n} follow from the eigenvalues $\lambda_n = \omega_{0n}^2$ of the matrix

$$\Omega_{ij} = \delta_{ij}(\varepsilon_i - \varepsilon_0)^2 + 4\sqrt{(\varepsilon_i - \varepsilon_0)(\varepsilon_j - \varepsilon_0)} F_{ij}, \quad (18)$$

with

$$F_{ij} = \int \int \varphi_0(z) \varphi_i(z) f_{\text{hxc}}(z, z', \omega) \varphi_0(z') \varphi_j(z') dz dz', \quad (19)$$

where $f_{\text{hxc}} = f_h + f_{\text{xc}}$, and ε_i and φ_i are the KS eigenvalues and eigenstates introduced earlier. Here $i, j > 0$ denote occupied-unoccupied single-particle transitions $0 \rightarrow i$, and we have already taken into account that the two-electron singlet is a spin-unpolarized system where only the lowest KS orbital is (doubly) occupied.

The oscillator strengths can be derived from the normalized eigenvectors x^n of Ω_{ij} through

$$s_n^{\text{d}} = 4 \left| \sum_i \sqrt{(\varepsilon_i - \varepsilon_0)} x_i^n \int z \rho_{s,0i}(z) dz \right|^2 \quad (20)$$

for dipole and

$$s_n^{\text{q}} = 4 \left| \sum_i \sqrt{(\varepsilon_i - \varepsilon_0)} x_i^n \int z^2 \rho_{s,0i}(z) dz \right|^2 \quad (21)$$

for quadrupole excitations. In the limit of the infinite-dimensional eigenvalue problem s_n^{d} and s_n^{q} should satisfy the appropriate oscillator sum rules, cf. Appendix A.

C. Adiabatic approximation and static linear response

The susceptibilities χ^{-1} and χ_s^{-1} are both retarded functions of time. Their frequency dependence is inherited by f_{xc} , which is the functional derivative of the exact v_{xc} . This is in line with v_{xc} also being a retarded function of time, i.e., v_{xc} is nonlocal-in-time with respect to its functional dependence on the time-dependent density.

An important concept both in linear and nonlinear TD-DFT is provided by the AE approximation. For the latter, v_{xc} is replaced by the exact $v_{\text{xc},0}$ of static DFT. Equivalently, f_{xc} is substituted by its static limit $f_{\text{xc},0}$. Obviously this step will change the correct transition energies that come out of the frequency-dependent Casida matrix approach of Eq. (18). However the extent and details of this error are still far from being completely understood.

To proceed toward a better understanding of the adiabatic approximation we need to obtain $f_{\text{xc},0}$ which is related to the static response functions by

$$\chi_{s,0}(z, z')^{-1} = \chi_0(z, z')^{-1} + V_{\text{ee}}(|z - z'|) + f_{\text{xc},0}(z, z'). \quad (22)$$

The static response limit ($\omega=0$) [2] is characterized by

$$\delta n_0^{\text{resp}}(z) = \int dz' \chi_0(z, z') \delta v_{\text{ext},0}^{\text{exact}}(z') \quad (23)$$

with

$$\chi_0(z, z') = -\frac{2}{\hbar} \sum_{n>0} \frac{\rho_{0n}(z) \rho_{0n}(z')}{\omega_{0n}} \quad (24)$$

and, for the noninteracting KS system, by

$$\delta n_0^{\text{resp}}(z) = \int dz' \chi_{s,0}(z, z') \delta v_{s,0}^{\text{exact}}(z'), \quad (25)$$

where

$$\chi_{s,0}(z, z') = -\frac{2}{\hbar} \sum_{n>0} \frac{\varphi_0(z) \varphi_n(z) \varphi_0(z') \varphi_n(z')}{\omega_{s,0n}}. \quad (26)$$

The adiabatically exact xc kernel thus belongs to the realm of ground-state linear density response as introduced in Sec. II A.

D. Symmetry properties and sum rules

Before we embark on the reconstruction of $f_{xc,0}$ it is helpful to summarize a few exact properties of the static xc kernel and the involved response functions. Due to the symmetry properties of the transition densities

$$\rho_{0n}(z) = \pm \rho_{0n}(-z), \quad (27)$$

where the sign is determined by the parity of ψ_n , χ_0 satisfies $\chi_0(z, z') = \chi_0(-z, -z')$. Naturally, $\chi_0(z, z') = \chi_0(z', z)$ does also hold. These properties do apply to $\chi_{s,0}$ and the inverse response functions, too.

Another exact constraint on the density-density response functions is provided by the sum rules [41]

$$\int \chi(z, z', \omega) [\partial_z v_{\text{ext},0}(z') - m\omega^2 z'] dz' = \partial_z n_0(z), \quad (28)$$

$$\int \chi_s(z, z', \omega) [\partial_z v_{s,0}(z') - m\omega^2 z'] dz' = \partial_z n_0(z). \quad (29)$$

They connect the complex, frequency-dependent response function to the static potential and ground-state density. As we are interested in the static response function χ_0 we take the limit $\omega \rightarrow 0$ and arrive at

$$\int \chi_0(z, z') \partial_z v_{\text{ext},0}(z') dz' = \partial_z n_0(z). \quad (30)$$

The analogous relation

$$\int \chi_{s,0}(z, z') \partial_z v_{s,0}(z') dz' = \partial_z n_0(z) \quad (31)$$

holds for the noninteracting KS system.

Inverting relations (28) and (29) one obtains the corresponding sum rules for the inverse response functions,

$$\int \chi^{-1}(z, z', \omega) \partial_z n_0(z') dz' = \partial_z v_{\text{ext},0}(z) - m\omega^2 z \quad (32)$$

and

$$\int \chi_s^{-1}(z, z', \omega) \partial_z n_0(z') dz' = \partial_z v_{s,0}(z) - m\omega^2 z. \quad (33)$$

Again, the limit $\omega \rightarrow 0$ leads to sum rules for the static versions of the inverse response functions. More importantly, making use of Eq. (22) it follows directly that the xc kernel satisfies

$$\int f_{xc}(z, z', \omega) \partial_z n_0(z') dz' = \partial_z v_{xc,0}(z). \quad (34)$$

It is important to note that the frequency-independent $f_{xc,0}$ does exactly satisfy the sum rule (34). This is a consequence of the fact that the AE approximation becomes exact for motion according to the harmonic potential theorem [39,41]. The sum rules also provide a useful test for response functions obtained from numerical schemes.

III. DENSITY-DENSITY RESPONSE FUNCTIONS

χ_0 AND $\chi_{s,0}$

A. Reconstruction of the response functions

One might think of two approaches to calculate the density-density-response functions: first, one could try to directly compute their Lehmann representations (24) and (26). However, this approach is not practical because it requires all the excited states and eigenenergies of the system. The numerical computation of a sufficient number of (correlated) eigenstates is not feasible even for a simple system such as the 1D two-electron singlet.

A second route is based directly on the response equations (23) and (25). In principle it should be possible to extract χ_0 from this integral relation by evaluating the linear response δn_0 to each of a large number of independent perturbations $\delta v_{\text{ext},0}^{\text{exact}}$ similarly to a tomographic reconstruction scheme. This concept becomes much clearer when it is used directly for the discrete version of the response equation

$$\delta n_0^{\text{resp}}(i) = dz \sum_j \chi_0(i, j) \delta v_{\text{ext},0}^{\text{exact}}(j), \quad (35)$$

which applies for a numerical approach. Here, $i, j = 0, \dots, N-1$ label points on a N -point real-space grid with $z(i) = -\frac{N-1}{2} dz + idz$, where dz is the grid spacing. The sum in Eq. (35) collapses for a perturbation of the type $\delta v_{\text{ext},0}^k(j) = \frac{c}{dz} \delta_{jk}$, where c is a (small) constant and δ_{jk} is the Kronecker delta, i.e., we have

$$\chi_0(i, k) = \frac{\delta n_0^k(i)}{c}. \quad (36)$$

The density perturbation

$$\delta n_0^k(i) = n_0^k(i) - n_0(i) \quad (37)$$

can be obtained from the ground-state solutions of the SE (cf. Sec. II A) with $v_{\text{ext,gs}}$ and $v_{\text{ext,gs}} + \delta v_{\text{ext},0}^k$, respectively. Repeating this procedure for all k of the coordinate grid the full χ_0 can be reconstructed. The constant c has to be chosen small enough to ensure that we are within the linear-response regime and that $v_{\text{ext,gs}} + \delta v_{\text{ext}}^k$ is sufficiently smooth on the chosen grid. On the other hand c has to be chosen large enough to achieve stable numerics.

The KS density-response function can be reconstructed analogously. Notably this procedure only requires the solution of the single-particle problem (5) for localized perturbations $v_{s,gs} + \delta v_{s,0}^k$. The static xc potential is not even needed here.

TABLE I. Ground-state properties of 1D two-electron singlet systems studied in this paper. All values are in Hartree atomic units. Further details about these systems can be found in Ref. [39].

System	$v_{\text{ext,gs}}(z)$
Helium	$-2W(z)$
A6-Hooke	$0.05(z^2+0.01z^6)$

We have applied this reconstruction scheme to two very different two-electron singlet systems: the helium atom and the anharmonic Hooke's atom (A6-Hooke system). The corresponding ground-state potentials $v_{\text{ext,gs}}(z)$ are given in Table I. These systems have been chosen because of their distinct behavior in earlier real-time linear-response studies [12]: while the AE approximation reproduces the lower transition energies of helium extremely well, it fails spectacularly for the A6-Hooke system, signaling the great importance of memory effects in the latter case. These failures were found to be related to the strong double excitation character of the problematic excitations. As those features are crucial also for the Casida formalism, the two systems provide suitable test cases for the present study. Furthermore, helium and A6-Hooke system differ in another important property: whereas the 1D helium atom shows a Rydberg series and a continuous part of the spectrum, there are only discrete energy levels in the A6-Hooke system. We will come back to this qualitative difference toward the end of this paper.

The reconstructed density-density response functions for helium and A6-Hooke system are shown in Figs. 1–4. Here positive (negative) values of $\chi_0(z, z')$ or $\chi_{s,0}(z, z')$ imply that a potential increase at z causes a density increase (drop) at z' . This provides the plausible qualitative picture that, locally, the increase of the potential leads to a reduction of the density. Due to particle number conservation this is accompanied by a nonlocal reaction, namely, the increase of the density in other parts of the system. It is also important to note that the nonzero parts of the response functions are localized

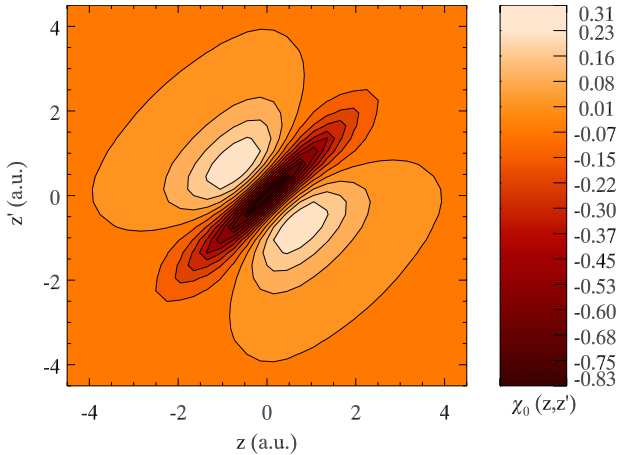


FIG. 1. (Color online) Interacting density-density response function $\chi_0(z, z')$ for helium.

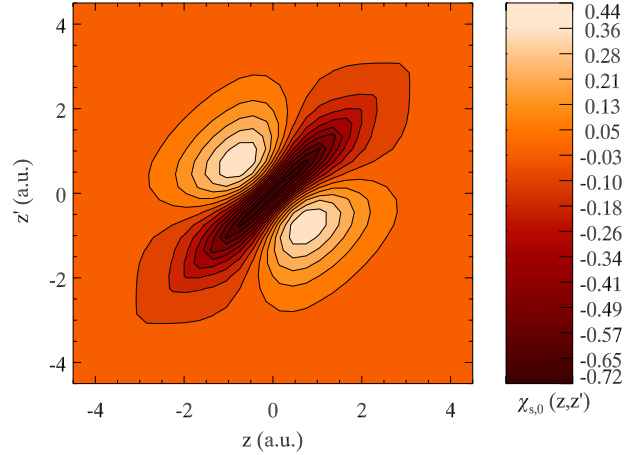


FIG. 2. (Color online) Noninteracting KS density-density response function $\chi_{s,0}(z, z')$ for helium.

in the central region, where n_0 is sufficiently large. Obviously the whole density is mostly unimpressed by potential perturbations localized far from the center.

As apparent from Figs. 1–4 the reconstructed response functions do indeed fulfill the symmetry conditions (cf. Sec. II D) except for tiny deviations that are due to unavoidable limitations in numerical accuracy. As any inversion scheme applied later amplifies these features we perform a further symmetrization of the response functions according to

$$\chi_0(i, j) \rightarrow \frac{1}{2}[\chi_0(i, j) + \chi_0(j, i)] \quad (38)$$

and

$$\chi_0(i, j) \rightarrow \frac{1}{2}[\chi_0(i, j) + \chi_0(N-1-i, N-1-j)], \quad (39)$$

where the latter operation ensures the symmetry under sign change of both spatial coordinates.

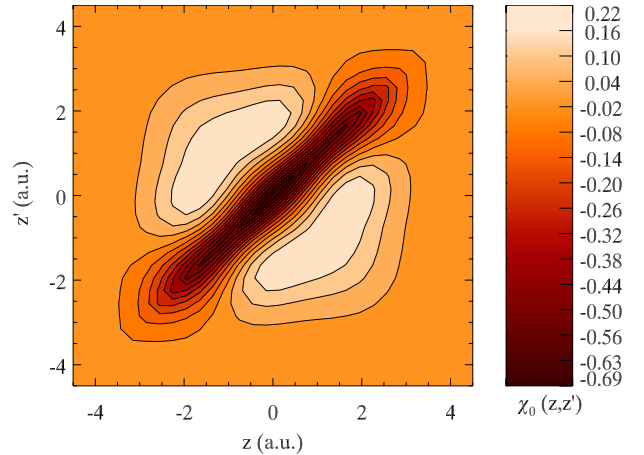


FIG. 3. (Color online) Interacting density-density response function $\chi_0(z, z')$ for the A6-Hooke system.

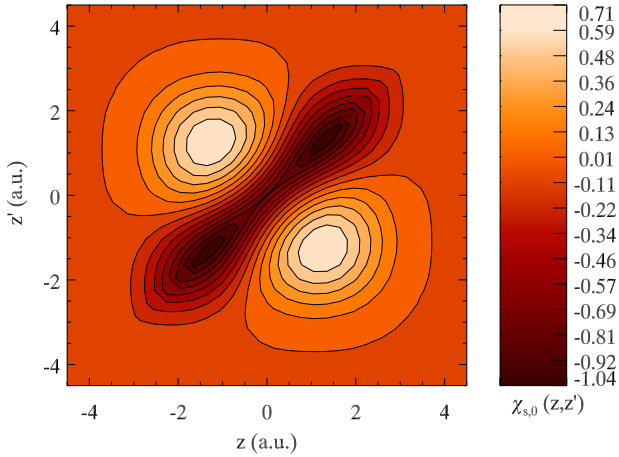


FIG. 4. (Color online) Noninteracting KS density-density response function $\chi_{s,0}(z, z')$ for the A6-Hooke system.

B. Test of the response functions

The quality of the obtained response functions can be tested in the following way: for a given potential perturbation $\delta v^{\text{exact}}(z)$ we perform both the gs calculation (cf. Sec. II A) and the response calculation according to Eq. (35). The resulting density perturbations $\delta n_0^{\text{exact}}$ and δn_0^{resp} can then be compared to judge the quality of the response function. For our test calculations we use the nonlocal potential changes of Table II and Fig. 5.

The interacting density response to these perturbations is shown in Fig. 6 for the helium atom. For all perturbations tested δn_0^{resp} and $\delta n_0^{\text{exact}}$ agree very well demonstrating the usefulness of the proposed reconstruction scheme. The reconstructed KS density-response function performs equally well.

As a further test we determine the violation of the static sum rules (30) and (31) by computing their left-hand side independently from their right-hand side, $\partial_z n_0(z)$. The results for helium are shown in Fig. 7, indicating that the sum rules are well satisfied quantitatively. As the KS and the exact density are identical by construction the curves lie all on top of each other. Both the response calculations and the sum

TABLE II. Nonlocal perturbations of the exact or KS ground-state potential used for testing the response functions. The choice of the amplitudes η_q , $q=1, \dots, 5$ ensures that the perturbation is within the linear-response regime of the particular system. Perturbations 3 and 4 are modified with a Gaussian cutoff in regions of very low density to prevent large values of $\delta v^{\text{exact}}(z)$ on the spatial grid.

Perturbation	$\delta v^{\text{exact}}(z)$
1	$\eta_1 \frac{-1}{\sqrt{(z-0.5)^2+1}}$
2	$\eta_2 \sin z$
3	$\eta_3 z$
4	$\eta_4 z^2$
5	$\eta_5 \cos z$

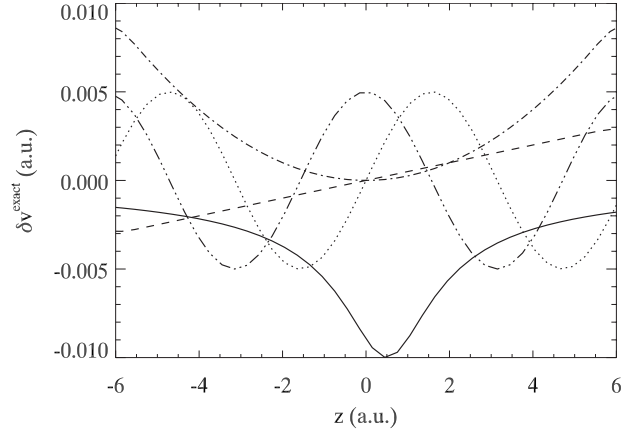


FIG. 5. Nonlocal potential perturbations $\delta v^{\text{exact}}(z)$ from Table II adapted for the perturbation of $v_{\text{ext,gs}}(z)$ of the helium atom (perturbation type 1–5: solid, dotted, dashed, dotted-dashed, triply-dotted-dashed).

rule analysis can also be performed for the A6-Hooke system, leading to results of similar quality.

IV. INVERSE RESPONSE FUNCTIONS AND THE STATIC XC KERNEL

In this section we show how to obtain the inverse response functions and the xc kernel. The latter is then used in response calculations for the static xc potential, which are compared to exact ground-state results. We also investigate how well the kernel fulfills the applicable sum rule. Finally we discuss in how far these integral properties determine the full xc kernel without ambiguity.

A. Inversion of the response functions

After the reconstruction of the density-density response function our next step is to obtain their inverse. On the dis-

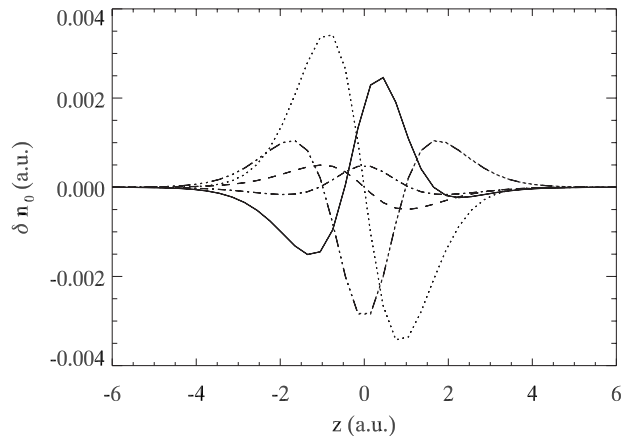


FIG. 6. Exact gs density response $\delta n_0^{\text{exact}}$ to the potential perturbations of Fig. 5 obtained from solving the interacting SE for the helium atom (perturbation type 1–5: solid, dotted, dashed, dotted-dashed, triply-dotted-dashed). The response calculation results δn_0^{resp} according to Eq. (35) lie directly on top of the corresponding $\delta n_0^{\text{exact}}$.

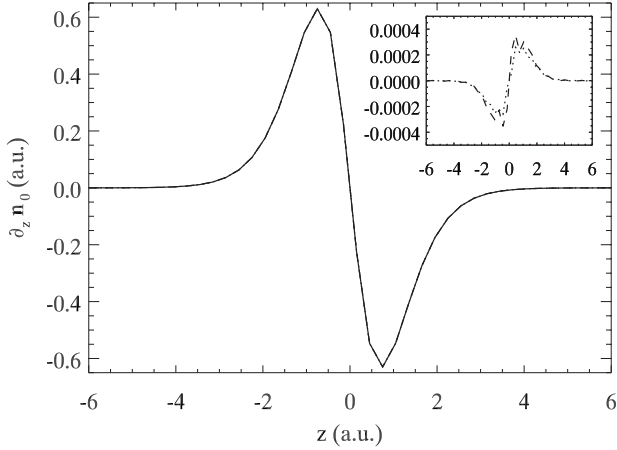


FIG. 7. Test of the sum rules (30) and (31) for helium: $\partial_z n_0(z)$ from direct differentiation (solid) and as obtained from $\int \chi_0(z, z') \partial_z v_{\text{ext},0}(z') dz'$ (dotted) and $\int \chi_{s,0}(z, z') \partial_z v_{s,0}(z') dz'$ (dashed). As all curves lie on top of each other on this scale, the inset shows the (tiny) differences between first and second (dotted) and first and third (dashed) curves.

create numerical grid this task amounts to inverting the matrix $\chi_0(i, j)$, i.e., finding $\chi_0^{-1}(i, j)$ so that

$$dz^2 \sum_j \chi_0^{-1}(i, j) \chi_0(j, k) = \delta_{ik}. \quad (40)$$

There exist many standard numerical routines for the inversion of real and symmetric matrices like the ones we are interested in. On the other hand, the inverse response functions are known to be singular by definition. This is a consequence of the fact that they describe the potential response, with the potential being defined only up to a constant. The singularity of, e.g., χ_0^{-1} corresponds to χ_0 being zero for $|z-z'| \rightarrow \infty$, i.e., the response of the density to a remote potential perturbation vanishes in the limit of infinite distance. Although this exact limit can never be represented on any finite numerical grid, the discrete response functions will have a number of rows and columns for large z or z' that are effectively zero for practical computational purposes. As a result the corresponding matrix is ill-conditioned.

In order to deal with this difficulty we restrict the following analysis to the inner region of the numerical grid, where $\chi_0(i, j)$ is sufficiently nonzero. This is not a particularly big loss as anyway several other necessary tools such as the inversion of the KSE are accurate only in the inner region of sufficiently high density. To the restricted matrix on the inner region we then apply a standard Gauss-Jordan matrix inversion algorithm [42].

To make sure that we choose the optimal grid interval for the inversion, we scan the possible inversion intervals on which Eq. (40) is satisfied, for the interval \mathcal{A} with the best performance of inverse response calculations,

$$\delta v_{\text{ext},0}^{\text{resp}}(i) = dz \sum_{j \in \mathcal{A}} \chi_0^{-1}(i, j) \delta n_0^{\text{exact}}(j). \quad (41)$$

Here we plug in the density perturbations $\delta n_0^{\text{exact}}$ corresponding to the potential changes of Table II and compare $\delta v_{\text{ext},0}^{\text{resp}}(i)$ to the original $\delta v_{\text{ext},0}^{\text{exact}}(i)$ for $i \in \mathcal{A}$.

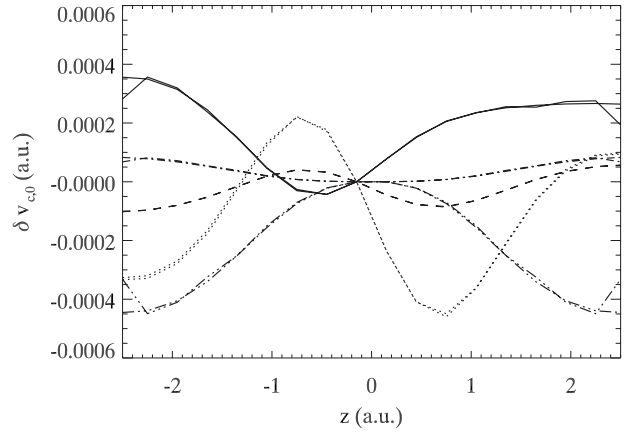


FIG. 8. $\delta v_{c,0}^{\text{exact}}$ and $\delta v_{c,0}^{\text{resp}}$ corresponding to perturbations of the helium gs density caused by external potential perturbations of type 1 (solid), 2 (dotted), 3 (dashed), 4 (dotted-dashed), and 5 (triply-dotted-dashed) according to Table II. All potentials are shifted by constants so that they are zero at the origin.

For the inversion of $\chi_{s,0}$ we proceed exactly in the same way. As an aside we note that $\chi_{s,0}^{-1}$ can also be computed analytically for the two-electron singlet system. More details on this topic are given in Appendix B.

B. Test of the static xc kernel

As soon as we have obtained the inverse response functions (in our case on a common truncated coordinate grid) it is straightforward to construct the xc kernel from Eq. (15). The ingredient f_h can directly be computed on the restricted grid. We will first investigate the performance of the kernel for static response calculations. As the nontrivial part of $f_{xc,0}$ is the correlation contribution we focus on $f_{c,0}$ and $v_{c,0}$ for these studies.

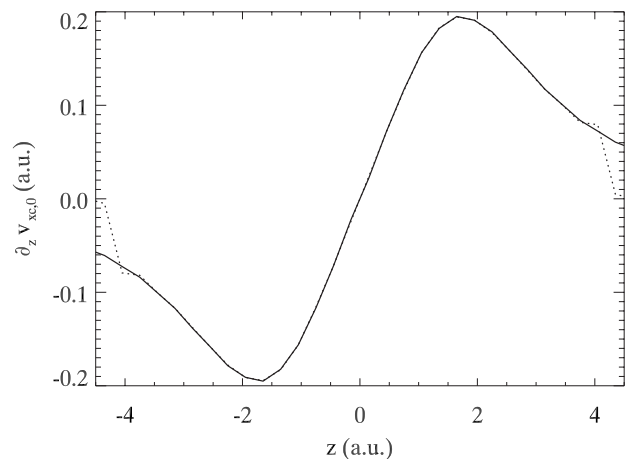


FIG. 9. Test of the sum rule (34) for helium: $\partial_z v_{xc,0}(z)$ from direct differentiation (solid) and as obtained from $\int f_{xc,0}(z, z') \partial_z n_0(z') dz'$ (dotted). Deviations at the edges are due to the finite size of the inversion interval.

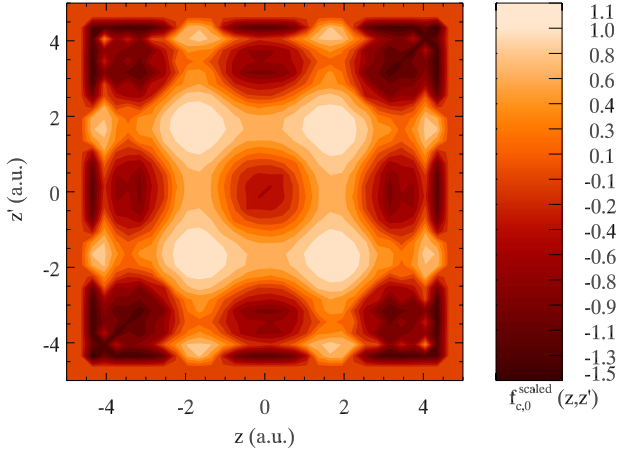


FIG. 10. (Color online) Static correlation kernel for helium on a restricted grid of roughly 9×9 a.u. For better visualization the xc kernel has been scaled according to $f_{c,0}^{\text{scaled}}(z, z') = \arctan[f_{c,0}(z, z')]$.

The static correlation kernel is the response function of $v_{c,0}$, i.e., for $i \in \mathcal{A}$,

$$\delta v_{c,0}^{\text{resp}}(i) = dz \sum_{j \in \mathcal{A}} f_{c,0}(i, j) \delta n_0^{\text{exact}}(j). \quad (42)$$

To test how well the reconstructed $f_{c,0}$ performs in this context we proceed in the following way: given a physical density perturbation $\delta n_0^{\text{exact}}$ corresponding (via a ground-state calculation) to the external potential perturbation $\delta v_{\text{ext},0}^{\text{exact}}$ we can compute $\delta v_{c,0}^{\text{resp}}$ via Eq. (42). The latter can be compared with the exact correlation potential perturbation

$$\delta v_{c,0}^{\text{exact}}(i) = \delta v_{s,0}^{\text{exact}}(i) - \delta v_{\text{ext},0}^{\text{exact}}(i) - \delta v_{\text{hx}}^{\text{exact}}(i), \quad (43)$$

where $\delta v_{\text{hx}}^{\text{exact}}$ and $\delta v_{s,0}^{\text{exact}}$ follow from $\delta n_0^{\text{exact}}$ by direct computation and inversion of the KS equation [cf. Eq. (B1)].

We have performed this test for the five perturbations $\delta v_{\text{ext},0}^{\text{exact}}$ given in Table II. The results are compared in Fig. 8 showing that $\delta v_{c,0}^{\text{resp}}$ and $\delta v_{c,0}^{\text{exact}}$ agree well in the central region of the grid, where the density is sufficiently large. Thus the reconstructed $f_{xc,0}$ provides a correct response function for $v_{c,0}$. Generally the results of inverse response calculations (density \rightarrow potential) do not have the same accuracy as the original ones (potential \rightarrow density). This is a consequence of the truncated grid, on which the inverse response function is obtained, and also due to the fact that little errors in the response function get amplified by the matrix inversion procedure (see below).

As a further test we explore how well $f_{xc,0}$ satisfies the sum rule (34). The results shown in Fig. 9 indicate that the sum rule is well fulfilled on the inversion interval. As for the response results presented above the violation of the inverse sum rule is somewhat larger than for the original sum rules. Once again, similar results can be obtained for the A6-Hooke system.

To finish the discussion of the reconstructed static kernel it is important to realize that all the properties tested previously just rely on integrals over $f_{c,0}(z, z')$. On the other hand our reconstruction scheme provides a numerical representa-

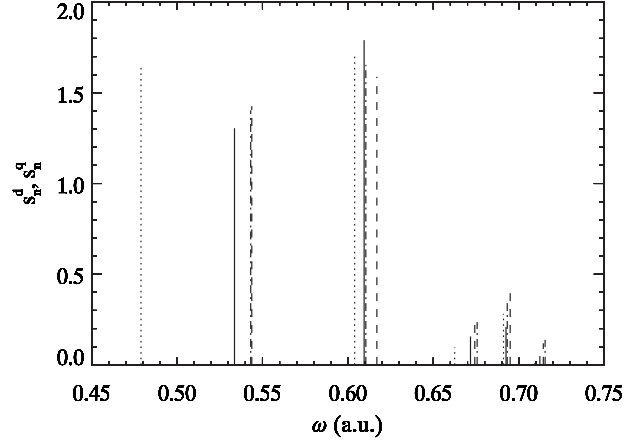


FIG. 11. Oscillator strengths of transition energies obtained from the bare KS values (dotted), EXX-Casida (dashed), AE-Casida (dotted-dashed), and from the exact eigenstates (solid) for helium. For each transition we plot only the dominant oscillator strength, i.e., either dipole or quadrupole. The quadrupole oscillator strengths have been rescaled for better visualization.

tion of $f_{c,0}$ as a full function of two coordinates. So how does the exact static correlation kernel actually look like? Figure 10 provides a visualization of $f_{c,0}$ for the helium model atom. However, we find that unlike the integral properties this picture is highly sensitive to the numerical parameters. The same naturally applies to similar plots of χ_0^{-1} and $\chi_{s,0}^{-1}$. Thus it seems not advisable to analyze the features of the kernel as a function of two spatial coordinates with our present methods. The high sensitivity is a consequence of the matrix inversion operation, which amplifies also small features of the response functions. However, this does not significantly affect the integral properties which have been found to be stable with respect to small changes of χ_0 and $\chi_{s,0}$.

One should recall that the presented reconstruction method for $f_{c,0}$ is based on the availability of the (numerically) exact solution of the interacting SE (cf. Sec. III A). As a consequence, the predominant value of this approach is that it allows to study properties of the exact $f_{c,0}$. Its usefulness as a practical DFT scheme to obtain the static kernel for a many-electron system is limited as the difficulty to compute the exact interacting solution increases with the complexity of the system. In principle, though, the approach can be extended to more than two electrons in three dimensions.

V. STATIC XC KERNEL IN TDDFT

Probably the most important application of the static xc kernel is within time-dependent linear-response theory. As explained above, $f_{xc,0}$ provides the adiabatically exact approximation of the frequency-dependent f_{xc} , which is crucial to obtain the exact transition energies and oscillator strengths. As the common approximations of f_{xc} are both adiabatic in time and approximate in space, it is of considerable interest to see how the adiabatically exact kernel actually performs.

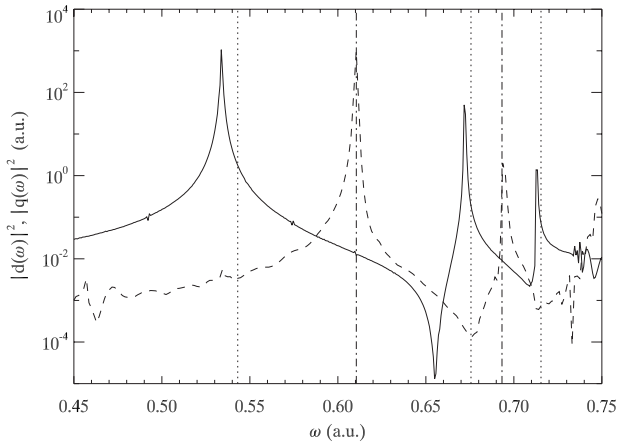


FIG. 12. Helium dipole (solid) and quadrupole (dashed) power spectrum from AE real-time propagation of Ref. [12]. The vertical lines indicate the dipole (dotted) and quadrupole (dotted-dashed) transition energies obtained from the present AE Casida approach (cf. Fig. 11).

To obtain the adiabatically exact excitation energies, we compute the five (ten) lowest KS eigenstates φ_i and eigenvalues ε_i for helium (A6-Hooke) and use them together with the system's $f_{\text{hxc},0}$ to construct the Casida matrix according to Eq. (18). Diagonalization of the latter directly leads to the adiabatically exact transition energies ω_{0n}^{ae} . Due to the orbitals' rapid falloff for large z the Casida results are stable with respect to the size of the inversion interval on which the kernel is available. Note that the coupling terms of the Casida matrix involve already two integrals over $f_{\text{xc},0}$. Hence the static kernel, which has been found to perform well for one-integral properties, is expected to be even more reliable. Finally, the oscillator strengths follow from Eqs. (20) and (21).

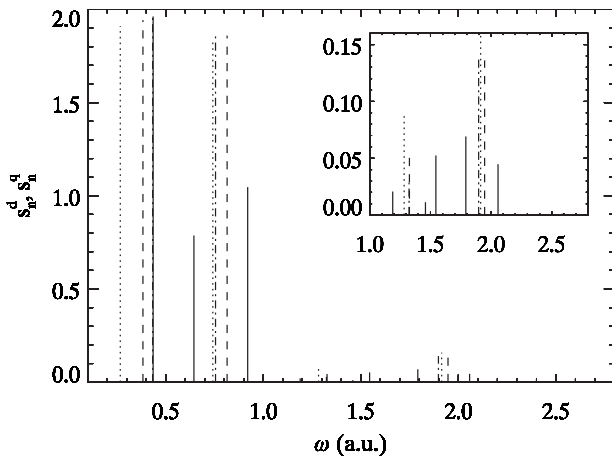


FIG. 13. Oscillator strengths of transition energies obtained from the bare KS values (dotted), EXX-Casida (dashed), AE-Casida (dotted-dashed), and from the exact eigenstates (solid) for the A6-Hooke system. For each transition we plot only the dominant oscillator strength, i.e., either dipole or quadrupole. The quadrupole oscillator strengths have been rescaled for better visualization. The inset shows a magnification of the higher energy regime.

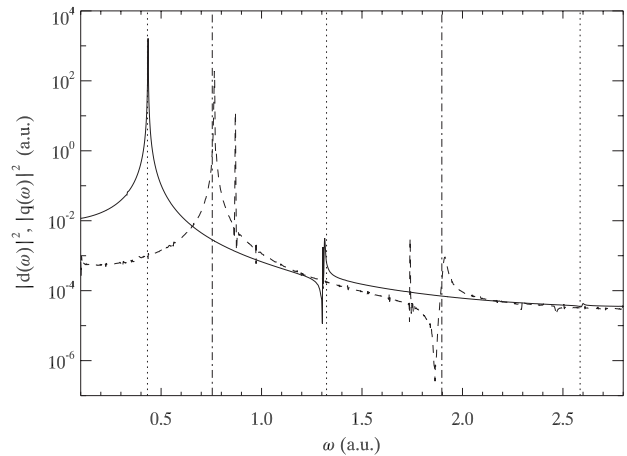


FIG. 14. A6-Hooke dipole (solid) and quadrupole (dashed) power spectrum from AE real-time propagation of Ref. [12]. The vertical lines indicate the dipole (dotted) and quadrupole (dotted-dashed) transition energies obtained from the present AE Casida approach (cf. Fig. 13).

It is instructive to study how the adiabatically exact transition energies and oscillator strengths differ from the exact values and those obtained from other approximations. Here, the exact quantities are readily available from the E_i and ψ_i of the static SE (cf. also Appendix A). On the other hand the bare KS transition energies and oscillator strengths following from ε_i and φ_i can serve as a zeroth-order approximation that corresponds to setting $f_{\text{hxc}}=0$ in the Casida matrix. A first correction to these values is provided by using only the exact exchange (EXX) kernel f_{hx} , which is independent of frequency for two-electron singlet systems.

The different approaches are contrasted in Fig. 11 for the case of helium. We can see how the bare KS values are shifted toward the exact ones by the combined effort of f_{hx} and $f_{\text{c},0}$. Whereas for the first transition the Hartree-exchange contribution is dominant, the second peak benefits from a correlation effect, which corrects the overshooting caused by f_{hx} . For increasing energies the KS transition frequencies gradually come closer to the exact ones implying that the single-particle picture becomes more and more relevant here.

Apparently the AE Casida method is able to reproduce the correct number of transitions at about the exact energies. However there are still some deviations between the exact and the AE transition energies and oscillator strengths. Is this a consequence of nonadiabatic memory effects that are not covered by the static kernel or is this a numerical error?

This question can be answered by comparing the present findings to a recent real-time study of the AE excitation energies for the same system [12]. This comparison, shown in Fig. 12, indicates that the transition energies obtained from real-time propagation agree much better with the exact ones than their Casida counterparts. So why do the latter deviate from the propagation results? This is a consequence of the atomic nature of the helium system: the KS spectrum quickly enters the Rydberg series and the continuum, so that the five lowest orbitals used by us are quite far from satisfying the corresponding oscillator strength sum rules, i.e., they do not

provide a complete set necessary for the correct description of the systems' properties within the Casida approach [43]. This problem does not exist in the real-time approach, which therefore has some advantages for atomic systems. We may thus conclude that the contributions of memory effects are negligible for the lower excitations of the helium model atom.

Finally we turn to the Casida results for the anharmonic Hooke's atom shown in Fig. 13. We find that the AE approximation does only reproduce the first transition energy and oscillator strength correctly. The remaining excitation energies are at wrong values or completely missing in the AE Casida results signaling the importance of memory effects.

Once again we are in a position to compare these findings with the corresponding real-time results of Ref. [12] shown in Fig. 14. In contrast to the helium atom we find no discrepancy between the two methods in this case. The good performance of the Casida method is not surprising as the ten lowest KS states of the A6-Hooke system satisfy their sum rule very well. This is a consequence of the fact that the anharmonic Hooke's atom has a completely discrete spectrum.

The Casida results for both systems imply once more that the reconstruction procedure for the xc kernel is working correctly. For completely confined systems like the A6-Hooke system, where a sufficient number of KS states can be computed with moderate effort, it is thus possible to reach energy ranges where the AE propagation scheme [12] is no longer reliable. The difficulties of the real-time approach are already apparent in Fig. 14. Here the AE power spectrum is on the one hand plagued by higher-order effects (sharp peaks) at intermediate energies and on the other it does not provide reliable predictions beyond $\omega \approx 2$ a.u.. For these issues the Casida approach based on the reconstructed adiabatically exact kernel provides valuable complementary and additional information.

VI. CONCLUSION

In this paper we have shown how the static xc kernel for one-dimensional two-electron singlet systems can be obtained. This approach is based on the reconstruction of the static density-density response functions on a discrete grid and their inversion on a smaller subgrid. The different steps of this reconstruction scheme can be checked by performing test response calculations which are then compared to exact ground-state results. The inverse response functions lead directly to a numerical representation of the static xc kernel.

Properties involving the integral kernel are found to be well converged and reliable in our approach. This is shown by conducting response calculations for the correlation potential and by checking the appropriate sum rules. Most importantly we have used the static xc kernel to calculate adiabatically exact transition energies from Casida-type matrix equations. These energies could be compared to transition frequencies that have been obtained from complementary adiabatically exact real-time linear-response calculations [12] and to exact transition energies from the correlated SE.

This comparison indicates that the reconstructed kernel is also reliable for this type of calculation. Furthermore we find

that, for a system with a continuum part of the spectrum such as the helium atom, the propagation approach is more accurate. On the other hand the real-time construction of the adiabatically exact approximation for v_{xc} becomes difficult for higher excitation energies. Here the approach based on the adiabatically exact kernel offers an attractive alternative for systems with a discrete spectrum such as the anharmonic Hooke's atom.

The latter is a useful prototype system for which the adiabatically exact approximation breaks down and memory effects become important. The accessibility of this regime with Casida matrix and real-time propagation methods enables new insights into memory effects in time-dependent density-functional theory.

ACKNOWLEDGMENTS

The authors acknowledge stimulating discussions with Manfred Lein and support by the Deutsche Forschungsgemeinschaft.

APPENDIX A: OSCILLATOR STRENGTHS AND SUM RULES

For 1D systems the dipole and quadrupole oscillator strengths are defined as

$$s_n^d = 2 \frac{m}{\hbar} \omega_{0n} |\langle 0 | z | n \rangle|^2 \quad (\text{A1})$$

and

$$s_n^q = 2 \frac{m}{\hbar} \omega_{0n} |\langle 0 | z^2 | n \rangle|^2. \quad (\text{A2})$$

The corresponding sum rules then follow from the energy weighted sum rule [44]

$$\sum_n \omega_{0n} |\langle 0 | V_{\text{pert}}(z) | n \rangle|^2 = \frac{\hbar}{2m} \int n_0(z) |\partial_z V_{\text{pert}}(z)|^2 dz. \quad (\text{A3})$$

Consequently we obtain

$$\sum_n s_n^d = N \quad (\text{A4})$$

for the dipole case [$V_{\text{pert}}(z) = z$] and

$$\sum_n s_n^q = 4q_0 \quad (\text{A5})$$

for the quadrupole case [$V_{\text{pert}}(z) = z^2$] where $q_0 = \int z^2 n_0(z) dz$ is the quadrupole moment of the ground state.

APPENDIX B: ANALYTIC REPRESENTATION OF $\chi_{s,0}^{-1}$

Due to the explicit representability of $v_{s,0}$ in terms of the ground-state density n_0 , i.e. [39],

$$v_{s,0} = \frac{\hbar^2}{2m} \frac{\partial_z^2 \varphi_0(z)}{\varphi_0(z)} = \frac{\hbar^2}{2m} \frac{\partial_z^2 \sqrt{n_0(z)}/2}{\sqrt{n_0(z)}/2}, \quad (\text{B1})$$

which is characteristic of the two-electron singlet system, we can perform the functional derivative $\chi_{s,0}^{-1}(z, z') = \delta v_{s,0}(z) / \delta n_0(z')$ analytically. This leads to

$$\frac{\delta v_{s,0}(z)}{\delta n_0(z')} = \frac{1}{2\sqrt{n(z)}} \partial_z^2 \left(\frac{\delta(z-z')}{2\sqrt{n(z)}} \right) - \frac{\delta(z-z')}{4[n(z)]^{3/2}} \partial_z^2 \sqrt{n(z)}, \quad (\text{B2})$$

where we have set $\hbar=m=1$. The appearance of spatial derivatives of delta functions in this analytic expression is no reason to worry: in any physically meaningful context $\chi_{s,0}^{-1}$ appears as an integral kernel and the derivatives can be shuffled to other functions by partial integration.

This analytical approach also applies to $\chi_s^{-1}(z, z', t-t') = \delta v_s(z, t) / \delta n(z', t')$ as [39]

$$v_s(z, t) = v_{s,0}(z, t) - \hbar \left\{ \dot{\alpha}(z, t) + \frac{\hbar}{2m} [\partial_z \alpha(z, t)]^2 \right\}, \quad (\text{B3})$$

where the KS phase α is related to the KS current j_s via

$$j_s(z, t) / n(z, t) = \frac{\hbar}{m} \partial_z \alpha(z, t) \quad (\text{B4})$$

and hence can be reexpressed in terms of the time-dependent density using the relation

$$j_s(z, t) = - \int_0^z \partial_t n(z', t) dz', \quad (\text{B5})$$

which follows from the 1D continuity equation. Here the functional differentiation will not only lead to spatial derivatives of $\delta(z-z')$ as for $\chi_{s,0}^{-1}$ but also to temporal derivatives of $\delta(t-t')$. These are the equal-time singularities that have been found to occur in functional derivatives of the potential with respect to the density and that are also present in the time-dependent xc kernel [45].

-
- [1] E. Runge and E. K. U. Gross, Phys. Rev. Lett. **52**, 997 (1984).
- [2] E. K. U. Gross, J. F. Dobson, and M. Petersilka, in *Density Functional Theory*, edited by R. F. Nalewajski (Springer, Berlin, 1996), pp. 81–172.
- [3] *Time-Dependent Density Functional Theory*, edited by M. Marques, C. Ullrich, F. Nogueira, A. Rubio, K. Burke, and E. Gross (Springer, Berlin, 2006).
- [4] M. Petersilka, U. J. Gossmann, and E. K. U. Gross, Phys. Rev. Lett. **76**, 1212 (1996).
- [5] M. E. Casida, in *Recent Advances in Density Functional Methods, Part I*, edited by D. P. Chong (World Scientific Publishing, Singapore, 1995), pp. 155–192.
- [6] S. Hirata and M. Head-Gordon, Chem. Phys. Lett. **302**, 375 (1999).
- [7] D. J. Tozer and N. C. Handy, Phys. Chem. Chem. Phys. **2**, 2117 (2000).
- [8] N. T. Maitra, F. Zhang, R. J. Cave, and K. Burke, J. Chem. Phys. **120**, 5932 (2004).
- [9] R. J. Cave, F. Zhang, N. T. Maitra, and K. Burke, Chem. Phys. Lett. **389**, 39 (2004).
- [10] J. Neugebauer, E. J. Baerends, and M. Nooijen, J. Chem. Phys. **121**, 6155 (2004).
- [11] K. J. H. Giesbertz, E. J. Baerends, and O. V. Gritsenko, Phys. Rev. Lett. **101**, 033004 (2008).
- [12] M. Thiele and S. Kümmel, Phys. Chem. Chem. Phys. **11**, 4631 (2009).
- [13] I. D’Amico and G. Vignale, Phys. Rev. B **59**, 7876 (1999).
- [14] P. Hessler, N. T. Maitra, and K. Burke, J. Chem. Phys. **117**, 72 (2002).
- [15] M. Thiele, E. K. U. Gross, and S. Kümmel, Phys. Rev. Lett. **100**, 153004 (2008).
- [16] K. Yabana and G. F. Bertsch, Phys. Rev. B **54**, 4484 (1996).
- [17] U. Saalmann and R. Schmidt, Z. Phys. D: At., Mol. Clusters **38**, 153 (1996).
- [18] F. Calvayrac, P. G. Reinhard, and E. Suraud, Ann. Phys. (N.Y.) **255**, 125 (1997).
- [19] M. Marques, A. Castro, G. Bertsch, and A. Rubio, Comput. Phys. Commun. **151**, 60 (2003).
- [20] M. Mundt and S. Kümmel, Phys. Rev. B **76**, 035413 (2007).
- [21] M. Lein, E. K. U. Gross, and J. P. Perdew, Phys. Rev. B **61**, 13431 (2000).
- [22] I. V. Tokatly and O. Pankratov, Phys. Rev. Lett. **86**, 2078 (2001).
- [23] G. Onida, L. Reining, and A. Rubio, Rev. Mod. Phys. **74**, 601 (2002).
- [24] H. Appel, E. K. U. Gross, and K. Burke, Phys. Rev. Lett. **90**, 043005 (2003).
- [25] G. Adragna, R. Del Sole, and A. Marini, Phys. Rev. B **68**, 165108 (2003).
- [26] A. Scherz, E. K. U. Gross, H. Appel, C. Sorg, K. Baberschke, H. Wende, and K. Burke, Phys. Rev. Lett. **95**, 253006 (2005).
- [27] C. A. Ullrich and K. Burke, J. Chem. Phys. **121**, 28 (2004).
- [28] M. Grüning, A. Marini, and A. Rubio, J. Chem. Phys. **124**, 154108 (2006).
- [29] D. Varsano, A. Marini, and A. Rubio, Phys. Rev. Lett. **101**, 133002 (2008).
- [30] R. Baer, e-print arXiv:0808.3848, J. Mol. Struct.: THEOCHEM (in press).
- [31] A. J. Krueger and N. T. Maitra, Phys. Chem. Chem. Phys. **11**, 4655 (2009).
- [32] S. L. Haan, R. Grobe, and J. H. Eberly, Phys. Rev. A **50**, 378 (1994).
- [33] D. Bauer, Phys. Rev. A **56**, 3028 (1997).
- [34] S. L. Haan and R. Grobe, Laser Phys. **8**, 885 (1998).
- [35] D. G. Lappas and R. van Leeuwen, J. Phys. B **31**, L249 (1998).
- [36] M. Lein, E. K. U. Gross, and V. Engel, Phys. Rev. Lett. **85**, 4707 (2000).
- [37] R. Panfili and W.-C. Liu, Phys. Rev. A **67**, 043402 (2003).

- [38] R. Püttner, B. Grémaud, D. Delande, M. Domke, M. Martins, A. S. Schlachter, and G. Kaindl, *Phys. Rev. Lett.* **86**, 3747 (2001).
- [39] M. Thiele and S. Kümmel, *Phys. Rev. A* **79**, 052503 (2009).
- [40] P. Hohenberg and W. Kohn, *Phys. Rev.* **136**, B864 (1964).
- [41] G. Vignale, *Phys. Lett. A* **209**, 206 (1995).
- [42] W. H. Press, S. A. Teukolsky, W. T. Vetterling, and B. P. Flannery, *Numerical Recipes in FORTRAN*, 2nd ed. (Cambridge University Press, Cambridge, 1992).
- [43] The numerical computations become increasingly involved for higher-lying states in the helium system.
- [44] R. A. Broglia, G. Coló, G. Onida, and H. E. Roman, *Solid State Physics of Finite Systems* (Springer, Berlin, 2004).
- [45] G. Vignale, *Phys. Rev. A* **77**, 062511 (2008).